Quantum Oscillations in High Magnetic Fields

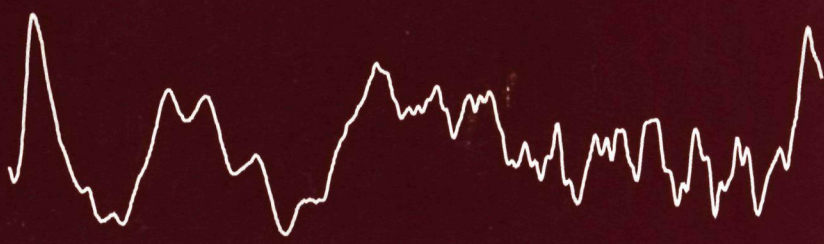

Paul Teunissen

Quantum Oscillations in High Magnetic Fields

CIP-GEGEVENS KONINKLIJKE BIBLIOTHEEK, DEN HAAG

Teunissen, Paulus Antonius Andreas

Quantum Oscillations in High Magnetic Fields/ P A A
Teunissen [S l s n] - Ill
Proefschrift Nijmegen - Met lit opg - Met samenvatting
in het Nederlands
ISBN 90 9005604-1
Trefw quantum oscillaties / gecorreleerde electronen /
metamagnetische overgang

Cover illustration quantum oscillations of the transverse magnetoresistance in the heavy fermion compound UPt_3 between 20 and 30 tesla (Julian, Teunissen, Wiegers see chapter 5)

Quantum Oscillations in High Magnetic Fields

een wetenschappelijke proeve op het gebied van
de Natuurwetenschappen

Proefschrift

ter verkrijging van de graad van doctor aan
de Katholieke Universiteit Nijmegen,
volgens besluit van het College van Decanen
in het openbaar te verdedigen op
woensdag 13 januari 1993
des namiddags om 1.30 uur precies

door

Paulus Antonius Andreas Teunissen

geboren op 20 juni 1965
te Eindhoven

Promotor: Prof. Dr. H. van Kempen
Copromotor: Dr. J.A.A.J. Perenboom

Van experimenteel onderzoek – zeker het soort dat in dit proefschrift beschreven staat – komt alleen maar iets terecht als vele mensen daaraan hun bijdrage leveren Enkelen van hen zou ik hier met name willen noemen

Om te beginnen ben ik veel dank verschuldigd aan Herman van Kempen en Jos Perenboom Op moeilijke momenten hebben ze mij uitstekend gecoached

Veel metingen heb ik samen met Stef Wiegers verricht Ik vond het heel plezierig en leerzaam om met hem samen te werken en als dat weer eens nodig was de aanwezige apparatuur, een weigerachtige mengkoeler bijvoorbeeld, "alle hoeken te laten zien", zoals hij wel vaker beeldrijke taal hanteert Ook wil ik hem bedanken voor het werpen van een kritische blik op de inhoud van dit boekje

Een belangrijk deel van hoofdstuk twee is mogelijk gemaakt door Henk Neijenhuisen, die mij erg heeft geholpen bij het transformeren van elektronische ontwerpen tot handelbare en werkende componenten Samen met Henk vormden Marijn Devillers, Louis Schreurs en Martha Geurts de kleine maar harde kern van Vaste Stof 1 en zorgden voor een fijne werksfeer

Veel dank ook aan alle medewerkers van het magnetenlab Met name Klaas van Hulst, een echte meedenker en altijd in voor een ongebruikelijk veld-tijd profiel, Jos Rook voor zijn onmisbare vakmanschap en Hung van Luong voor de prima asystentie

It was quite an experience to work with Stephen Julian Without him I would never have been a witness of ingenious sample rotation techniques (remote tapping on insert included) I have enjoyed our co-operation very much and I would like to thank him for his comments on chapter five

Op het gravel van de tennisbaan was in ander opzicht ook sprake van "alle hoeken" Samen met Paul van der Wel heb ik ze grondig kunnen verkennen en verrassende inzichten gekregen in de wetten van de tennismechanica

Tot besluit wil ik mijn ouders bedanken voor hun steun en belangstelling en Astrid omdat ze zoveel voor mij betekent

"It was a large room. Full of people. All kinds. And they had all arrived at the same building at more or less the same time. And they were all free. And they were all asking themselves the same question:
What... is behind... that curtain?"

Laurie Anderson, "Big Science".

Voor Astrid

Contents

Chapter 1

de Haas – van Alphen effect in theory

1.1 Introduction

When the first experimental observation of oscillatory magnetic behaviour was made by de Haas and van Alphen [1] in 1930 in bismuth, it was not realised just then what the underlying physical explanation should be A few months before, Landau had published a paper [2] in which he remarked that the magnetisation of a metal would be expected to exhibit a periodic variation because of the quantisation of the helical orbits of the conduction electrons Curiously enough both sides were unaware of the other's contribution at the time

In 1952 Onsager [3] was the first to show that the period of these so-called de Haas – van Alphen (dHvA) oscillations was inversely proportional to the extremal area of the cross section of the Fermi surface A few years later Lifshitz and Kosevich [4] worked out a more complete theory which not only confirmed Onsager's prediction concerning the periodicity of the oscillations but which also resulted in a quantitative expression for their amplitude and phase

This chapter is meant to give a compact derivation of the Lifshitz–Kosevich expression and to explain the physical origin of the oscillations It is based on the semi-classical picture of Bloch electrons moving through a crystal lattice in addition to the Bohr–Sommerfeld quantisation rule The electrons are assumed to be independent particles, the influence of many-body interactions on the Lifshitz–Kosevich expression is briefly sketched

Some excellent reviews on the subject the dHvA effect are available, though not of recent date a detailed treatment by Shoenberg [5], an older overview by Gold [6] and a collection of relevant topics by several authors, edited by Springford [7]

1.2 Electron motion in a magnetic field

The semi-classical description of a Bloch electron in the presence of a magnetic field $\mathbf{B}$ is based on the Lorentz force equation

$$\hbar\dot{\mathbf{k}} = -e(\mathbf{v} \times \mathbf{B}) \tag{1 1}$$

where $\mathbf{k}(t)$ is the electron wave vector and $\hbar\mathbf{k}$ its crystal momentum The velocity $\mathbf{v}$ is given by

$$\mathbf{v} = \frac{1}{\hbar}\frac{\partial\epsilon(\mathbf{k})}{\partial\mathbf{k}} \tag{1 2}$$

where $\epsilon(\mathbf{k}(t))$ is the electron energy It follows immediately from these equations that both $\epsilon(\mathbf{k}(t))$ and the component of the wave vector along the magnetic field, $k_{\|}$, are constants of motion Integration of (1 1) with respect to time gives

$$\hbar(\mathbf{k} - \mathbf{k_0}) = -e(\mathbf{r} - \mathbf{r_0}) \times \mathbf{B} \tag{1 3}$$

where $\mathbf{r}$ is the position vector of the electron in its classical trajectory The projection $\mathbf{r}'$ of the (helical) orbit on to the plane perpendicular to $\mathbf{B}$ is a scaled version of the trajectory of $\mathbf{k}$ in the reciprocal space The scaling factor is $\hbar/eB$ Furthermore the

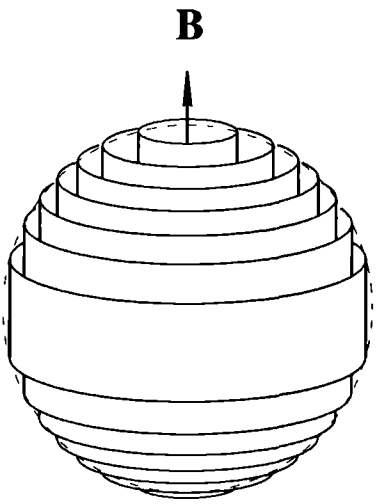

Figure 1.1 Semi-classical representation of the allowed states in the reciprocal space for a free electron metal when a magnetic field **B** is applied. Only states with energy less than the Fermi energy are shown.

projected **r**-orbit is rotated 90° with respect to the **k**-orbit. In the free electron case the constant energy surfaces are spheres and the orbits are circular. In general the **k**-space orbits will not be circular and they often are not even closed. The angular frequency with which the $\mathbf{r}'$ orbit is traversed is the so-called cyclotron frequency

$$\omega_c = \frac{eB}{m^*} \tag{1.4}$$

which depends on the cyclotron or orbit effective mass

$$m^*(\epsilon, k_{\|}) = \frac{\hbar^2}{2\pi}\left(\frac{\partial \mathcal{A}}{\partial \epsilon}\right) \tag{1.5}$$

where $\mathcal{A}$ is the cross-sectional area of the Fermi surface at $k_{\|}$. For those trajectories in **k**-space which are closed, the projected **r**-space orbit will also be closed and according to the Bohr-Sommerfeld rule the periodic motion is expected to be quantised:

$$\oint \mathbf{p} \cdot \mathrm{d}\mathbf{r}' = \oint (\hbar\mathbf{k} - e\mathbf{A}) \cdot \mathrm{d}\mathbf{r}' = (n + \gamma)2\pi\hbar \tag{1.6}$$

where $\nabla \times \mathbf{A} = \mathbf{B}$, n is an integer and γ is an undetermined phase factor. This quantum condition can be rewritten in terms of the flux Φ of **B** through the $\mathbf{r}'$-orbit:

$$\Phi = \frac{2\pi\hbar}{e}(n + \gamma) \tag{1.7}$$

expressing that only those orbits are permitted through which the flux, apart from the phase factor, is an integral multiple of the fundamental flux quantum $2\pi\hbar/e$ The areas of the allowed orbits in real-space are therefore given by $(n+\gamma)2\pi\hbar/eB$, corresponding to allowed areas A_n in **k**-space

$$A_n(\epsilon_n, k_\parallel) = \frac{2\pi e}{\hbar}(n+\gamma)B \tag{1 8}$$

It is known as the Onsager relation, and shows that the effect of a magnetic field is to constrain the allowed states in **k**-space to lie on a series of so called Landau tubes with energies ϵ_n (figure 1 1) Typically the quantum numbers n are large and in the limit of the correspondence principle which relates quantum behaviour at high quantum numbers with classical motion the degeneracy of each Landau level is expected to be such that it can just accommodate all the $(V/4\pi^3)\Delta\mathcal{A}\delta k_\parallel$ electrons which would be contained at zero magnetic field in an annular area $\Delta\mathcal{A} = 2\pi eB/\hbar$ surrounding the orbit On average, the number of electron states δD on a length of tube lying between $k_\parallel$ and $k_\parallel + \delta k_\parallel$ will be

$$\delta D = \frac{eBV}{2\pi^2\hbar}\delta k_\parallel \tag{1 9}$$

The area of the **k**-space orbit with quantum number n grows with increasing magnetic field and at the same time the projected area of the real-space orbit decreases in order to conserve the magnetic flux When the Landau state approaches an extremal cross-section of the Fermi surface $\mathcal{A}_{extr}$, the free energy will increase to a maximum If the magnetic field is increased a bit further, the tube becomes depleted, causing a sudden lowering of the free energy Now the Landau state with quantum number $(n-1)$ is the outermost non-empty tube and will again give rise to an increase of the free energy until a new maximum is reached The maxima occur whenever $A_n = \mathcal{A}_{extr}$, at regularly spaced intervals in 1/B given by

$$\Delta\left(\frac{1}{B}\right) = \frac{2\pi e}{\hbar}\frac{1}{\mathcal{A}_{extr}} \tag{1 10}$$

This expression directly relates the periodicity of the oscillations of the free energy to the extremal cross section of the Fermi surface, i e , it provides information about the Fermi surface topology

1.3 The oscillatory part of the free energy

In order to derive the magnetic moment of the electron system it proves convenient to start from the thermodynamic grand potential defined by

$$\Omega = \mathcal{F} - N\mu \tag{1 11}$$

where $\mathcal{F}$ is the free energy of the electron gas μ is the chemical potential and N is the number of electrons The vector magnetic moment is given by

$$\mathbf{M} = -\left(\frac{\partial\Omega}{\partial\mathbf{B}}\right)_\mu \tag{1 12}$$

Although $\mathbf{M}$ is derived from Ω by differentiation at constant μ, it does not imply that μ in fact *is* constant as B changes. The free energy $\mathcal{F}$ of an electron gas is given by

$$\mathcal{F} = N\mu + k_B T \sum_n \ln(1 - f(\epsilon_n)) \tag{1.13}$$

where f is the Fermi–Dirac distribution function and the summation is over all available states. The thermodynamic potential Ω is then

$$\Omega = -k_B T \sum_n \ln(1 + e^{(\mu - \epsilon_n)/k_B T}) \tag{1.14}$$

Keeping in mind the degeneracy as specified in (1.9), the summation may be transformed into an integral over $k_\parallel$

$$\Omega = -k_B T \int_{-\infty}^{+\infty} \mathrm{d}k_\parallel \left(\frac{eBV}{2\pi^2\hbar}\right) \sum_n \ln(1 + e^{(\mu - \epsilon_n)/k_B T}) \tag{1.15}$$

The levels ϵ_n are assumed *not* to be broadened. So at $T = 0$ the contribution $\delta\Omega$ of a thin slab through the Fermi surface normal to the magnetic field between $k_\parallel$ and $k_\parallel + \delta k_\parallel$, is then

$$\delta\Omega = \delta k_\parallel \left(\frac{eBV}{2\pi^2\hbar}\right) \sum_{n=0}^{N} (\epsilon_n - \mu) \tag{1.16}$$

where N is the highest value of n. The summation over n can now be worked out via the Poisson summation formula [5, p. 481]:

$$\sum_n \to \mathrm{d}n + 2 \sum_p \int \mathrm{d}n \cos(2\pi p n) \tag{1.17}$$

When only the oscillatory terms in the summation are retained, the result for the thin slab becomes

$$\delta\tilde{\Omega} = \delta k_\parallel \left(\frac{e^2 B^2}{4\pi^4 m^*}\right) \sum_{p=1}^{\infty} \frac{1}{p^2} \cos\left[2\pi p \left(\frac{\hbar \mathcal{A}(k_\parallel)}{2\pi e B} - \gamma\right)\right] \tag{1.18}$$

The next step is the summation over all parallel slices through the Fermi surface, i.e., to integrate over $k_\parallel$. For large N the argument of the cosine function is approximately $2\pi pN$ so the integrand will oscillate rapidly as $\mathcal{A}(k_\parallel)$ varies from slice to slice. Only in the neighbourhood of stationary $\mathcal{A}$ will the contributions of the various slices add constructively, leading to

$$\tilde{\Omega} = \frac{e^2}{4\pi^4 m^*} \left(\frac{2\pi e}{\hbar}\right)^{1/2} \left|\frac{\partial^2 \mathcal{A}}{\partial k_\parallel^2}\right|^{-1/2} \sum_{p=0}^{\infty} \frac{B^{5/2}}{p^{5/2}} \cos\left[2\pi p \left(\frac{F}{B} - \gamma\right) \mp \frac{\pi}{4}\right] \tag{1.19}$$

where F is the so called dHvA frequency given by

$$F = \frac{\hbar}{2\pi e} \mathcal{A}_{extr} \tag{1.20}$$

and the term $\left|\frac{\partial^2 \mathcal{A}}{\partial k_\parallel^2}\right|^{-1/2}$ is the Fermi surface curvature factor.

1.4 Modifications of the ideal case

It is very illustrative to treat the effect of finite temperature, electron scattering and electron spin on the amplitude of the harmonics p as a result of "phase smearing", i.e., to consider the dHvA frequency F to be varied over a small range around the value corresponding to the idealised situation. The distribution of F depends on the mechanism that is considered but in general will be a peaked function with a certain width.

Let the argument of a cosine term in (1.19) be the variable ψ. The net effect of a distribution in F is the replacement of $\cos\psi$ by

$$\frac{\int D(\phi/\lambda)\cos(\psi+\phi)\mathrm{d}\phi}{\int D(\phi/\lambda)\mathrm{d}\phi} \tag{1.21}$$

where ϕ is the departure from the standard value ψ and $D(\phi/\lambda)$ is the distribution function of the phase smearing. It is defined in such a way that the probability of ϕ lying between ϕ and $\phi+\mathrm{d}\phi$ is proportional to $D(\phi/\lambda)\mathrm{d}\phi$. The scaling parameter λ is characteristic of the particular kind of phase smearing under consideration and stands for the width of the phase smearing distribution function. If $\lambda \ll 1$ only small values for ϕ will contribute to (1.21) and reduces it to $\cos(\psi)$ indicating that the phase smearing is unimportant. For $\lambda \geq 1$, the dephasing is considerable and (1.21) can be written as

$$Re\left[\frac{e^{i\psi}\int D(\phi/\lambda)e^{i\phi}\mathrm{d}\phi}{\int D(\phi/\lambda)\mathrm{d}\phi}\right] = Re\left[e^{i\psi}G(\lambda)/G(0)\right] \tag{1.22}$$

where $G(\lambda)$ is the Fourier transform of $D(z)$

$$G(\lambda) = \int_{-\infty}^{\infty} e^{i\lambda z}D(z)\mathrm{d}z \tag{1.23}$$

and $z = \phi/\lambda$. From (1.22) it is clear that – in general – the effect of the phase smearing is not only to reduce the amplitude of $\tilde{\Omega}$ by $|G(\lambda)|/G(0)$ but also to introduce a phase shift. In the case that $D(z)$ is a symmetrical function of z, $G(\lambda)$ is real and the phase shift is zero.

The following sections show the effects of $T > 0$, finite lifetimes and electron spin splitting.

1.4.1 Thermal damping

At finite but low temperatures the Fermi surface becomes slightly diffuse and the depletion of the states associated with the outermost tubes becomes less abrupt, leading to a thermal damping of the oscillations. The Fermi–Dirac function f for $T > 0$ with chemical potential μ can be regarded as resulting from a distribution of zero temperature Fermi–Dirac functions, with their chemical potentials ζ distributed around μ. Since the dHvA frequency F is a function of μ, a distribution of ζ is

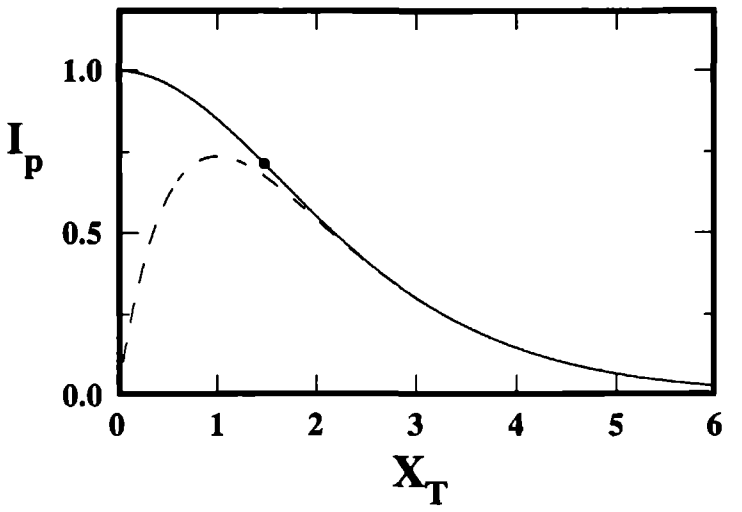

Figure 1.2 The thermal damping factor I_p as a function of X_T The dashed curve represents the approximation $2X_T e^{-X_T}$ for large X_T The dot corresponds to $m^* = m_e$, $T = 1$ K and $B = 15$ T

equivalent to a smearing of the phase ψ The distribution function D is proportional to

$$-\frac{\mathrm{d}f(\zeta)}{\mathrm{d}\zeta} = \frac{1}{2k_\mathrm{B}T\,(1+\cosh(\zeta-\mu)/k_\mathrm{B}T)} \tag{1 24}$$

The change ϕ of the phase that corresponds to a change $(\zeta - \mu)$ of the Fermi energy is given by

$$\phi = \frac{2\pi p}{B}(\zeta-\mu)\frac{\mathrm{d}F}{\mathrm{d}\mu} = \frac{2\pi p}{B}(\zeta-\mu)\frac{m^*}{e\hbar} \tag{1 25}$$

Then the distribution function can be written as $1/[1+\cosh(\phi/\lambda)]$ with the parameter $\lambda = 2\pi p m^*/Be\hbar$ so the effect of a finite temperature on the amplitude of each harmonic p of $\tilde{\Omega}$ is an extra factor

$$I_p = \frac{X_T}{\sinh X_T} \tag{1 26}$$

where

$$X_T = 2\pi^2 p \frac{m^* k_\mathrm{B} T}{e\hbar B} \tag{1 27}$$

In figure 1 2 the thermal damping factor is shown as a function of X_T To obtain some quantitative feeling for I_p, the point which corresponds to $m^* = m_e$ (free electron mass), $T = 1\,0$ K and $B = 15$ T is marked by a dot

1.4.2 Finite lifetimes

In real metals the scattering of electrons causes a finite lifetime of the states and the otherwise sharp quantum levels ϵ_n become broadened according to the uncertainty principle. As was first shown by Dingle this results in a reduction of the oscillation amplitude. Assuming that the level broadening has a Lorentzian line shape and that the scattering time τ can be considered to be independent of ϵ, $\mathbf{k}$ and $\mathbf{B}$ the effect of this broadening is equivalent to a spread of the chemical potential around the actual value μ. The probability that the Fermi energy lies between μ and $\mu + \mathrm{d}\mu$ is given by

$$\frac{\mathrm{d}\zeta}{(\zeta - \mu)^2 + (\hbar/2\tau)^2} \tag{1.28}$$

This can be expressed in terms of phase smearing with a distribution

$$D(\phi/\lambda) = \frac{1}{1 + (\phi/\lambda)^2} \tag{1.29}$$

with $\lambda = \pi p \hbar k_\circ / B e l_\circ$, where $1/l_\circ$ is the reciprocal mean free path of the quasiparticle, averaged around the extremal orbit and $k_\circ$ is the average Fermi wave vector defined by $\mathcal{A} = \pi k_\circ^2$. It is assumed that $1/\tau = \hbar k_\circ / m^* l_\circ$. This leads to the Dingle reduction factor for every harmonic p

$$K_p = \exp\left(-\frac{p\pi\hbar k_\circ}{eBl_\circ}\right) = \exp\left(-\frac{p\pi}{\omega_c \tau}\right) \tag{1.30}$$

The mean free path $l_\circ$, as defined above, reflects the effect of all scattering processes. Therefore it is normally much smaller than the value of the mean free path derived from electrical resistivity. A proper discussion of the influence of electron scattering on the dHvA amplitude should involve a detailed consideration of the actual electron scattering mechanism and the effect of an applied magnetic field.

1.4.3 Effect of electron spin

The electron spin moment will interact with the magnetic field to produce a symmetrical Zeeman splitting of each Landau level for any slice by the amount of $ge\hbar B/2m^*$. The electronic g-factor may differ from its free electron value $g_0 = 2.0023$ because of the effect of spin-orbit coupling on the spin moment.

Thus for any slice through the Fermi surface there are two sets of levels giving rise to a phase difference

$$\Delta\phi = \frac{2\pi p}{B} \Delta E \frac{\mathrm{d}F}{\mathrm{d}\mu} = \frac{2\pi p}{B} \Delta E \frac{m^*}{e\hbar} \tag{1.31}$$

between the oscillations coming from the spin-up and the spin-down electrons. The distribution function can be written as

$$D(\phi/\lambda) = \delta\left[(\phi/\lambda) - \frac{1}{2}\right] + \delta\left[(\phi/\lambda) + \frac{1}{2}\right] \tag{1.32}$$

and, after a Fourier transformation, this leads to a reduction factor

$$\cos\left[\frac{p\pi q}{2}\left(\frac{m^*}{m_e}\right)\right] \tag{1 33}$$

1.5 The Lifshitz – Kosevich formula

A rigorous quantitative description of the dHvA effect was first given by Lifshitz and Kosevich (LK) [4] After correcting the expression for $\tilde{\Omega}$ by including the amplitude reducing factors I_p and K_p, the oscillatory part of the magnetisation for one spin component is finally

$$\widetilde{\mathbf{M}} = -\left(\frac{\partial\tilde{\Omega}}{\partial\mathbf{B}}\right)_\mu = \sum_{p=1}^{\infty}\frac{1}{p^{3/2}}\mathbf{M}_p \sin\left[2\pi p\left(\frac{F}{B}-\gamma\right)\mp\frac{\pi}{4}\right] \tag{1 34}$$

where

$$\mathbf{M}_p = D(\mathbf{B})\left[\mathbf{B}-\frac{1}{F}\frac{\partial F}{\partial\Theta}\boldsymbol{\Theta}-\frac{1}{F\sin\Theta}\frac{\partial F}{\partial\Phi}\hat{\boldsymbol{\Phi}}\right]\frac{X_T}{\sinh X_T}\mathrm{e}^{-X_D} \tag{1 35}$$

$$X_T = \alpha p\left(\frac{m^*}{m_e}\right)\frac{T}{B} \tag{1 36}$$

$$X_D = \frac{p\pi\hbar k_\circ}{eBl_\circ} = \frac{p\pi}{\omega_c\tau} \tag{1 37}$$

$$\alpha = \frac{2\pi^2 k_B m_e}{e\hbar} \approx 14\,69\ \mathrm{TK}^{-1} \tag{1 38}$$

$$D(\mathbf{B}) = -\frac{e^2}{4\pi^3}\left(\frac{2\pi e}{\hbar}\right)^{1/2}\left|\frac{\partial^2\mathcal{A}}{\partial k_\parallel^2}\right|^{-1/2}\frac{F\sqrt{B}}{m^*} \tag{1 39}$$

and where $(\hat{\mathbf{B}}, \hat{\boldsymbol{\Theta}}, \hat{\boldsymbol{\Phi}})$ is the set of orthogonal unit vectors when the field is expressed in spherical polar coordinates The negative (positive) sign in the argument of the sine term in (1 34) corresponds to a maximum (minimum) extremal cross-sectional area

The effective mass m^* can be enhanced due to many-body interactions of the electrons with each other, with phonons or magnons, etc , meaning that the independent quasi-particle picture, on which the LK formula is based, is no longer valid However, it turns out that the effect on the dHvA behaviour is normally restricted to a substitution of the mass in the thermal damping term by $m^* = (1+\lambda)m_B$, where m_B is the mass before many-body interactions are taken into account and λ represents the degree of mass enhancement Its value is in the order of one in most cases of electron-phonon interactions The electron-electron value is typically 10^{-2} Recently there has been a considerable interest in the class of the so-called *heavy fermion* compounds When dHvA measurements on these materials are interpreted in terms of the standard LK theory, the effective quasi-particle masses are measured to have stunningly high values The largest observed to date is 170 m_e

in UPt_3 (see section 5 7) Chapter 5 is dedicated to this member of the heavy fermion family, where the many-body interactions and their influence on quantum oscillatory behaviour will be considered in more detail

The LK formula is of course only describing the effect of a single extremal area of the Fermi surface In general a Fermi surface can have more than one extremal area normal to the applied field direction and each extremal orbit will contribute to the total magnetisation with an expression like (1 34)

As pointed out in (1 20) the measured frequency F is directly related to an extremal area of the Fermi surface, thus making it possible to extract information about the shape of the Fermi surface from measurements of F as a function of the crystallographic orientation

From the temperature dependence $X_T/\sinh X_T$ of the amplitude of $\mathbf{M}_p$ at constant field, m^* can be determined Note that m^* is orientation dependent so it enables one (in principle) to assign a value to the effective mass to a certain part of the Fermi surface For relatively simple topologies of the Fermi surface it is possible to determine the average velocity around the extremal orbit

$$\left\langle \frac{1}{v_F} \right\rangle = \frac{m^*}{\hbar} \left(\frac{\pi}{A_{extr}} \right)^{1/2} \tag{1 40}$$

Once m^* has been determined one can derive from the field dependence of $\mathbf{M}_p$ the reciprocal quasiparticle mean free path, averaged around the relevant orbit on the Fermi surface

$$\frac{1}{l_o} = \left\langle \frac{1}{l_{\mathbf{k}}} \right\rangle_{\mathbf{k}_F} \tag{1 41}$$

The oscillations associated with spin-up and spin-down electrons need not have equal amplitudes and furthermore the spin splitting of the energy levels is not necessarily proportional to $\mathbf{B}$, as has been assumed in section 1 4 3 The effect of spin can then no longer be described by the simple constant cosine factor (1 33) in the harmonic amplitudes If the spin degeneracy at $\mathbf{B} = \mathbf{0}$ in the electronic structure has been removed by a ferromagnetic splitting of the bands, as in Fe or Ni, the shape of the Fermi surface for each spin orientation may be quite different and their dHvA effect is better described by two separate oscillations, each having its own frequency, amplitude and phase

The oscillatory behaviour of $\mathbf{M}$ is not the only manifestation of the variation of Ω with magnetic field Related effects can also be observed in other thermodynamic quantities which can be directly derived from $\tilde{\Omega}$ Examples are variations in sample temperature (in adiabatic conditions), specific heat, sample dimensions (magnetostriction), elastic properties (ultrasound velocity) and the chemical potential μ Also indirect effects like oscillations in transport properties (e g magnetoresistance) are observable although the interpretation requires knowledge of the relaxation processes in magnetic fields (see the Adams Holstein theory [8] of the Shubnikov–de Haas oscillations in the magnetoresistance)

Before continuing with an outline of a widely used experimental method to

observe the dHvA effect I will give a brief description of two phenomena that can complicate the observation and interpretation of the dHvA effect

1.6 Magnetic breakdown

In 1963 Priestley [9] observed a giant orbit frequency in the dHvA frequency spectrum of Mg The frequency corresponded to an orbit area that is larger than the hexagonal cross-section of the Brillouin zone This mystery was solved shortly afterwards by Cohen and Falicov [10], who pointed out that when a sufficiently strong field is applied electrons can *tunnel* from an orbit on one part of the Fermi surface to an orbit on another part, if they are separated by a small enough energy barrier ϵ_g A distinction must be made between intra and inter-band transitions Intra band transitions on the Fermi surface can occur only for an infinitely narrow range of $k_{\|}$, while inter-band transitions can take place over a much wider range

The range of phenomena associated with interband transitions is known as "magnetic breakdown" and is the cause of the appearance and disappearance of orbits The criterion for magnetic breakdown is given by

$$\hbar\omega_c \geq \epsilon_g^2/E_F \tag{1 42}$$

where E_f is the Fermi energy [11] In the case that magnetic breakdown is appreciable, the concept of well defined semi-classical trajectories on the Fermi surface has become invalid In the intermediate regime between very low and very high fields, this leads to a complicated dHvA frequency spectrum showing combination and difference frequencies of the frequencies characteristic of the low field regime

Magnetic breakdown can also cause dramatic changes in the magnetoresistance For instance open orbits at low magnetic fields may become closed as magnetic breakdown sets in, or hole orbits may give way to electron orbits and in this way upset the balance in a compensated material The possibility of magnetic breakdown must always be kept in mind when interpreting electronic properties in very strong magnetic fields

1.7 Magnetic interaction

In order to explain an abnormally rich harmonic content in certain samples, Shoenberg proposed [12] that the effective magnetising field should be $\mathbf{B} = \mu_0(\mathbf{H} + \mathbf{M})$ rather than $\mathbf{B} = \mu_0\mathbf{H}$ (this is ignored in the LK formula) Thus the oscillatory magnetisation $\widetilde{\mathbf{M}}$ should be determined self-consistently from the implicit relation

$$\widetilde{\mathbf{M}} = \sum_{p=1}^{\infty} \frac{1}{p^{3/2}} \mathbf{M}_p \sin\left[2\pi p\left(\frac{F}{\mu_0(H+\widetilde{M})} - \gamma\right) \mp \frac{\pi}{4}\right] \tag{1 43}$$

Here $\mathbf{M}$ is chosen to be parallel to $\mathbf{H}$ Since $M \ll H$ the amplitude of $\mathbf{M}_p$ will hardly vary However, the value of the sine terms in equation (1 34) can change

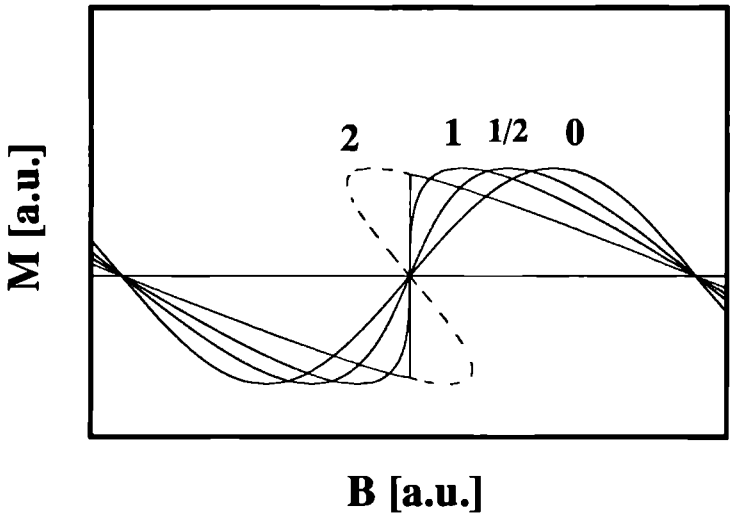

Figure 1.3 The magnetisation as a function of magnetic field for increasingly stronger magnetic interaction, characterised by the quantity a (see text) For $a > 1$ the magnetisation becomes multivalued, leading to a discontinuous jump when this happens

considerably because $F/H \gg 1$

As a consequence of the nonlinear character of the magnetic interaction the standard LK formula will be affected In the case of weak oscillations the magnetic interaction will also be small Still, its effect on the harmonic content can be noticeable Furthermore, as a result of mixing, new frequencies can be generated from two or more fundamental terms associated with different extremal cross-sections through the Fermi surface I refer to work of Devillers [13] who analysed strong interaction spectra in Au, showing up to 10 harmonics of the [111] neck orbit as well as an abundance of satellite peaks caused by frequency mixing

The following simple model illustrates the mechanism Suppose the magnetisation can be thought of as being periodic in B rather than in $1/B$

$$\widetilde{M} = M_0 \sin(B/B_0) \tag{1 44}$$

which is not unreasonable if B_0 hardly changes over one cycle of oscillation Writing $B = \mu_0(H + \tilde{M})$ gives

$$\widetilde{M} = M_0 \sin(\mu_0(\tilde{M} + H)/B_0) \tag{1 45}$$

In the case of a long thin sample the magnetic field H will be the same inside and out and the solution of (1 45) is straightforward In figure 1 3 several possibilities are shown of the behaviour of $\tilde{M}$ as a function of magnetic field The degree of distortion of the sine wave depends on the value $a = \mu_0 M/B_0$ In the case that $\mu_0 M$ becomes comparable with $\Delta B = B^2/F$ of the fundamental oscillations, the

magnetisation can even become multivalued over certain field regions, which means in practice that the magnetisation will jump periodically. This leads to a tremendous increase of the harmonic content of the dHvA signal. The actual criterion that determines whether magnetic interaction effects need to be taken into account is given by $\mu_0(\mathrm{d}M/\mathrm{d}B) < 1$. In the above example crystal anisotropy and sample shape were totally ignored. Both, however, can have a considerable influence on the wave shape of the observed quantum oscillation in the case of magnetic interaction. A comprehensive treatment on this subject as well as magnetic breakdown can be found in Shoenberg's book [5] and references therein. A more compact discussion on magnetic interaction by Pippard can be found in reference [7, p. 124].

References

[1] W.J. de Haas and P.M. van Alphen, Leiden Comm. **208d**, **212a**, (1930) and **220d** (1932).

[2] L.D. Landau, Z. Physik **64**, 629 (1930).

[3] L. Onsager, Phil. Mag. **43**, 1006 (1952).

[4] I.M. Lifshitz and A.M. Kosevich, Zh. Eksperim. i Theor. Fiz. **29**, 730 (1955) [English translation: Soviet Phys. – JETP **2**, 636 (1956)].

[5] D. Shoenberg, *Magnetic oscillations in metals*, Cambridge University Press (1984).

[6] A.V. Gold in *Solid State Physics, vol. 1: Electrons in Metals*, p. 39, edited by J.F. Cochran and R.R. Haering, New York: Gordon and Breach (1968).

[7] *Electrons at the Fermi Surface*, edited by M. Springford, Cambridge University Press (1980).

[8] E.N. Adams and T.D. Holstein, J. Phys. Chem. Solids **10**, 254 (1959).

[9] M.G. Priestley, Proc. Roy. Soc. A **276**, 258 (1963).

[10] M.H. Cohen and L.M. Falicov, Phys. Rev. Lett. **7**, 231 (1961).

[11] E.I. Blount, Phys. Rev. **126**, 1636 (1962).

[12] D. Shoenberg, Phil. Trans. Roy. Soc. (London) **A 255**, 85 (1962).

[13] M.A.C. Devillers, Sol. St. Comm. **52**, 23 (1984).

Chapter 2

Observation of quantum oscillations

2.1 In general

In order to be able to observe quantum oscillations in materials, a number of conditions have to be fulfilled First of all, the oscillations are a *low temperature* phenomenon, requiring at least liquid helium temperatures but often lower Secondly, they are a *high field* phenomenon An electron wave packet must be able to round the extremal orbit at least once before it is scattered ($\omega_c\tau > 1$) This is why the studied materials need to be as pure as possible with as little defects as possible The application of a high magnetic field increases the value for ω_c, thus relaxing the constraint on τ Also, the variation of the magnetic field over the volume of a sample has to be small compared with the oscillation period considered Since the phase of the sine term in the Lifshitz-Kosevich formula (1 34) changes by 2π over a field range $\Delta B = B^2/F$, a sufficiently high and homogeneous magnetic field is needed in order to avoid resolution difficulties

This chapter deals with the techniques necessary for dHvA measurements in high field Bitter magnets The principle of detection is discussed in 2 2 The noisy conditions in these Bitter magnets are dealt with, using an electronic feedback system as described in 2 3 Finally, in 2 4, some digital analysis techniques as well as their pitfalls are briefly discussed

2.2 Field modulation technique

The most thoroughly developed method to study the dHvA effect is the inductive field modulation method [1] It is based on superimposing a small periodic field $b_0\cos(\omega t)$ on a background field B In this way the magnetisation is made to vary periodically with time The sample is placed inside one of a balanced pair of pick-up coils The induced electromotive force can be examined by means of a phase sensitive detector (PSD) at the angular frequency ω or at higher harmonics $k\omega$ Assume that $b_0 \ll B$ then the fundamental dHvA term in (1 34) can be written as

$$\begin{aligned} M(t) &= A\sin\left[\frac{2\pi F}{B + b_0\cos\omega t} + \phi\right] \approx A\sin\left[\frac{2\pi F}{B} - \frac{2\pi F b_0\cos(\omega t)}{B^2} + \phi\right] \\ &= A\left\{\sin\left[\frac{2\pi F}{B} + \phi\right]\cos\left(\lambda\cos(\omega t)\right)\right. \\ &\quad \left. - \cos\left[\frac{2\pi F}{B} + \phi\right]\sin\left(\lambda\cos(\omega t)\right)\right\} \qquad (2\,1) \\ \lambda &= \frac{2\pi F b_0}{B^2} \qquad (2\,2) \end{aligned}$$

The functions $\cos(\lambda\cos(\omega t))$ and $\sin(\lambda\cos(\omega t))$ can be expressed as the sum of time-harmonics $\cos(k\omega t)$ with coefficients proportional to Bessel functions of the first kind $J_k(\lambda)$

$$\cos(\lambda\cos(\omega t)) = J_0(\lambda) + 2\sum_{k=1}^{\infty}(-1)^k J_{2k}(\lambda)\cos(2k\omega t) \qquad (2\,3)$$

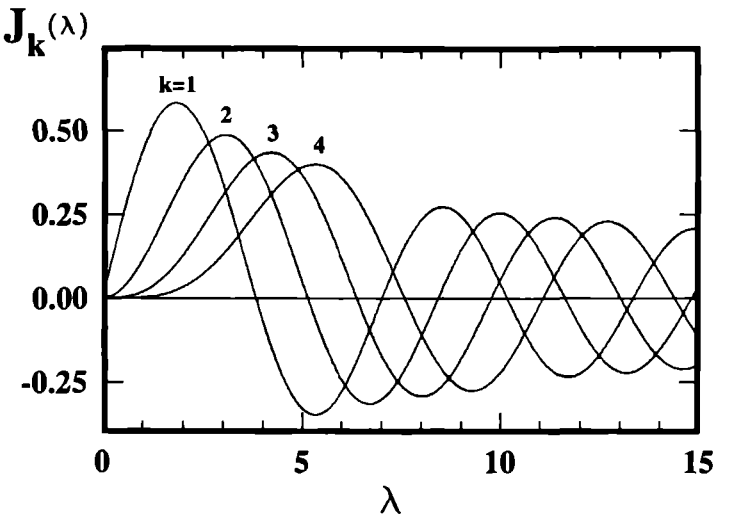

Figure 2.1 Bessel functions $J_k(\lambda)$ of the first kind of order k =1, 2, 3 and 4

$$\sin(\lambda\cos(\omega t)) = 2\sum_{k=1}^{\infty}(-1)^k J_{2k+1}(\lambda)\cos((2k+1)\omega t) \tag{2 4}$$

Now (2 1) can be written as

$$M(t) = A\left\{J_0(\lambda)\sin\left[\frac{2\pi F}{B}+\phi\right] + 2\sum_{k=1}^{\infty}J_k(\lambda)\cos(k\omega t)\sin\left[\frac{2\pi F}{B}+\phi-\frac{k\pi}{2}\right]\right\} \tag{2 5}$$

so the induced e m f in the pick-up coil is

$$V_{pu} = c\frac{\mathrm{d}M}{\mathrm{d}t} = \sum_{k=1}^{\infty} v_k \sin(k\omega t) \tag{2 6}$$

$$v_k = -2cA\omega k J_k(\lambda)\sin\left[\frac{2\pi F}{B}+\phi-\frac{k\pi}{2}\right]$$

where c is a factor representing the coupling of the sample to the detection coil It appears that every time-harmonic v_k of V_{pu} is weighed by a coefficient $J_k(\lambda)$ Figure 2 1 shows the behaviour of $J_k(\lambda)$ for several values of k The amplitude of a time-harmonic can be drastically influenced by the choice of λ, i e , the amplitude of the modulation field compared with frequency F and the background field B Note that the amplitude can even become zero for certain values of λ The Bessel function dependence of v_k can be very helpful in sorting out a complicated dHvA frequency spectrum

In general the magnetisation is a sum of dHvA-harmonics with index p (equation (1 34)) and following the same line of reasoning the coefficients for the time-harmonics become

$$v_k = -2c\omega k \sum_{p=1}^{\infty} A_p J_k(p\lambda) \sin\left[\frac{2p\pi F}{B} + \phi_p - \frac{k\pi}{2}\right] \qquad (2\ 7)$$

2.2.1 Principle of detection

The pick-up coil surrounding the sample measures the time derivative of the total flux through the coil when a uniform magnetic field ($\mathbf{B} + \mathbf{b}_0 \cos(\omega t)$) is applied, with $\mathbf{b}_0 \parallel \mathbf{B}$ It detects not only the small magnetic moment of the sample, also the modulation field $\mathbf{b}_0 \cos(\omega t)$ induces a voltage across the pick-up coil Therefore another coil is added to the circuit which has a much weaker inductive coupling to the sample but picks up the same voltage due to the modulation field Thus the net induced voltage will be entirely due to the magnetic moment of the sample itself The design of the pick-up coils depends very much on the demands of the experiment, for instance sensitivity calibration, the shape of the sample or the necessity of an in situ orientation study I refer to section 2 2 2 for the actual pick up coil configuration used in the Bitter magnets

Due to the presence of the $J_k(r\lambda)$ terms, the observed voltage v_k as a function of $1/B$ will – in general – not resemble the behaviour of $M(1/B)$ Only in the case of very weak modulation the Bessel functions are proportional to p^k The observed waveform for v_k is then proportional to $\mathrm{d}^k M/\mathrm{d}B^k$

For several reasons it proves to be advantageous to monitor the behaviour of the pick-up voltage at a *harmonic* rather than at the fundamental modulation frequency First of all, if the pick-up coils are not quite balanced, the net voltage fed into the PSD contains a considerable $\sin(\omega t)$ component which is *not* associated with the magnetisation of the sample but stems directly from the modulation field itself If this component is too large, it influences the detection resolution By monitoring a harmonic of ω this problem is avoided Another reason for avoiding detection at the fundamental frequency is that, even at low ω, the balance of the pick-up coils is upset by eddy currents induced in the sample Because of magnetoresistance this effect is field dependent, i e , the (un)balance is field dependent, causing a sloping baseline on top of which the oscillations appear Again, detection at 2ω or higher harmonics almost completely eliminates this complication Finally, the current in the modulation coil causes eddy currents to flow in metal parts of the cryostat, which results in a vibration noise component at ω, yet another reason to detect at harmonics

2.2.2 Using Bitter magnets

Although superconductive magnet technology is pushing the limit to 20 T nowadays, it is still the class of hybrid magnets that holds the record (33 5 T) for *static magnetic fields* In these hybrid magnets the total magnetic field is produced by

a superconductive solenoid with a large inner diameter, in combination with a resistive, water cooled magnet placed inside the superconductive coil The resistive magnet consists of two nested Bitter magnets In the Nijmegen High Field Magnet Laboratory (NHFML) two hybrid magnets are in operation The Nijmegen-I is able to generate 25 T in a room temperature bore of Ø 53 mm, while the Nijmegen II (Ø 32 mm) can obtain a maximum magnetic field of 30 4 tesla Two 3 MW power supplies, operated in parallel, serve to energise the magnets Each unit is able to generate a current of 10 kA at 300 V I refer to [2] for an extensive description of the NHFML installation and will only give technical details if it is relevant

There are several drawbacks in the use of resistive or hybrid magnets compared with purely superconductive magnets First of all, during operation the noise level in the dHvA signal is much higher than with superconductive magnets Magnetic field noise is produced by temperature fluctuations in the plates of the Bitter stacks which lead to current path fluctuations However, the main noise source is the three-phase rectifier bridge of the power supply It not only generates 'white" noise but also harmonics of 50 Hz in the electrical current which passes through the magnets Consequently the magnetic noise spectrum is not flat at all, but shows peaks at these frequencies Figure 2 8(**a**) on page 38 shows the typical spectral content of the magnetic field noise The major component is the 300 Hz ripple and has a maximum amplitude of approximately 1×10^{-4} T in a 20 T Bitter magnet Furthermore, mechanical vibrations caused by the water cooling system result in a motion of the sample, pick-up coils and other wiring relative to the magnetic field, thus increasing the noise level considerably

The homogeneity of the Bitter magnets may be another experimental concern, for instance in the case of high dHvA frequencies and large sample dimensions In hybrid magnets the homogeneity is determined by the homogeneity of both the superconductive coil and the resistive coil but also by the relative positions of the maxima of the two magnets The homogeneity of a 20 T Bitter magnet is approximately one part in 10^3 over a sphere 1 cm in diameter For the hybrid magnets this number is worse three parts in 10^3

In order to limit the influence of these effects several precautions have to be taken During a dHvA experiment it is of the utmost importance to minimise the amount of induced e m f not associated with the quantum oscillations Therefore wires running from the top of the cryostat down to the field maximum have to be firmly mechanically anchored Pairs of wires must be carefully twisted and, in case they are soldered or otherwise connected to another twisted pair, one must prevent introduction of a small pick-up loop at this point

Another important effect, especially for high ω and high modulation amplitude, is the unwanted heating of the (metallic) sample itself due to induced eddy currents [3] since the amplitude of the dHvA oscillations are drastically reduced if the sample temperature is too high (equation (1 26)) For a cylindrical sample with

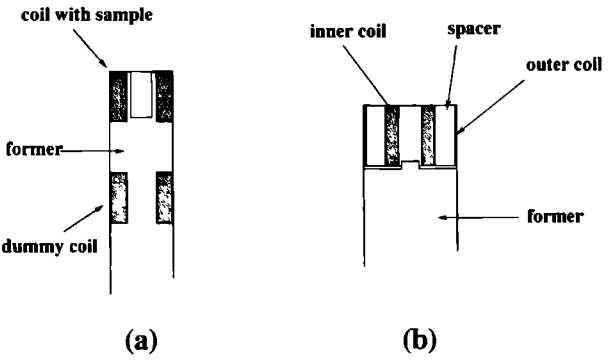

Figure 2.2 Arrangement of compensated pick-up coils (**a**) coaxially above each other and (**b**) with the dummy coil wound on top of the sample coil and spacer.

radius a, length l and resistivity ρ the skin depth is given by

$$\delta = \left(\frac{2\rho}{\mu_0\omega}\right)^{-1/2} \tag{2.8}$$

If $(a/\delta)^2 \ll 1$ there is still full penetration of the magnetic field and the generated power in the sample will be approximately

$$P = \frac{\pi l a^4}{8\ \rho}\left(\frac{\mathrm{d}B}{\mathrm{d}t}\right)^2 \tag{2.9}$$

If for example $a = 0.5$ mm, $l = 1$ mm and $\rho = 10^{-10}$ Ωm while the modulation frequency $\omega/2\pi = 20$ Hz and the modulation amplitude is 100 Gauss, the induced heating is in the order of 1 μW. The temperature of the sample will be determined by the thermal boundary resistance R of the heat flow $\dot{Q}$ across the interface from metal to liquid ^{4}He. For a given interface with total area A and a heat flux $\dot{Q}/A$, the temperature drop across the boundary is

$$\Delta T = \frac{\dot{Q}}{A} R \tag{2.10}$$

where $R = KT^{-3}$, with $K \approx 10^{-2}$ K^{4}m^2/W for metals and $T < 0.1$ K. If the liquid helium temperature T is around 100 mK the resulting sample temperature will be in the order of 1 K!! It is therefore extremely important to thermally connect the sample to a silver sinter which has a large surface area of contact with the helium.

The design of the pick-up coils used in a dHvA measurement is governed by

the noisy conditions of the Bitter magnets. In view of the (time dependent) field inhomogeneity it proves to be beneficial to wind the two pick-up coils on top of each other instead of coaxially above each other (figures 2.2(**b**) and (**a**), respectively). For the same reason the whole pick-up coil system must preferably be as small as possible. The inner coil is wound with Ø 20 μm copper wire and has an inner diameter of 1.0 mm and its length is 1.9 mm. Each layer has approximately 100 turns and the total number of layers is 14. It has an estimated effective cross-sectional area of 20 cm^2. The outer coil has an inner diameter of approximately 4.0 mm and is wound on top of a cylindrical spacer that separates the two coils and reduces the flux coupling of the second coil with the sample. It has approximately 170 windings and the effective cross-sectional area is carefully made equal to that of the inner coil (better than 0.5% at 77 K). During winding, each time a layer was completed, a small amount of GE varnish (diluted in ethanol) was allowed to soak the coil. After the balancing of the coils, the set was impregnated with STYCAST-1266 epoxy resin [4], which was heated to 50 °C to make it more fluid.

2.2.3 Experimental set up

Since the dHvA set up has gone through several stages of improvement I will describe only its final form, i.e., a 25 mK, fixed orientation set up for a 20 T Bitter magnet (figure 2.3). The dilution refrigerator needed for those temperatures will be discussed separately in chapter 3.

The modulation field is generated by a single layer of nominal Ø 0.71 mm copper wire, which is wound directly on the stainless steel core tube of the Bitter magnet. The heat generated in this coil is removed by the same water flow that cools the Bitter stacks. The maximum modulation field is 0.18 T (peak-peak) and is generated by a BRÜEL & KJÆR 2708 (1200 VA) power supply. In order to prevent movement of the windings due to Lorentz forces acting on them (900 Nm^{-1}, which gives a hoop stress of 16 N for each winding), the copper wire is pre-stressed during winding with a force of 30 N. Afterwards the coil was impregnated with STYCAST 2850-GT epoxy [4]. The homogeneity of the modulation coil is one part in 10^3 over a Ø 1 cm sphere.

The current through the Bitter magnet is controlled by means of a manually operated 18-bit DA converter unit, which provides a reference voltage for the 6-MW power supply and can be programmed for linear field sweeps. It is equipped with a speed limiter, such that the maximum sweep time from 0 to 20 tesla is 40 seconds. The magnetic induction is usually measured indirectly by monitoring the electrical current through the Bitter magnet via shunt resistors.

The net signal from the set of pick-up coils is first amplified by a low noise preamplifier. Due to the presence of a sample the balance for the $\sin(\omega t)$ component is affected. In general the signal can be thought of as being the sum of two pick-up voltages having a slightly different amplitude and a slightly different phase. If this net signal turns out to be too strong so as to upset the amplifiers or the PSD it is necessary to suppress this ω component and thus making 2ω detection

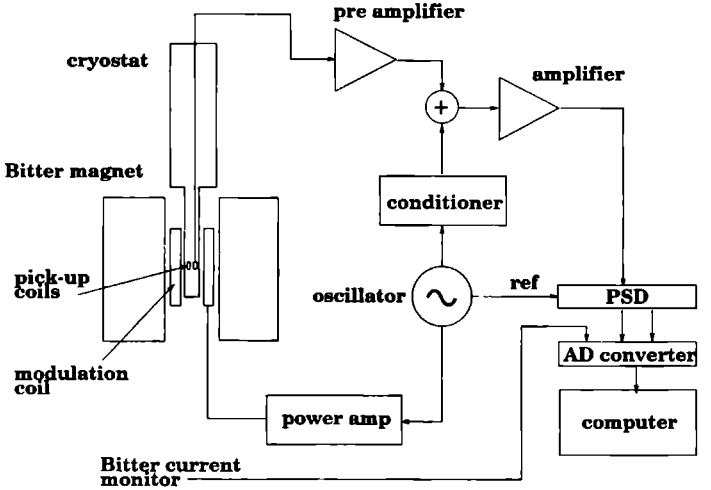

Figure 2.3 Schematic diagram of the dHvA experimental setup for a 20 T Bitter magnet system

more accurate Suppression is accomplished by adding to the net pick-up voltage another voltage which is derived from the oscillator that drives the modulation coil at frequency ω This voltage can be varied in amplitude and shifted in phase before it is added to the preamplified pick-up voltage After the ω suppression the signal is further filtered and amplified to (preferably above) the 10 mV level before feeding it into a lock-in amplifier

It is possible to make a quantitative estimate of the coupling constant c in (2 7) (see also equation (1 34)) for the pick-up coil and a sample of typical dimensions When using second harmonic (2ω) detection, the amplitude of the first (p=1) dHvA-harmonic in terms of the pick-up voltage is given by

$$v_{2\omega} = 2\,6093\omega cuGJ_2(\lambda)\frac{TF}{B^{1/2}|A''|^{1/2}}\frac{\exp(-X_D)}{\sinh(X_T)}\cos(\pi gm^*/2m_e) \qquad (2\,11)$$

where u is the sample volume and G is the electronics gain For calibration purposes we used a [111] neck orbit in a $Au_{1-x}Ag_x$ sample [5] with $x = 2\,5 \times 10^{-3}$ and dimensions 0 6×0 6×1 9 mm The Dingle temperature can be determined by plotting $\ln(v_{2\omega}\sinh(X_T)B^{1/2}/J_2(\lambda))$ versus $1/B$ The curve will be linear with a slope $\alpha p(m^*/m_e)T_D$ The Dingle temperature for the Au-Ag sample was measured to be 1 2 K The values of m^* and $|A''|$ were taken from the literature [6] The detected voltage of 1 0 μV at the pick-up coils and ω = 195, with modulation amplitude of 85 Gauss, a background field of 10 5 T and a temperature of 600 mK, yields $c \sim 0\,16$ TA^{-1} This value is as expected since the coupling constant of a 500 turn coil is typically 0 1 TA^{-1} [7]

The standard dHvA procedure is to measure both the in phase and quadra-

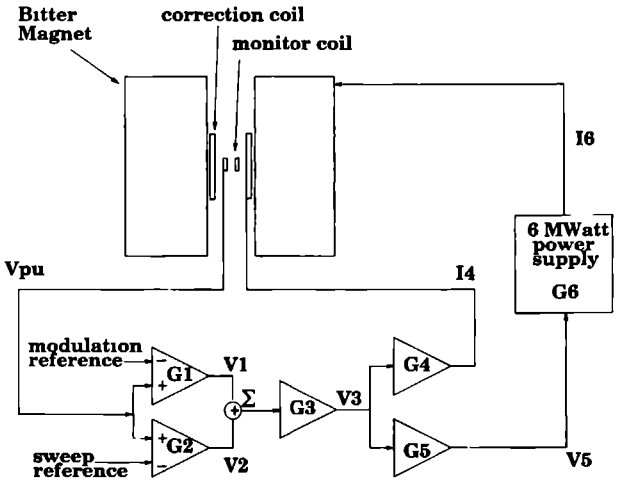

Figure 2.4 Schematic diagram of the feedback circuit

ture signal of the lock-in as a function of magnetic field This is done by digitising the analog data either by a built-in 13-bit AD converter of the lock in or by a 16-bit scanning ADC if higher resolution is needed Normally the field is swept linearly in time although it is possible to program other field-versus-time relations The actual data taking is controlled by a self written application program, using commercially available scientific software tools It allows easy data acquisition, analysis and presentation of data The menu-driven program not only takes care of the actual measurements, also extensive analysis of the acquired data is possible (some of which will be discussed in section 2 4)

2.3 Field stabilisation

As already discussed in section 2 2 2 the magnetic field generated in Bitter magnets is rather noisy This problem can be greatly reduced by placing a superconducting screen around the sample The superconductive material that is used for this purpose must have a sufficiently high critical current density at high fields in order to be useful This possibility is described by Tarnawski *et al* [8] who use a cylinder of ceramic $YBa_2Cu_3O_{7-\delta}$

However when it is necessary to modulate the magnetic field, another approach is needed Instead of a passive shielding of the field-fluctuations, it is possible to suppress them by means of an active negative-feedback system Figure 2 4 shows a simplified block diagram of the broad band feedback loop developed for Bitter magnet configurations The frequency response function of each component is given by $G1(\omega)$, , $G6(\omega)$, where the noise in the field, which is present in a tiny volume

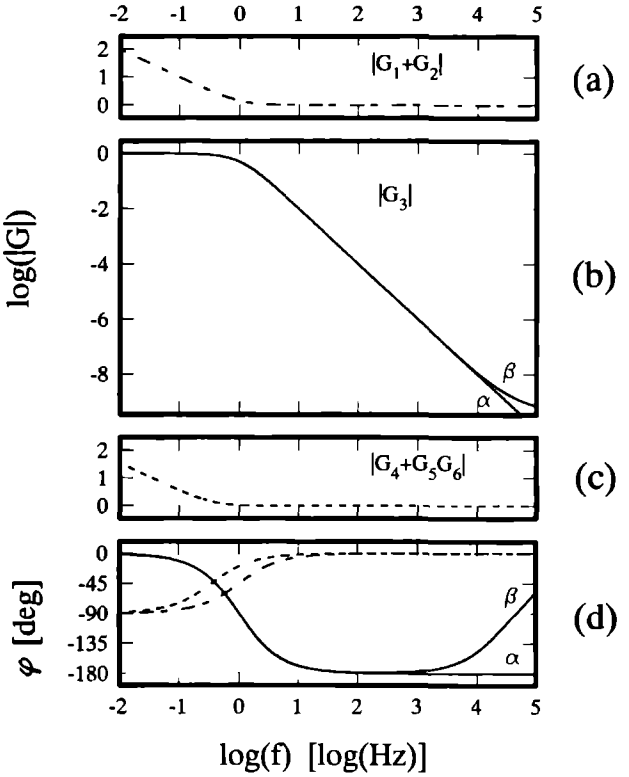

Figure 2.5 Frequency response functions of (**a**) the input stage, (**b**) the middle stage and (**c**) the output stage of the feedback amplifier, in (**d**) the phase lags are shown

around the sample, is monitored by a 2300 turn pick-up coil (Ø 7 0 mm, height 10 mm) It has an effective cross-sectional area of 0 088 m^2

Roughly spoken, the pick-up voltage V_{pu} is integrated *twice* before it is fed back as a magnetic field In order to combine a low integrator drift with a large bandwidth, the input stage as well as the output stage of the feedback amplifier circuit are split into two parallel branches At the input stage the pick-up voltage is fed both into a 100× preamplifier G1 with a 120 kHz bandwidth and into an integrating circuit G2 which is thermally stabilised The gain of the integrator is 100 at 1 Hz

The outputs of both circuits, V_1 and V_2, are summed in point Σ and further amplified by two first-order (active) low-pass filters, both with cut-off frequencies at 1 Hz The output stage transforms the resulting voltage V_3 into a magnetic field again

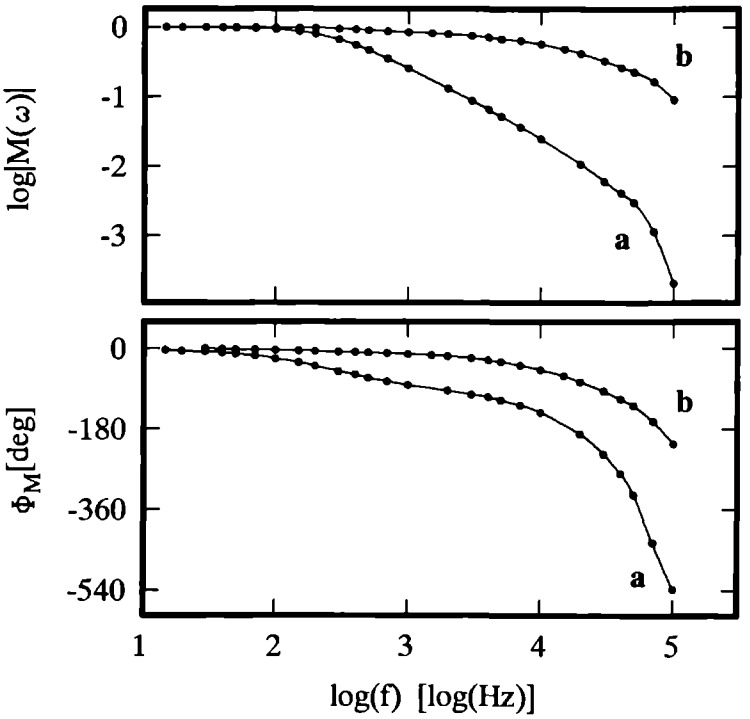

Figure 2.6 The modulus and argument of the mutual inductance between the primary correction coil and the secondary pick up coil Curves (**a**) are measured when the cryostat is filled with liquid ^{4}He and the copper radiation shield is cooled with liquid N_2, curves (**b**) are measured under the same circumstances but after a slot has been milled in the radiation shield

For the high frequencies a 100 kHz flat-band power amplifier G4 is used which generates a correcting magnetic field in a 10^{-2} T coil For low frequency field variations, including sweeping of the field, the other branch takes over The output voltage V5 of integrator G5 serves as the reference voltage for the 6-MW power supply of the Bitter magnet Again the magnetic fields of the Bitter and the correction coil are summed at the sample position The voltage-to-field gain of the high frequency branch is made equal to that of the low frequency branch at 0 35 Hz The magnitude of the frequency response functions of the input, middle and output stage are shown in figure 2 5(**a**), 2 5(**b**)[α] and 2 5(**c**) respectively In figure 2 5(**d**) the phase lags, introduced by the corresponding response functions, are shown in a single graph

In order to obtain an open loop gain of a few hundred at 100 Hz, the frequency response characteristics of all components of the feedback amplifier circuit need to

be under control up to a few times 10 kHz Since the whole point of this negative feedback is to provide a stabilisation of the magnetic field, it is of great importance to make sure that no oscillations arise due to unforeseen phase shifts in the open loop frequency response function $G_{OL}(\omega)$ This implies that the mutual induction $M(\omega)$, defined by

$$V_{pu} = j\omega M(\omega) I_{prim} \quad (2\ 12)$$

$$M(\omega) = |M(\omega)|\, e^{j\Phi(\omega)} \quad (2\ 13)$$

between the (primary) correction coil and the (secondary) pick-up coil has to be known as a function of frequency Here I_{prim} is the current through the primary coil and V_{pu} is the pick-up voltage Note that $M(\omega)$ is a complex quantity and introduces a phase shift Φ There are several circumstances that have quite a dramatic effect on the behaviour of $M(\omega)$

First of all the metal tubes of the cryostat, surrounding the sample, cause a decrease of $|M(\omega)|$ as well as a phase lag between the primary and secondary circuit Especially a copper radiation shield which is cooled with liquid nitrogen has a dominating effect It makes the mutual induction even temperature dependent because the resistivity of the copper changes considerably with temperature Another complication can be the internal capacitance of both the correction coil and the pick-up coil, influencing their high frequency behaviour The latter effect is assumed to be incorporated in $M(\omega)$ Curve (**a**) of figure 2 6 shows the measured mutual inductance between the two coils when the cryostat is filled with liquid ^{4}He, and the copper shield is cooled with liquid nitrogen The influence of the copper screen could be considerably reduced (curve (**b**)) by milling a narrow slot in it, parallel to the field direction over a length of 15 cm Moreover, because of the slot, $M(\omega)$ turned out to be virtually independent of temperature, which facilitated further tests on the feedback loop

Stability of the loop is achieved when the open loop gain is *smaller than unity* at the frequency where the total phase lag around the loop is 180° In order to neutralise the phase shift introduced by $M(\omega)$ even more, some additional corrections were made in amplifier G3 (curve β in figure 2 5(**b**)) In figure 2 7 is shown what the effect of this correction is on the total response function $G_{OL}(\omega)$ Curve (**a**) shows the maximum possible open loop gain when $G3(\omega)$ is not corrected while curve (**b**) represents the case that $G3(\omega)$ is of the form β, shown in figure 2 5(**b**) In the latter case the open loop gain $|G_{OL}|$ can be increased to a few hundred at 100 Hz

The performance of the feedback loop can be directly judged from figure 2 8 It shows two spectra of the magnetic field noise The upper curve is taken when the feedback loop is not used The lower one is collected under exactly the same circumstances, but in this case the feedback loop is in operation It is clear from this figure that not only all harmonics of 50 Hz are suppressed but also the "white' background noise is reduced appreciably

It is possible to sweep the magnetic field by simply applying a constant DC sweep reference voltage at the negative input of amplifier G2 (figure 2 4) For this

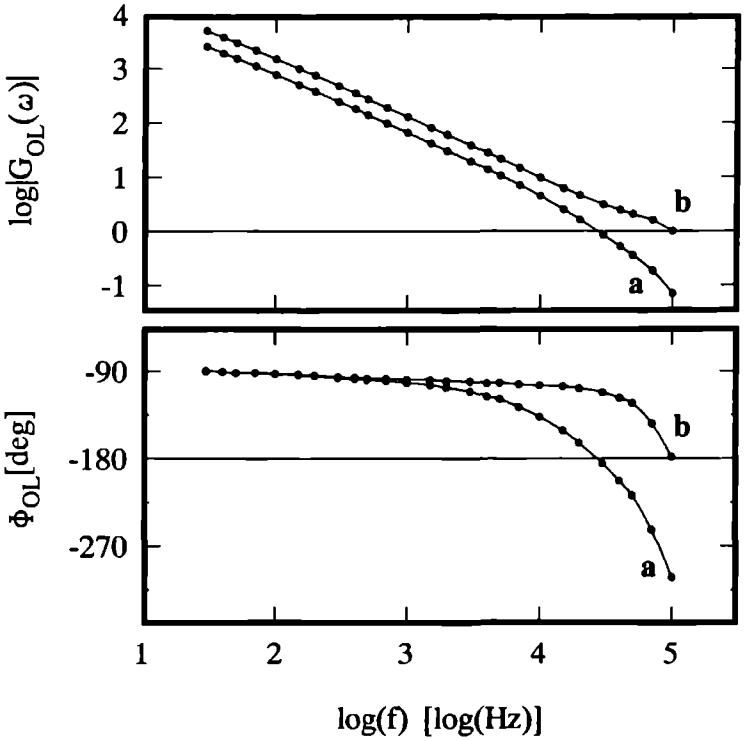

Figure 2.7 Open loop response function for different frequency dependence of G3(ω) (**a**) in the case of a frequency dependence α and (**b**) when G3 is corrected (β)

purpose a DIGISTANT DC-voltage standard was used The minimum drift in 10 minutes of the magnetic field is measured to be 10^{-3} tesla Field modulation (above 1 Hz) is obtained by feeding an appropriate signal to the negative input of G1 Note that these reference voltages represent the time derivative of the desired magnetic field, which is proportional to V_{pu} The difference between the desired value for V_{pu} and its actual value is given by

$$Err(\omega) = \frac{1}{1 + G_{OL}(\omega)} V_{ref}(\omega) \qquad (2\ 14)$$

which becomes very small for $|G_{OL}(\omega)| \gg 1$

Although the advantages of a feedback mechanism are obvious, it is necessary to consider possible pitfalls Since the field stabilisation relies on the performance of the monitor pick-up coil and the input stage of the feedback amplifier, it is very important to avoid induced voltages at any other point than the sample region This demands more-than-average precautions The pair of wires from the monitor

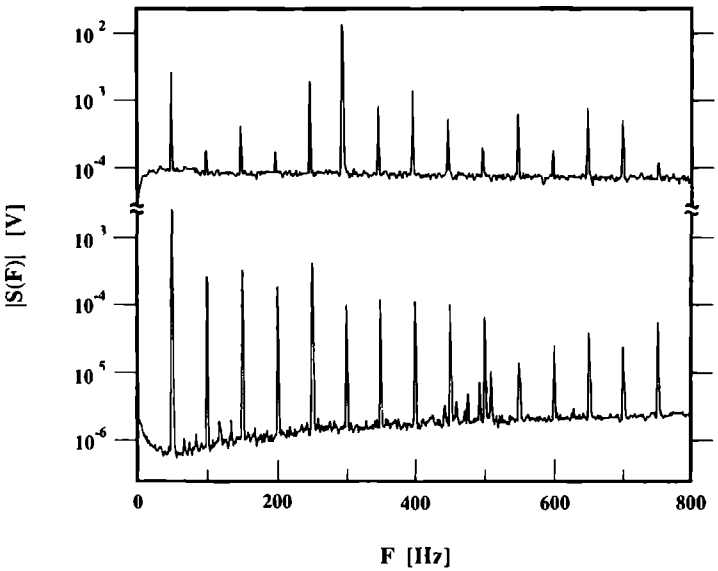

Figure 2.8 Noise spectrum $|S(F)|$ of the magnetic field (**a**) in case the feed back mechanism is not active and (**b**) when the feedback loop is closed

coil must be carefully twisted and glued down to some rigid part of the cryostat The wires should preferably be non-interrupted from pick-up coil to the top of the cryostat so as to avoid thermally induced voltage differences at soldered connections which can result in magnetic field drift Also the monitor coil should be rigidly connected to the sample because only then will movement of the sample in the field not result in field noise but it will be corrected for by the feedback loop

2.4 Analysis of measurements

Digitisation of all relevant quantities has the great advantage that a wide range of digital analysis techniques can be applied to extract useful information In case of dHvA(-like) experiments it is often desirable to make some estimate of the spectrum of the quantum oscillations The reliability of such an estimate depends on several conditions

In the case of a periodic signal in $1/B$ with dHvA-frequency f_0 and which is observed for an infinitely long interval in $1/B$, the spectrum $S(f)$ will be a delta function $\delta(f - f_0)$ In reality the finiteness of the interval in $1/B$ results in a broadening of this peak The intrinsic resolution Δf depends on the length L of the interval and is given by $\Delta f \ L \geq 1/2$ The sampled data array can be written as the product of an infinitely long array and a rectangular pulse function which specifies

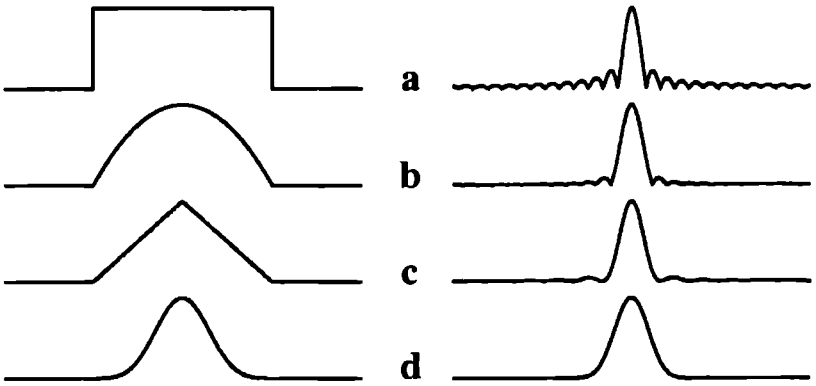

Figure 2.9 Several types of window used to calculate an estimate of a frequency spectrum On the left are the windows in the time domain On the right their Fourier transforms are shown for (**a**) Rectangular pulse, (**b**) X(1-X) window, (**c**) Triangular window, (**d**) 3-term Blackmann window

the interval over which the data are known The Fourier transform of the product of two functions is equal to the convolution of their individual Fourier transforms This means that the delta function must be convoluted with the Fourier transform of the pulse function, which is the sinc function $\sin(2\pi fL)/(2\pi fL)$ The value for the full width half maximum (FWHM) of this function is $0\,6/L$ Furthermore there exist numerous additional peaks, called side lobes or feet These side lobes cause a leakage of the spectral intensity, i e , the intensity is not strictly localised at f_0 but contributes also to these side lobes The largest side lobe amplitude of the sinc function is 22% of the main peak amplitude In order to suppress this leakage it is necessary to truncate the sampled data array less abruptly as in the case of the rectangular cutoff function A few examples of alternative choices for a cutoff or window function are shown in figure 2 9 Their Fourier transforms show fewer side lobes than the sinc function, but at the cost of intrinsic resolution since the main peaks are broadened Apart from a smaller resolution, the use of a window also means throwing away information Therefore the choice of a particular window function depends mainly on what one is aiming at when analysing a spectrum An extensive overview of possible windows is given by Harris [9]

If the data show strong low frequency components (for instance a changing background) this can result in wiggles in the spectrum which can completely dominate higher frequency signatures Weighing the data with a window that is exactly zero at both ends can partially solve this problem but it is better to subtract a fitted background before Fourier transforming A quadratic background fit is sufficient in most cases

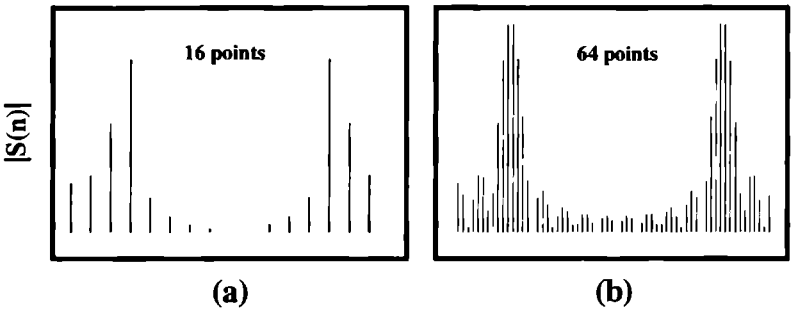

Figure 2.10 (**a**) 16-points Fourier transform and (**b**) 64-points transform on the same 16-points wave form but 3 x 16 zero's are added before Fourier transforming The example waveform $A(n) = \sin(\frac{1}{3}(2\pi n/N))$ As a result of the zero padding the spectrum is calculated in more points The intrinsic spectral resolution, however, remains unaltered

The actual calculation of the spectrum $S(f)$ of a digitised signal is usually done by means of the discrete Fourier transform (DFT)

$$S(k\ \ \mathrm{d}f) = \sum_{n=0}^{N-1} A(n\ \ \Delta L)e^{i(2\pi kn/N)}\ ,\quad k = 0, 1,\quad , N-1 \qquad (2\ 15)$$

where $A(n)$ is the digitised waveform, consisting of N equidistant points The spacing $\mathrm{d}f$ in the spectrum is related to the sampling interval ΔL of the the waveform by $\mathrm{d}f = 1/(N\ \ \Delta L)$ In practice the DFT algorithm is rarely used because it is highly redundant Instead a number of so-called fast Fourier transforms (FFT's) are in use, which result in a reduced computer calculation time A small price to be paid for this is that the number of points N has to be a power of two This is easily arranged by adding zero's to the end of the (windowed) array $A(n)$ until this condition is fulfilled Moreover, the zero filling has the effect of reducing the spacing $\mathrm{d}f$ with which the spectrum is scanned As a rule of thumb one should always at least double the length of the original waveform $A(n)$ by zero filling In figure 2 10 the effect of padding zero's is illustrated

Another possible source of error due to the use of DFT or FFT is known as aliasing From equation (2 15) follows that $|S(N-k)| = |S(k)|$ which means that the DFT of an N-point waveform yields only $N/2$ meaningful output points $k = (0,\ \ (N/2)-1)$ since the other $N/2$ points $k = (N/2,\ \ ,N-1)$ form a mirror image of the first set The mirror frequency is given by the Nyquist frequency $f_N = 1/(2\Delta L)$ In order to avoid the situation that the spectrum overlaps with its mirror image one must take care that the frequency content of the waveform *before* it is digitised has no contribution for frequencies above $1/(2\Delta L)$ or half the sample frequency This is done by installing a low pass filter in front of the AD converter In case the output of a PSD is being sampled, one can make use of its low pass filters As a rule of thumb the sample interval has to be at least three times as small

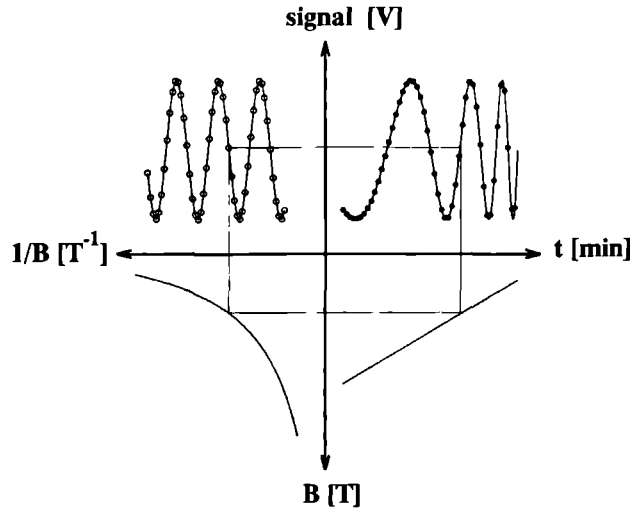

Figure 2.11 Procedure of transposing data that are equidistant in time, to data equidistant in $1/B$.

as the value of the PSD time constant.

To conclude the list of contemplations on the pitfalls one must avoid while calculating dHvA spectra, I mention the errors introduced when calculating an array of equidistant points in $1/B$. In practice the dHvA signal from the PSD is digitised at fixed *time* intervals with sample frequency f_s, not at fixed $1/B$ intervals. The transpositioning of data equidistant in time to points equidistant in $1/B$ is illustrated schematically in figure 2.11. It is assumed that the magnetic field is swept linearly in time between B_{min} and B_{max}. The value of $\Delta L = \Delta(1/B)$ is determined to be $\Delta B/B^2_{min}$ where ΔB is the average field interval between digitised points. In turn ΔL determines the number N of equidistant points to be calculated in the interval $(1/B_{max}, 1/B_{min})$. N is equal to $(B_{min}/B_{max})\times$(the number of points in B). This reduction in points is not necessary if the original data are digitally filtered with a cutoff frequency of $(B_{min}/B_{max}) \times f_s$ before transposing. One must be aware that high-dHvA-frequency features can be suppressed because of this filtering.

Thus the procedure is first to construct a mesh of equidistant points in $1/B$ points and then, for every value of $1/B$, estimate the value of the dHvA signal at the corresponding point in B. That makes it necessary to interpolate between field values surrounding this desired point in B (1^{st} quadrant in figure 2.11). If the sampled waveform is filtered enough, a simple two point linear interpolation will suffice. When more elaborate interpolation schemes are used and more than two points are involved the effect is, one way or another, some form of low pass filtering. From my experience, going beyond a three point quadratic interpolation did not result in

better or more reliable dHvA spectra.

References

[1] D. Shoenberg and P.J. Stiles, Proc. Roy. Soc. (London) **A 281**, 62 (1964).

[2] K. van Hulst and J.A.A.J. Perenboom, IEEE-Trans. Magn. **24**, 1397 (1988);
K. van Hulst and J.A.A.J. Perenboom, Physica B **164**, 13 (1990);
"Research in High Magnetic Fields", International workshop, Nijmegen, The Netherlands; editors J. Franse, J. Fuggle, H. van Kempen, W. Mattens and J. Perenboom (1987).

[3] B. Knecht, G.G. Lonzarich, J.M. Perez, and D. Shoenberg, J. Low-Temp. Phys. **29**, 499 (1977).

[4] STYCAST 1266 and STYCAST 2850-GT, Grace N.V., Westerlo, Belgium.

[5] Kindly provided by Prof. Dr. M. Springford, H.H. Wills Physics Laboratory, Bristol, U.K.

[6] D.H. Lowndes, K.M. Miller, R.G. Poulsen, and M. Springford, Proc. Roy. Soc. Lond. A **331**, 497 (1973).

[7] M. Springford, private communications.

[8] Z. Tarnawski, H.P. van der Meulen, J.J.M. Franse, K. Kadowaki, P.A. Veenhuizen, and J.C.P. Klaase, Cryogenics **28**, 614 (1988).

[9] F.J. Harris, Proceedings of the IEEE **66**, 51 (1978).

Chapter 3

A 25 mK dilution refrigerator for use in high magnetic fields

3.1 Introduction

The field of low temperature physics is a vast area in fundamental research The application of high magnetic fields provides an extra experimental parameter Its effect on electronic properties of materials may be used to obtain information on zero field properties, such as the Fermi surface effective masses, et cetera However, a magnetic field can also induce a new physical state with phenomena that are absent when the field is zero, for example the (fractional) quantum Hall effect, field induced Wigner solid or the quenching of spin fluctuations in itinerant ferromagnets and heavy fermion systems

Although it is possible to design and build helium dilution refrigerators that provide temperatures of a few millikelvin, it is less easy to incorporate a 30 T hybrid magnet in the experimental set up without giving in too much on the minimum temperature I will now describe a novel dilution refrigerator which has been built and designed at the Nijmegen HFML, following original ideas of Dr K Neumaier [1] It has already proved its use in several high-field experiments, including the successful observation of quantum oscillations in the heavy fermion compound UPt_3 in fields up to 30 T, which will be discussed in chapter 5

3.2 Design

The design of the refrigerator is illustrated in figure 3 1 It is placed in a ^{4}He bath cryostat, which in turn loads into the room temperature bore of a magnet There are two characteristic features in the design First the total system fits the Ø 32 mm room temperature bore of the Nijmegen-II 30 T hybrid magnet system, over a length of approximately 60 cm Furthermore the heat exchanger and mixing chamber are made of plastic so as to avoid eddy current heating during operation in magnetic fields

The condenser line passes a pumped ^{4}He pot followed by a restriction before it enters the still The ^{3}He is led through a single continuous heat exchanger and emerges into the mixing chamber

The heat exchanger consists of an epoxy rod [2] in which a spiral channel is machined, with a rectangular cross-section of 2 5×2 5 mm^2 Inside this groove runs a spiraled capillary containing the concentrated phase A KAPTON polyimide film is wrapped around and glued on the outside of the rod, preventing short-circuits of the channel The top section of the capillary is Ø 0 3-0 6 mm copper-nickel, 1 5 m in length Further down it becomes Ø 0 7-1 0 mm also 1 5 m long and for the last section 3 m of Ø 1 3 mm inner diameter teflon capillary is used The effective exchange surface area is estimated to be around 200 cm^2 The plastic tail is surrounded by a stainless steel tube, which is at 4 2 K, and spacers are necessary to prevent vibrations or direct touches The cylindrical mixing chamber contains a concentric shield which forces the ^{3}He to cross the phase boundary on the inside of the shield Several thermometers and a heater are mounted and the wires run up through the groove

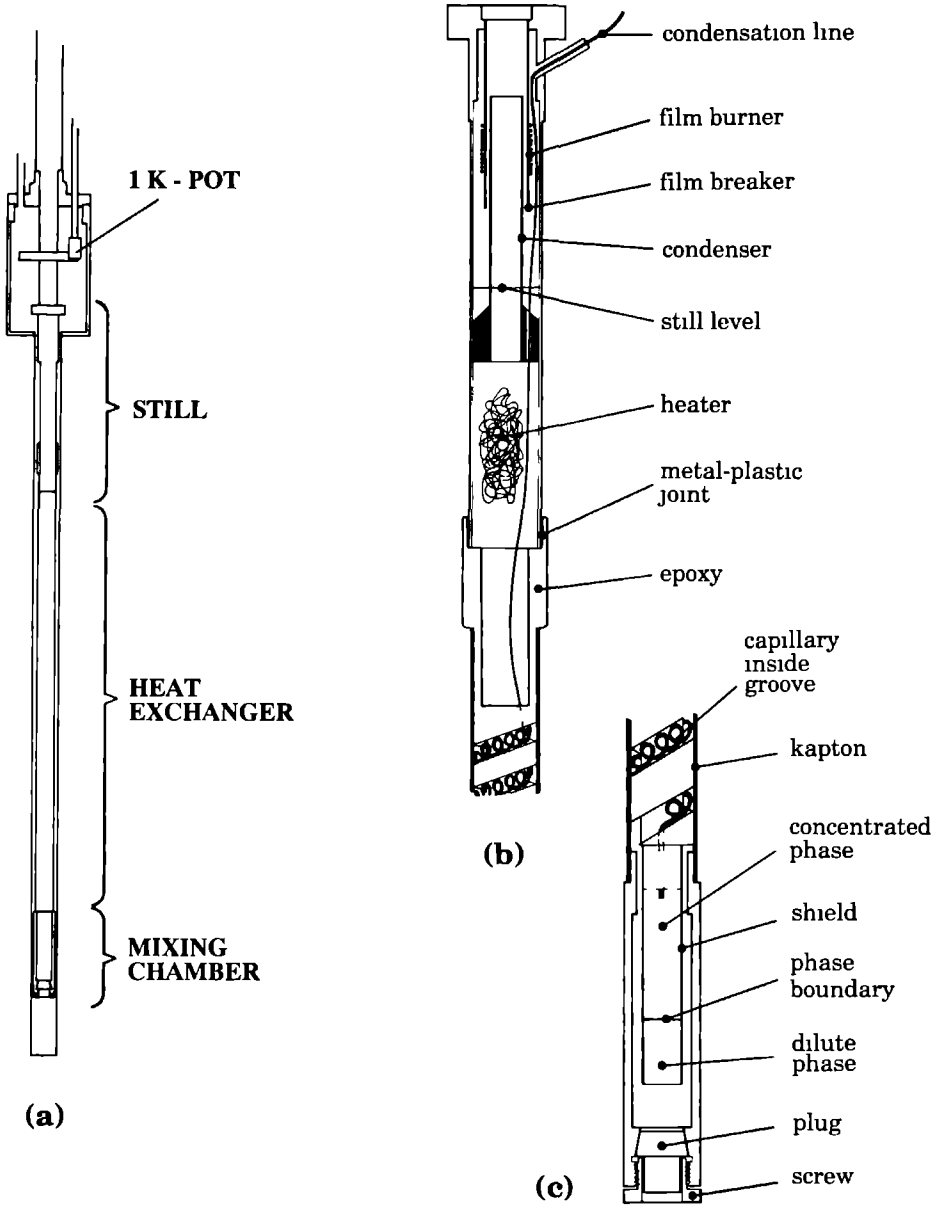

Figure 3.1 (**a**) Schematic diagram of the dilution refrigerator design The still (**b**) and the mixing chamber (**c**) are shown in more detail

sample space inside mixing chamber	Ø 9×45	mm
sample space below mixing chamber	Ø 16×50	mm
base temperature (zero field)	25	mK
base temperature (30 tesla)	30	mK
^{3}He charge	7	dm^3 NTP
total mixture	15	dm^3 NTP
^{3}He flow rate at base temperature	45	μmol/s
cooling time 300 K → 4 2 K	6	h
cooling time 4 2 K → 25 mK	3	h
surface area of heat exchanger	200	cm^2

Table 3.1 Specifications of the plastic tail dilution refrigerator

to the still where they exit the tail via a vacuum seal

Samples can be mounted in the mixture on a leak tight conical plug at the bottom of the mixing chamber All wiring necessary for the experiment itself is fed through the plug and runs up on the outside of the heat exchanger and via the still to the copper 1 K plate On several occasions we have also mounted a sample on the outside of the mixing chamber and made a thermal link between the experiment and the mixture via high purity silver wires which were fed through the plug and connected in the mixing chamber to some sintered silver powder

The still consists of metal components and between the heat exchanger and the still there is a plastic to metal junction, sealed with STYCAST 2850-GT resin [3] The still heater consists of a bundle of manganine wire There is a ^{4}He superfluid film breaker and a film burner which heats the outer stainless steel shield and evaporates the ^{4}He film A small clearance between the two shields prevents the ^{4}He to be pumped away while the cold inner copper shield serves as a condenser The film burner is able to decrease the ^{4}He/^{3}He molar flow ratio of the circulating mixture by a factor of two

The modular construction of the refrigerator and the fact that there are relatively few parts involved, make it a reliable machine In the rare case of trouble it is easy to make repairs The compact design also makes the instrument easy to move from one magnet unit to another Furthermore there is the advantage of the refrigerator being a fully in-house product This assures a high flexibility for the experimentalists that have to work with it

3.3 Thermometry

For thermometry at millikelvin temperatures in high fields we mainly use commercial carbon composition resistors (SPEER MATSUSHITA) or ruthenium oxide thick film chip resistors These secondary thermometers have a high sensitivity, and a rea-

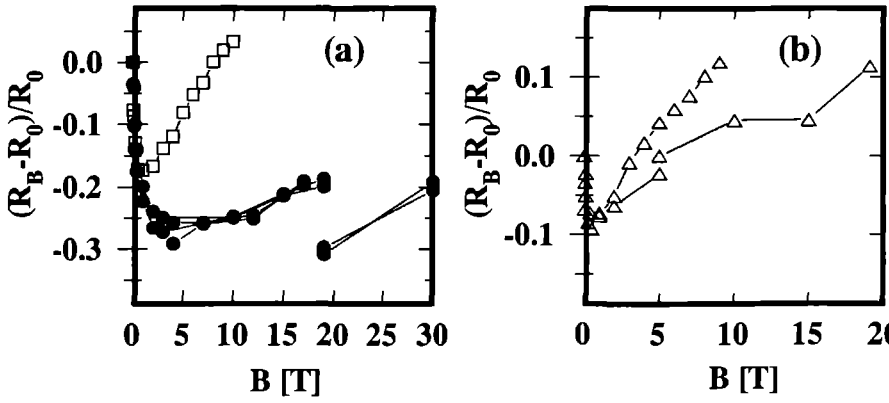

Figure 3.2 Magnetoresistance of (•) Speer resistors, (□) Matsushita resistors, and (△) RuO_2 thick film chips

sonably good reproducibility The insulating cover of the carbon resistors is removed and the core is cut into small slabs which gives a faster response and improves the thermal contact Leads are connected to the slabs with silver paint [4] Because of their dimensions they do not occupy valuable space in the refrigerator and thermal anchoring is simple The SPEER resistors have been calibrated in zero field against a CMN thermometer in the temperature range 0 01–4 2 K [5]

All types of resistor show a change in the resistivity when a magnetic field is applied The deviation from the zero field value becomes more and more important below 1 K and is considerable below 100 mK Figure 3 2 (**a**) shows the magnetoresistance $[R_B - R_0]/R_0$ for SPEER and MATSUSHITA carbon resistors, and (**b**) RuO_2 chip resistors at a temperature of 30 mK The data have been collected in the course of doing experiments in the dilution refrigerator

When a magnetic field is applied, all types of resistor show a similar behaviour After an initial drop, the magnetoresistance starts to rise again The position of the minimum, however, is different for each type The drop in resistance is approximately 25–30% for the SPEER sensors, 18% for the MATSUSHITA's, and 7–9% for the RuO_2 chips At a temperature of 30 mK this means an apparent increase in temperature of 9 mK, 5 mK and 2 5 mK respectively The effect is appreciably less at a temperature of 1 2 K Only 5% for the SPEER, 3% for the MATSUSHITA, and 1% for the RuO_2 resistors The data for the SPEER resistors taken at 19 T and 30 T, are shifted down due to a larger background heat leak during this particular hybrid magnet experiment as explained in section 3 4 The field dependence of the SPEER resistors above 5 T is approximately 1 2% T^{-1} at 30 mK

The observed behaviour is quantitatively more or less the same as described by others [6, 7, 8, 9, 10] There is however some scatter between the reports, also when one batch of resistors is compared with another batch of the same kind In

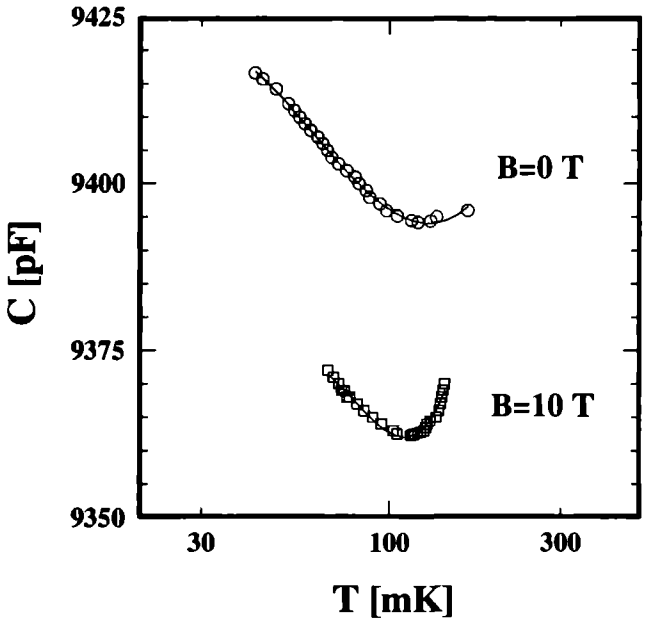

Figure 3.3 Temperature dependence of a SIEMENS capacitor (**a**) $B = 0$ T, and (**b**) $B = 5, 10, 15$ T Note the change of the position of the minimum

practice this means that every resistor has to be calibrated in field individually

The calibration is done under the assumption that there is no temperature change in the mixing chamber when a magnetic field is applied This is a realistic assumption since there are no metal parts in the tail which can cause eddy current heating due to field sweeps or the 300 Hz ripple in the field Furthermore it has been checked whether mechanical vibrations of the Bitter magnet cause heating of the mixing chamber

Glass capacitance sensors have been shown to be reliable field-independent thermometers (Wiegers *et al* [11] and references therein) The measured property is the dielectric constant of certain vitreous silica glasses In a further search for magnetic field independent temperature sensors, we have tested the performance of a SIEMENS capacitance thermometer [12] The capacitor was mounted inside the mixture and the wiring consisted of a pair of small Ø 0 6 mm coaxial cables [13] Each coax was contained in a Ø 0 7 1 0 mm stainless steel capillary The capacitance was measured with a high-sensitive automatic capacitance bridge [14] which operates at a fixed frequency of 1 kHz

In figure 3 3(**a**) the temperature dependence of the capacitance is shown The temperature has been measured with calibrated SPEER carbon resistors described above When the temperature is lowered, the capacitance initially drops then passes a minimum and finally starts to increase again The sensitivity $(1/C)\mathrm{d}C/\mathrm{d}\ln T$ at

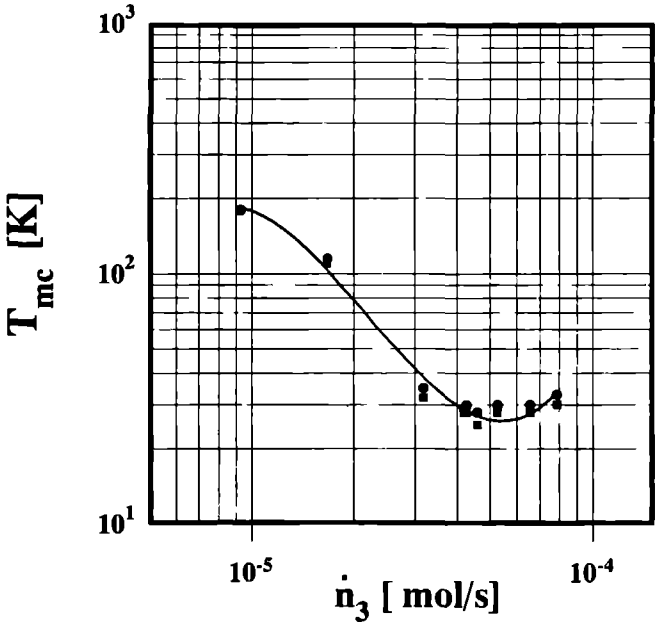

Figure 3.4 Performance of the plastic dilution refrigerator expressed in the relation between the mixing chamber temperature T_{mc} and the ^{3}He molar flow rate n_3

low temperatures is approximately -3×10^{-3}, which is an order of magnitude better than that of the vitreous silica sensors [11]

However, there are several features which make it a far from ideal sensor at low temperatures First of all, after cooling down the refrigerator, the capacitance shows a drift, which decreases fast with time (one or two days) This effect is acceptable A more serious one comes into play when a magnetic field is applied The capacitance-versus-temperature curve of figure 3 3(**a**) is being displaced to curve (**b**) as soon as a magnetic field is turned on The displacement in the plot is both horizontal and vertical As soon as a magnetic field is present, the capacitance is very insensitive to field variations! Calibration curves taken at 5, 10, and 15 tesla almost coincide with curve (**b**) A satisfying explanation for this behaviour is not found The wiring has been measured to produce no field dependent effects using an ordinary air-gap capacitor

3.4 Performance

The base temperature of the mixing chamber with a ^{3}He flow rate of 45 μmol/s without a magnetic field is 25 mK This can even be brought down to 21 mK when the ^{4}He bath is pumped, due to the reduced background heat leak through the

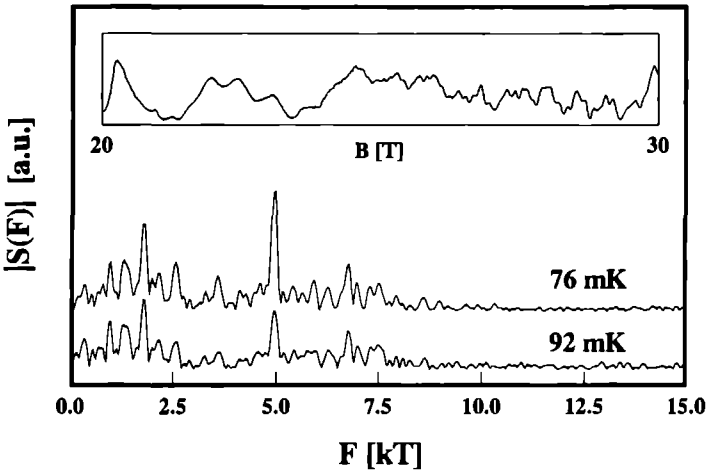

Figure 3.5 Quantum oscillation spectra in UPt_3 for 76 and 92 mK at high magnetic fields up to 30 T Note the strong temperature dependence of the peak near 5 kT The inset shows the oscillations as a function of the applied magnetic field **B** is parallel to the *b* axis of the hexagonal crystal structure The spectra are calculated for the interval 24 5 < B < 30 T

spacers The background heat load on the mixing chamber is measured to be 1 μW and is due to thermal conduction not only from the top through the plastic and the liquid He, but also through the spacers that touch the 4 2 K screen Although the spacers are made of VESPEL SP 22 [19] and the contact area with the stainless steel is smaller than 0 25 mm^2, the contribution to the background heat leak to the mixing chamber can not be neglected In figure 3 4 the performance of the dilution refrigerator is shown by plotting the temperature in the mixing chamber versus the ^{3}He flow rate The minimum indicates the balance between cooling power, the heat carried by the incoming ^{3}He, and the background heat leak

The dilution refrigerator has proved itself in several high-field (B > 20 T) experiments like measurements of the (fractional) quantum Hall effect [15, 16] and magnetisation measurements on pressurised ^{3}He [17] A good example of the flexibility of this refrigerator is the observation of quantum oscillations in the magnetoresistance of the heavy fermion compound UPt_3 (see chapter 5 and reference [18]) These measurements have been performed in the Nijmegen 30 T hybrid magnet system, the first above 20 T where a so-called metamagnetic transition takes place During operation a base temperature of 35 mK was achieved in the mixing chamber In order to make a rotation study, the sample had to be placed below the mixing chamber, i e , in the vacuum space Due to the construction of the rotator and the induction of eddy currents in some high purity silver wires (used for thermal linking), the background heat leak and thus the base temperature is slightly higher than found in other experiments For UPt_3 the amplitude of the quantum oscillations is

strongly influenced by the sample temperature A resistance-versus-magnetic field trace (inset) together with its frequency spectrum is illustrated in figure 3 5 The extreme temperature dependence of the oscillations is evidenced by the decrease of the peak around 5 kT when the sample temperature is increased from 76 to 92 mK

References

[1] Dr K Neumaier, Walther Meissner Institut, Garching, B R D

[2] HYSOL EPOXY CP4-4285, The Dexter Corporation, Olean, New York, U S A

[3] STYCAST 2850-GT, Grace N V , Westerlo, Belgium

[4] ELECTRODAG 1415, Acheson Colloiden B V , Scheemda, Holland

[5] The single batch SPEER resistors were kindly provided by Professor G Frossati, Kamerlingh Onnes Laboratorium der Rijksuniversiteit Leiden

[6] Y Koike, T Fukase, S Morita, M Okamura, and N Mikoshiba, Cryogenics **25**, 499 (985)

[7] Q Li, C H Watson, R G Goodrich, D G Haase, and H Lukefahr, Cryogenics **26**, 467 (1986)

[8] R W Willekers, F Mathu, H C Meijer, and H Postma, Cryogenics **30**, 351 (1990)

[9] M W Meisel, G R Stewart, and E D Adams, Cryogenics **29**, 1168 (1989)

[10] W A Bosch, F Mathu, H C Meijer, and R W Willekers, Cryogenics **26**, 3 (1986)

[11] S A J Wiegers, R Jochemsen, C C Kranenburg, and G Frossati, Rev Sci Instr **58**, 2274 (1987)

[12] SIEMENS X7R ceramic multilayer capacitor (0 10 μF)

[13] BIOMED wire AS 632-1SS, stainless steel, Cooner wire company

[14] ANDEEN-HAGERLING capacitance bridge, model 2500

[15] C V Brown, C J G M Langerak, P C Main, L Eaves, T J Foster M Henini, P A A Teunissen, and J A A J Perenboom, Physica B (to be published),
P J Rodgers *et al* , Physica B (to be published)

[16] G Grabecki, A Wittlin, T Dietl, P A A Teunissen, S A J Wiegers, and J A A J Perenboom, Semiconductor Science & Technology (to be published)

[17] S A J Wiegers *et al* , private communication

[18] S R Julian, P A A Teunissen, and S A J Wiegers, Physica B **177**, 135 (1992),
S R Julian, P A A Teunissen, and S A J Wiegers, Phys Rev B **46**, 9821 (1992)

[19] VESPEI SP 22 polyimide mixed with 30 vol % graphite,
Du Pont Vespel parts, Geneva, Switzerland

Chapter 4

de Haas – van Alphen oscillations in $YBa_2Cu_3O_{7-\delta}$

4.1 Introduction

The claim by Bednorz and Muller [1] in 1986 of evidence of a superconductive transition occurring at a temperature as high as 30 K in a La Ba-Cu-O system was rapidly confirmed by a number of laboratories in the U S , Japan and Europe It was established that a critical temperature T_c in the range of 20 40 K occurred for $La_{2-x}M_xCuO_{4-\delta}$, where M is Ba, Sr or Ca and δ represents an oxygen vacancy concentration Application of pressure led to a relatively strong increase of T_c, even higher than 50 K for M = Sr Since pressure was so effective, Wu *et al* [2] applied "chemical pressure", replacing La atoms in the La-Ba-Cu-O system by smaller isovalent Y atoms This produced a 90 K superconductor, later identified as $YBa_2Cu_3O_{7-\delta}$ Like the initial systems, this material was prepared by ceramic processing techniques High temperature annealing in an oxygen containing atmosphere was necessary to obtain the exact oxygen content and crystalline phase to give a high T_c Other preparation techniques have been developed since then, resulting in the production of small single-crystals and oriented films After the discovery of $YBa_2Cu_3O_{7-\delta}$ numerous other high T_c materials belonging to this class have been identified, the highest T_c reported being 125 K in the compound $Tl_2Ba_2CaCuO_{8-\delta}$

The macroscopic bulk properties of the high T_c superconductors (HTCS) are now rather well established On the other hand, the microscopic description of the basic mechanism(s) responsible for the occurrence of high temperature superconductivity, is still not settled and contradictory models are presented in the literature [3, 4] In the last four years a considerable amount of effort has been directed to elucidate the electronic ground state and the nature of the elementary excitations This has led to reports [5] on angle resolved photo emission spectroscopy and positron-annihilation two-dimensional angular correlation (2D-ACAR) measurements The results of these experiments have been interpreted as being supportive of the existence of a Fermi surface

Photo emission is, in general, a powerful tool for probing the electronic structure of materials It has proved somewhat erratic in the study of high T_c superconductors Because it is a surface sensitive probe, the major experimental hurdle has been the preparation of high quality surfaces in vacuum which are representative of the bulk Only after single-crystals of $YBa_2Cu_3O_{7-\delta}$ were cleaved *in situ* at T < 40 K, a distinct and stable Fermi edge was observed, which is consistent with metallic behaviour

Several measurements have been carried out on both insulating and metallic single-crystal oxides using the ACAR technique in order to investigate and to compare their electronic structure, in particular with respect to the possible existence of a Fermi surface In this case it is less clear how to interpret the experimental results Data obtained on the insulator La_2CuO_4 [6 7] have been well described by a model derived from a linear combination of atomic orbitals-molecular orbital scheme (LCAO MO) [8], thus excluding a dominance of Fermi surface related signals in ACAR measurements On the other hand, Tanigawa *et al* [9] interpret their data on the same compound in terms of Fermi surface topology Also Smedskjaer

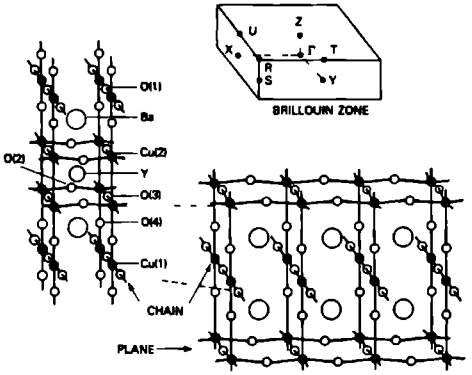

Figure 4.1 Crystal structure of $YBa_2Cu_3O_{7-\delta}$ together with the corresponding Brillouin zone

et al [10] and Bansil *et al* [11] deduce the existence of four Fermi surface sheets from their data measured on $YBa_2Cu_3O_{7-\delta}$

The possible presence of a Fermi surface in $YBa_2Cu_3O_{7-\delta}$ calls strongly for a conclusive, direct ground state measurement (like a de Haas – van Alphen experiment) Therefore, the main goal of the work described in this chapter is to establish the existence of dHvA quantum oscillations in this material

4.2 Fermi surface calculations on $YBa_2Cu_3O_{7-\delta}$

It is not my intention to give a review on the subject of the electronic structure of the HTCS nor will I mention the large amount of papers that use a model Hamiltonian to try to account for the (superconducting) properties of these materials I will confine myself to a short description of the crystal structure and the calculated Fermi surface for $YBa_2Cu_3O_{7-\delta}$, based on local-density-functional (LDF) theory

The crystal structure of $YBa_2Cu_3O_{7-\delta}$ is orthorhombic with a single formula unit per primitive cell It can be viewed as a defect perovskite lattice $(Y\text{-}Ba)_3Cu_3O_{9-\delta}$, based on three Cu-centered perovskite cubes with both O vacancy ordering and Y-Ba ordering along the c axis The structure is illustrated in figure 4 1 together with its corresponding Brillouin zone It is usually described in terms of Cu-O layers and Cu-O chains The chains consist of Cu(1) and O(1) atoms along the b axis The layers consist of Cu(2), O(2) and O(3) atoms The lattice constants are approximately $a = 3\,82$ Å, $b = 3\,89$ Å, and $c = 11\,86$ Å [12]

Several linear-augmented-plane-wave (LAPW) calculations have been reported [13, 14, 15] Although most calculations are generally in good agreement on a scale of a few tens of meV, there are differences in the bands near the Fermi level, resulting in somewhat different predictions regarding the Fermi surface shape Figure 4 2 shows the Fermi surface cross-sections in all symmetry planes, as calculated by

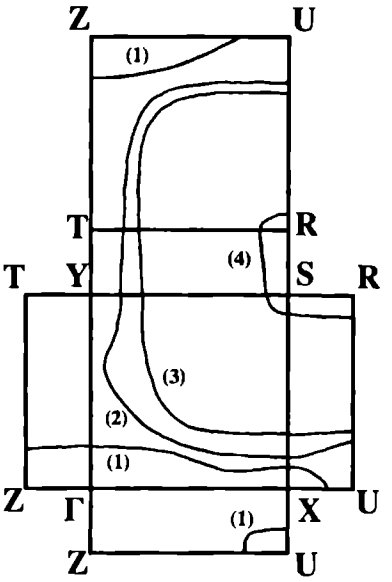

Figure 4.2 Calculated cross-sections of the Fermi surface of $YBa_2Cu_3O_{7-\delta}$ in all symmetry planes of the Brillouin zone [16]. Several surfaces can be distinguished; they are labeled (1)...(4), and described in more detail in the text.

Picket, Cohen and Krakauer (PCK) [16]. It is possible to discern which bands (i.e., which parts of the Fermi surface) arise from the Cu-O chains and which arise from the Cu-O planes. The Fermi surface bands labelled (1) and (4) are chain-derived whereas the bands (2) and (3) are plane-derived.

Speaking in terms of orbits around extremal cross-sectional areas it follows from these calculations that, in case the magnetic field is applied along the c axis, band (1) has a minimum electron orbit ("neck") at $k_z = \pi/c$. Furthermore there are two cylindrical, nearly degenerate, hole-like Fermi surfaces (2) and (3), with little dispersion along the k_z direction. The cross-sectional areas of these "barrels" are roughly squares with rounded corners. Finally one can deduce a cylindrical hole surface (4) along k_z with a small, undulating cross-sectional area, which is minimal at $k_z = 0$ and maximal at $k_z = \pi/c$. The above described calculation differs from a calculation by Yu *et al.* (YMFD) [17] at two points. The latter find an extra, chain-derived Fermi surface: an irregular shaped cylinder centered around Y-T. The other difference is that the pinching off around U of the planar Fermi surface does not occur in the calculation by Yu *et al.* (although it almost happens) which means an absence of the "neck" orbit. The extremal cross-sectional areas calculated by both groups are listed in table 4.1 together with experimental values, which will be

Extremal Fermi surface	Area (T)	m^* (m_e)	group
(4) minimum of small cylinder	530±20	7 0±2 5	LANL
	540±30	$2\ 1^{+2}_{-0\ 5}$	HFLTU
	170	-1 6	PCK
	400	-2.1	YMFD
(4) maximum of small cylinder	780±20	7 2±2 5	LANL
	—	—	HFLTU
	220	-1 7	PCK
	420	-2 3	YMFD
(1) "neck"	3510±100	7 4±2.6	LANL
	—	—	HFLTU
	3700	1 45	PCK
	—	—	YMFD
(3) inner "barrel"	—	—	LANL
	—	—	HFLTU
	12410	-1.4	PCK
	12050	-1.5	YMFD
(2) outer "barrel"	—	—	LANL
	—	—	HFLTU
	12570	-1.5	PCK
	12680	-1.6	YMFD

Table 4.1 Comparison of reported Fermi surface observations by two experimental groups (LANL [19] and HFLTU [21]) with extremal cross-sectional areas as calculated by two theoretical groups (PCK [16] and YMFD [17]).

discussed in the next section.

4.3 Reported quantum oscillations

Recent reports [18, 19, 20, 21, 22] claim the observation of dHvA oscillations in very high magnetic fields in the compound $YBa_2Cu_3O_{7-\delta}$. The samples used for these experiments are not single-crystals but consist of fine-grained powders embedded in a non-conducting epoxy. All grains have their c axes aligned along a certain direction. I will now shortly describe the findings of the above mentioned reports.

First there is the group of the Los Alamos National Laboratory (LANL) [18, 19], using a 105 T explosion driven flux compression system. The principle of generation of such high fields is the following. A capacitor bank is discharged

over a single turn coil of large cross-sectional area This results in a sinusoidal current in time When the magnetic field is at its maximum (just below 8 T) both ends of the coil are driven into each other by detonation of explosives This traps the flux in the metallic hoop As the explosion continues it squeezes the area containing the initial flux In this way the magnetic field strength inside is increased to just above 100 T The time scale of the pulse is 100 μs The radial expansion of the coil and Joule heating leads to a smooth but rapid decrease of the field The maximum time derivative of the field dB/dt is in the order of 5×10^6 tesla per second [23]! In order to detect magnetisation signals, a 100-turn single-layer coil has been wound on an aligned-powder-in-epoxy sample of dimensions Ø 1 0×4 5 mm A compensation coil has been wound on a dummy sample consisting of pure epoxy The measured signal is proportional to dM/dt It is needless to say that this experimental method (especially the explosive part) leads to the loss of both the sample and the pick-up coils

The oscillations reported to have been observed between 100 T and 60 T are listed in table 4 1 Their Fourier transform has contributions at (530±20) T, (780±20) T and (3510±100) T It is concluded that these frequencies correspond to the minimum of the small cylinder, the maximum of the small cylinder, and the "neck" orbit, respectively (see previous section) The derived orbital effective masses for all three frequencies are approximately 7 times the free electron mass The "barrel" orbits have not been observed

The second report stems from the High Field Laboratory of the Tohoku University (HFLTU), Sendai, Japan [21] Their method of detecting dHvA signals is of the conventional type the field modulation technique These experiments have been performed in hybrid magnets up to 27 T using a modulation frequency of 1000 to 2500 Hz and a modulation field of 200 Gauss peak-to-peak The modulation coil was mounted on the sample holder inside the cryostat Their construction led to intense vibrations of everything that is mechanically connected to this coil In order to suppress the vibrations, copper rings were attached to the sample holder, nearby the modulation coil, so as to counteract the movements of the vibrating coil with induced Lorentz forces in the rings For efficiency purposes four samples were measured simultaneously with four PSD's The magnetic field was swept between 10 and 27 T with a maximum rate of 1 0 T/min It is claimed that in this way a dHvA frequency is observed at (540±30) T corresponding to the minimum of the cross-section of the Fermi surface around point S (the small undulating cylinder) The effective mass for this extremal orbit is estimated to be 2 times the free electron mass No other frequencies have been observed

A very recent experiment by Nizhankovskii *et al* [24], using a totally different approach to quantum oscillations, is reported to have produced information on the Fermi surface of $YBa_2Cu_3O_{7-\delta}$ It shows a faint oscillatory behaviour of the contact potential difference between the plates of a capacitance, consisting of a thin epitaxial film of $YBa_2Cu_3O_{7-\delta}$ and a polycrystalline (in this case a bronze) counter electrode The underlying idea is that the chemical potential in a conductor – like all thermodynamic quantities – is expected to oscillate with the same periodicity as

that of the dHvA effect but with very small amplitude microvolts or less for most metals The effect was first predicted by Kaganov *et al* [25] The periodic variation of the contact potential of $YBa_2Cu_3O_{7-\delta}$, as measured by Nizhankovskii *et al*, has dHvA spectrum contributions at 250 T and 525 T No higher frequencies have been observed

It is important to be aware of the fact that all groups have observed oscillations in rather different experimental conditions, which calls for caution when making comparisons Also the sample material might not be the same for the LANL and HFLTU groups Finally one must be careful when comparing the measured orbit sizes to the theoretical values since small changes in the band structure near the Fermi level causes considerable variations in the cross-sectional areas, especially those of the smaller extremal orbits

4.4 The Nijmegen experiments

The decision to start experimenting on $YBa_2Cu_3O_{7-\delta}$ was based on the fact that we should be able to at least reproduce the results mentioned above, for high magnetic fields are easily produced as well as samples Furthermore a complete dHvA set up was ready at the time Our first aim was to look for quantum oscillations in more or less the same circumstances as the HFLTU group, meaning a modulation technique at high continuous background fields up to 20 T The dHvA set up is discussed in chapter 2 The samples have been prepared in the same way as in references [19] and [21] The ceramic pellets were produced in a rather standard way The materials $Y_2Cu_2O_5$ and $BaCuO_2$ were ground and thoroughly mixed in a molar ratio of 1 4 Next the mixture has been pressed into a pellet and was kept at a temperature of 950 °C for 48 hours in an oxygen-rich environment A resistance measurement on a fragment of this pellet showed a superconductive transition at 90 K with a 90%-10% width of $\sim$ 0 7 K

Immediately afterwards the pellet has been carefully ground in a mortar Optical inspection of cut samples revealed grain sizes ranging from a few μm to 30 μm, with an average of 10 μm The powder was then stirred into STYCAST 1266 epoxy resin and the slurry was cast in several Ø 1 0 mm cylindrical moulds which had been drilled in a small teflon piece In order to orient the grains, the mould was placed in a strong magnetic field generated by a Bitter magnet The axes of the tiny holes were parallel to the magnetic field direction The magnet was operated at a field of 10 T making excursions to 15 T every 5 minutes Due to the intrinsic crystal anisotropy the magnetisation is also anisotropic [26] Along the c axis of a crystallite it is much larger than along the a or b axis The torque on the crystallite will thus tend to align the c axis parallel to the magnetic field direction During the alignment the mould was heated to $\sim$ 50 °C, which served two purposes At first it makes the resin less viscous which facilitates the rotation of the small crystallites during the alignment The second reason is that after a while the epoxy hardens quicker, in this way shortening the alignment procedure to 2 hours

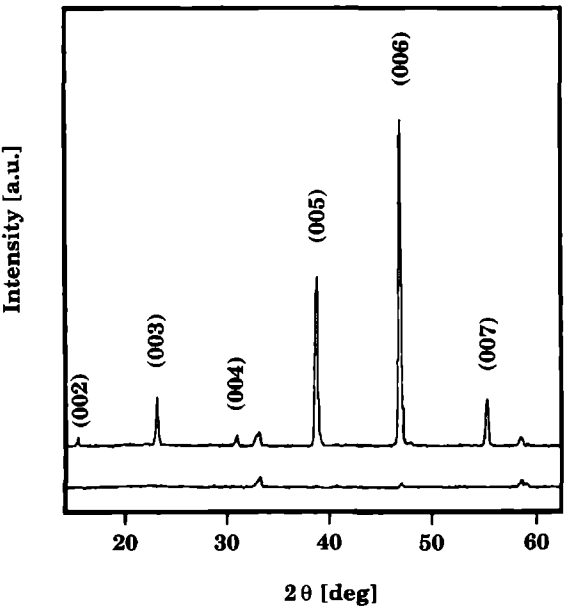

Figure 4.3 (a) X-ray powder diffraction pattern taken from grains of $YBa_2Cu_3O_{7-\delta}$ embedded in epoxy, (b) pattern obtained from a sample which has been oriented in a magnetic field (see text) Θ is the angle between the X-ray beam and a plane in the sample which is perpendicular to the applied field direction

In order to check the effect of the magnetic field on the orientation, powder diffraction patterns were taken with an X-ray spectrometer [27] The patterns are shown in figure 4 3 for two epoxy embedded samples one prepared with, the other without applying a magnetic field Although not visible on this scale, a large number of reflections could be identified in the spectrum of the non-oriented sample All the (hkl) reflections with $h, k = 0$ increase significantly in the aligned sample, confirming the anticipated c axis orientation The (006) peak has grown by a factor of 140 Other intensities in the diffraction pattern, like the (103)/(013) near 33° or the (123)/(213) near 69° seem to be hardly influenced by the alignment procedure possibly by a remnant randomness in crystal orientation This can be understood if a certain fraction of the grains in the epoxy does not consist of true single-crystals but of a conglomerate of several crystallites with non-parallel orientation, which hamper each other in the aligning process The possibility that these reflections stem from non-reacted $Y_2Cu_2O_5$ or $BaCuO_2$ can be ruled out since a diffraction pattern taken from unoriented powder which had been allowed to re-react again at 950° for 24 hours did not show a reduction of these peaks There is however clear evidence that a considerable fraction of the sample has been oriented along the desired direction

4.4.1 Attempts with the modulation technique

The modulation experiments have been performed with the sample in the mixing chamber of the dilution refrigerator, described in chapter 3 The reason for doing this is straightforward If an effective mass ratio of 7, as reported by the LANL group, is valid for magnetic fields around 15 T then a considerable gain in signal strength can be obtained by going from say 1 2 K to 50 mK The amplitude damping due to thermal smearing of the Fermi surface (1 26) will decrease from 200 to close to 1 Most of the times the magnetic field was swept between 10 T and 20 T, with a sweep rate varying between 0 1 and 1 0 T/min We have tried numerous combinations of modulation frequency and modulation amplitude, ranging from the full 1800 Gauss peak-to-peak at 10 Hz to 25 Gauss peak-to-peak at 1000 Hz Although we have focussed on a possible presence of the frequencies reported by LANL, we have found *no reproducible dHvA signatures* in $YBa_2Cu_3O_{7-\delta}$

Detection was usually done at the second harmonic of the modulation frequency In our first attempts we encountered enormous heating of the mixing chamber ($T \sim 1$ K) when the modulation field was turned on, especially when the background magnetic field was zero The pick-up signal was also rich in harmonics of the modulation frequency All these phenomena seemed to point in one direction the grains in the sample were probably arranged beyond the percolation threshold, causing hysteresis and dissipation due to flux flow

Further measurements were done on samples from a second batch which had a filling fraction that was smaller by a factor of two The heating of the samples due to modulation was still appreciable but noticeably smaller and we were able to collect a large number of traces which could be analysed and checked for reproducibility and "Bessel behaviour" (2 7) of the amplitude of possible frequency candidates All "peaks" we have ever observed stood out from the background noise level by a factor of three at most None of them were reproducible they could not be observed again if all experimental conditions were kept unchanged A dependence on the modulation depth or temperature has never been seen

In order to be more comparative with the LANL measurements we have also studied aligned samples which were manufactured by the Los Alamos group [28] and have a low filling fraction of 17% by volume Again we have used the same set up and checked for reproducibility in possible dHvA signatures With these samples we hardly experienced heating of the mixing chamber during field modulation It was possible to maintain a temperature of 70 mK at maximum modulation depth Nevertheless these experiments were just as fruitless as the ones on our own samples In order to get some idea of the reproducibility, figure 4 4 shows five traces on a LANL sample, each taken under exactly the same circumstances

4.4.2 The "pulsed" field method

In an attempt to simulate the experimental conditions of a pulse measurement we have ramped the field of a Bitter magnet as fast as possible and measured the induced voltage on the dHvA pick-up coil In the normal operation mode the 6-

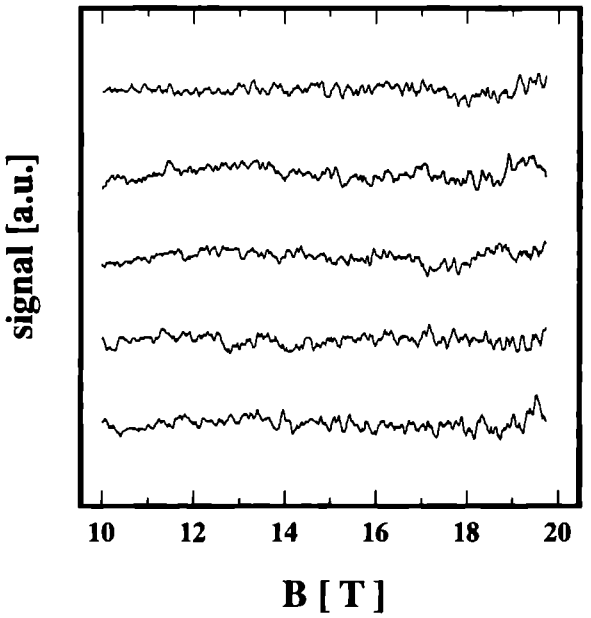

Figure 4.4 Several dHvA-traces on $YBa_2Cu_3O_{7-\delta}$, taken under equal experimental conditions using the field modulation technique No correlation has been found between the recordings

MW power supply is able to sweep the magnetic field with a maximum velocity of 0 5 T/s In this mode the transistor unit after each rectifier is able to reduce the presence of harmonics of 50 Hz in the magnet current It is possible to increase the sweep rate to 2 T/s However, in this case the transistor unit of the power supply is not working properly Normally this unit corrects for small deviations in the magnet current (mostly harmonics of 50 Hz from the rectifier units), but at this sweep rate the unit becomes overloaded and the 50 Hz harmonics are passed to the magnetic field without filtering, which leads to extra noise in the dHvA pick-up signal The position of the yoke of each rectifier unit is varied by means of filling and emptying oil-pressurised cylinders This process limits the sweep rate An extra complication of this rather uncontrolled ramping up and down is that during the "up-sweep" several bursts of noise appear in the magnetic field We have not been able to pinpoint and remove the cause of these bursts and decided to measure only during "down-sweeps", where they were absent In figure 4 5 an example is given of the time profile of the magnetic field

It is possible to derive from the LANL data what signal strength one can expect in a pulse experiment in Nijmegen, assuming that the Lifshitz–Kosevich relation is applicable in both experimental conditions Suppose that the oscillatory

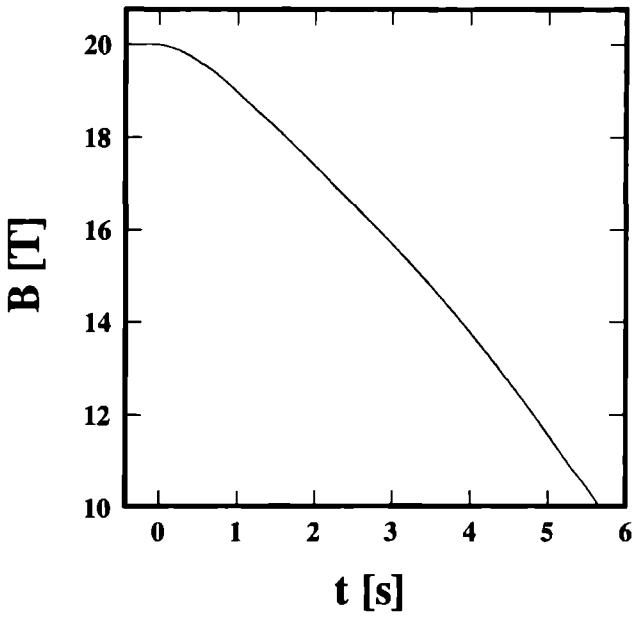

Figure 4.5 Field variation in time during a "pulse" with the Bitter magnet system.

magnetisation is given by

$$M(t) = M_0(B(t)) \cdot \sin\left(\frac{2\pi F}{B(t)} + \phi\right) \tag{4.1}$$

then the voltage, induced in the pick-up coil, is

$$\begin{aligned} V_{\mathrm{pu}} &= c\frac{\partial M}{\partial t} = c\frac{\partial M}{\partial B}\dot{B} \\ &\approx c\frac{2\pi F}{B^2} M_0(B(t)) \cos\left(\frac{2\pi F}{B(t)} + \phi\right)\dot{B} \end{aligned} \tag{4.2}$$

where M_0 is equal to the expression for the amplitude in equation (1.34). The approximation used here is that the magnetic field does not change considerable compared with the period of the dHvA signal. The quantity c stands for the coupling factor of the pick-up coil with the sample.

Several quantities in the above expression differ appreciably from the LANL set up. While the time derivative of the magnetic field is in the order of 10^6 T/s, in Nijmegen 2 T/s is the fastest we can do. On the other hand the pick-up coil in Nijmegen has a considerably better flux coupling to the sample than the one of LANL. The term F/B^2 will also be to our advantage. And again, if the effective

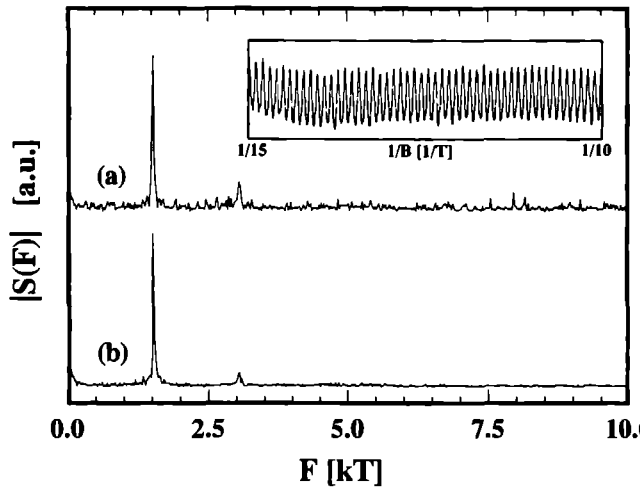

Figure 4.6 Amplitude spectra $|S(F)|$ of the dHvA signal of a $Au_{1-x}Ag_x$ ($x = 2.5 \times 10^{-3}$) test sample, taken with the "pulsed" field method, (**a**) spectrum of a single trace between 10 and 15 T, (**b**) spectrum of 20 averaged traces. The inset shows the data versus $1/B$ after averaging.

mass of 7 m_e is still applicable in fields around 15 T the thermal damping coefficient (1.26) will provide a relative gain of 200. Taking all factors into account, we expect the signal amplitude on the pick-up coil in the Nijmegen experiment to be in the order of 0.5 μV. The expected time frequency of a 550 T dHvA-signal will be

$$f = \frac{F}{B^2}\dot{B} \sim \text{a few Hz} \tag{4.3}$$

which is comfortably below the 50 Hz ripple and its harmonics. In order to increase the signal-to-noise ratio we have developed a semi-automatic pulse routine, which allowed us to pulse every 90 seconds and to collect 100 traces in a few hours. After preamplification and filtering, the signal from the pick-up coils together with some voltage proportional to the magnetic field are fed into a PC-based stereo AD converter with 2000 Hz sample rate [29]. The data have been processed by thoroughly tested routines. This includes digital filtering, conversion to $1/B$, and Fourier transforming. The averaging has been done in two ways. Either the data have been *averaged in the B domain*, followed by conversion to $1/B$ and calculation of the Fourier transform, or every trace was first transposed to the $1/B$ domain, next *averaged in the $1/B$ domain* and finally Fourier transformed. Both paths should lead to the same result. Furthermore all traces could optionally be divided by dB/dt so as to prevent possible oscillations in the sweep rate to show up as dHvA signals. A good way to check whether oscillations are periodic in $1/B$ is to compare the peak width in a Fourier transform of data in the B domain with a Fourier transform of

data in the $1/B$ domain a genuine dHvA peak should broaden in the B domain

Before starting measurements on $YBa_2Cu_3O_{7-\delta}$ we have checked the reliability of the "pulsed" method by making calibration measurements using the [111] neck oscillations of the same $Au_{1-x}Ag_x$ sample as has been used for testing the modulation set up (page 32) The magnetic field is derived directly from the current through the Bitter stacks The validity of this was verified by comparing it with simultaneous field registrations performed by integrating the pick-up voltage induced in a monitor coil which surrounds the sample and the set of dHvA coils (see section 2 3) It was deduced that measuring the field using the Bitter current is accurate within 7×10^{-4} The software routines could be tested and the analysis proved to be reliable the signal-to-noise ratio of the neck orbit improved roughly by $\sqrt{N}$ when averaging $N = 20$ "pulses" and the frequency determined for this orbit differed less than 1% from the literature value of 1532 tesla [30] (see figure 4 6) The peak height of the harmonic at 3 kT has reduced somewhat due to the averaging This is the result of a spread in the phase of the oscillations between the consecutive traces It is estimated from this decrease of the second harmonic amplitude that the reproducibility of a trace is in the order of 10 Gauss when expressed in magnetic field Also, averaging in the $1/B$ domain or averaging in the B domain resulted in similar Fourier spectra We have estimated the coupling constant c of the sample to the dHvA pick-up coil by means of an amplitude analysis of the gold signal It turned out to be 0 11 T/A which is comparable to the value of 0 16 T/A we have derived from modulation experiments on exactly the same sample in exactly the same coil configuration The outcome of these tests gave therefore enough confidence for us to be able to extract possible dHvA oscillations with frequencies around 500 T in the high T_c superconductor, provided they are strong enough

We have studied both our home-made samples and those of the LANL group [28] In comparison with the case of field modulation, the heating of the mixing chamber of the dilution refrigerator after a field "pulse" was almost negligible We have averaged the data obtained from 70 to 100 pulses and we have concentrated on the existence of dHvA peaks in the frequency interval 100–1500 tesla Although we sometimes believed to have pinpointed a peak, it turned out to be irreproducible, meaning the signal-to-noise ratio of this peak did not grow as the number of averaged pulses was increased In fact only one of the pulses in the ensemble turned out to be responsible for a strong "oscillation" After removal of this trace, the peak in the average spectrum had disappeared *All in all we must conclude that the only phenomena we were able to observe in $YBa_2Cu_3O_{7-\delta}$ were caused by sheer noise and incidental events*

Since we roughly know the sensitivity of our experimental set up, we can derive from the noise level in our measurements an estimate of the upper limit of the amplitude of the oscillatory magnetisation in $YBa_2Cu_3O_{7-\delta}$ From the modulation measurements we derive a maximum magnetisation of 8 7 Am^{-1} while the pulse measurements give an upper bound of 13 Am^{-1} The difference is mainly due to the difference in the coupling constants c, as determined for each technique This means that at least for the dHvA measurements on $YBa_2Cu_3O_{7-\delta}$ we have used two more

or less equally sensitive methods The values are only a factor of 15 smaller than the amplitude of the magnetisation caused by the [111] neck orbit of the $Au_{1-x}Ag_x$ test sample The reason for this is that the high T_c samples induce more noise in the pick-up system than the gold alloy does, possibly because of flux jumps

4.4.3 Interpretation of the results

In this concluding section I would like to discuss the mere possibility of detecting dHvA oscillations in $YBa_2Cu_3O_{7-\delta}$, since the upper critical field B_{c2} for B parallel to the c axis is very high (well over 100 T [31]) and consequently the magnetooscillations can only be measured in the superconducting (mixed) state In the past two decades there have been several reports on quantum oscillation measurements in Chevrel type superconductors Examples are magnetothermal oscillations in V_3Ge [32], and dHvA measurements on Nb_3Sb [33], Nb_3Sn and V_3Si [34] All these observations were done above B_{c2}

Only one Fermi surface measurement has been performed successfully both above and *below* B_{c2} by Graebner and Robbins [35] in the quasi-two-dimensional compound $2H$-$NbSe_2$ The oscillations were seen in the magnetisation as well as in temperature One might expect that the field inhomogeneity associated with the presence of a vortex lattice in the mixed state of the superconductor, would provide an obstacle to the observation of the dHvA effect However for a material like $NbSe_2$ the Ginzburg-Landau parameter κ is extremely large and it is estimated that the field variation along a cyclotron orbit is smaller than $\xi_{GL}/\lambda = 1\%$ From the field dependence of the oscillation amplitude it is derived that the Dingle temperature – a measure for the scattering rate – is somewhat increased from 0 96 K in the normal state at high fields to 1 35 K in the mixed state, just below B_{c2} The measured dHvA frequency below B_{c2} is slightly (3%) higher than above the transition This is explained by the fact that the Landau oscillations are periodic in $1/B$ and B in the mixed state is decreasing toward zero more rapidly (that is a higher apparent frequency) than it would in the case of $B = \mu_0 H$

The subject of orbital quantisation of quasiparticles and the dHvA effect in the mixed state of a superconductor has been addressed by several authors In 1968, Gruenberg and Gunther [36] showed, making a Green s function analysis of the modification of the gap equation near B_{c2}, that Landau level quantisation should have a significant effect on the properties of a superconductor and it followed that the superconductive transition temperature $T_c(B)$ would be an oscillatory function of the magnetic field Other authors studying quantum oscillatory behaviour in a type II superconductor [37, 38] also conclude that it should be possible to observe these effects, even below B_{c2}

One can estimate the number of vortices in $YBa_2Cu_3O_{7-\delta}$ that are surrounded by the extremal cyclotron orbit corresponding to a dHvA frequency of 550 T and in this way get a feeling for the field inhomogeneity experienced inside the superconductor The relation between real space and reciprocal space is given by $|\mathbf{r}| = (\hbar/eB)|\mathbf{k}|$ The vortex density can be approximated by $n_\phi \approx B/\Phi_S$ where Φ_S is the supercon-

ducting flux quantum ($2\,07\times10^{-15}$ Wb) At 15 T the extremal reciprocal area $\mathcal{A} = 2\pi eF/\hbar$ corresponds to a real-space orbit with radius $r_c \approx 60$ nm, which contains about $\pi r_c^2 n_\phi \simeq 80$ vortices The vortex separation is approximately 10 nm and this is about 5 times the Ginzburg–Landau coherence length ξ_{ab} in the $a-b$ plane of the crystal structure [39, 40, 41] The field penetration depth λ_{ab} is extremely large (>1500 Å [42]) and the field variation along a cyclotron orbit will be of the order of 0 5% At 15 T the period $B^2/F = 0\,14$ T, which is not much larger than 0 5% of 15 T Therefore one might expect some form of extra scattering due to the presence of the vortices and consequently a reduction of a dHvA amplitude

Very recently Stephen [43] and Maki [44] have studied the effect of orbit quantisation on the quasiparticle excitation spectrum above the gap, outside the vortex cores Both authors find that the gap $\Delta(B)$ in the mixed state behaves as an extra Dingle temperature and in this way reduces the amplitude of the dHvA oscillations This extra scattering by the vortices is given by

$$\frac{1}{\tau_v} \simeq \Delta(B)^2 \left[\frac{\pi}{\mu\omega_c}\right]^{1/2} \tag{4 4}$$

where μ is the Fermi energy and ω_c is the cyclotron frequency This effect is indeed observed by Graebner and Robbins although no field dependence of the Dingle temperature was reported and it was small enough to be able to observe quantum oscillations well below B_{c2}

Both Stephen and Maki find that only in a narrow region near B_{c2}, where $\Delta(B) \simeq \Delta(0)(1-B/B_{c2})^{1/2}$ is sufficiently small, it is likely to find dHvA effects The actual numbers become even more depressing considering the already high content of impurities in these materials Therefore a possible explanation for our negative results might very well be that the amplitude is indeed too small to be detected, since we operated in a field region well below B_{c2}

There are other considerations which make a successful dHvA measurement questionable The normal state properties of the high T_c superconductors - like resistivity, thermal conductivity, Hall coefficient, optical conductivity, Raman scattering intensity, tunneling conductance, and nuclear relaxation rate – are frequently unlike those expected for a Fermi liquid [45] In the light of this a phenomenological model by Varma [46] has gained considerable attention since it provides a unified description of the normal state properties mentioned above It is referred to as the *marginal Fermi liquid* model and it is based on the hypothesis that there exist spin and charge response functions of the Fermi liquid that have an *additional* contribution $\chi_A(k,\omega)$ to the polarisability where

$$\mathcal{I}m\left[\chi_A(k,\omega)\right] = \begin{cases} -N(0)\omega/T & |\omega| < T \\ -N(0)\mathrm{sgn}(\omega) & |\omega| > T \end{cases} \tag{4 5}$$

and is frequency limited by a sharp cut off $|\omega_X|$ Here $\mathcal{I}m$ is the imaginary part, T is the temperature, and $N(0)$ is the density of states at the Fermi level This unusual form for $\mathcal{I}m[\chi_A]$ has been observed very recently in neutron [47] and Raman [48]

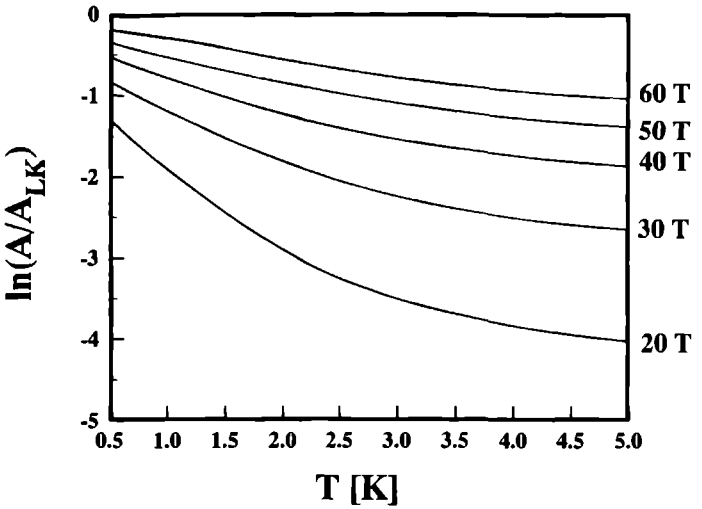

Figure 4.7 Reduction of the dHvA amplitude plotted as a function of temperature for several values of the magnetic field The amplitudes A_{LK} and A are the amplitude factors of the Lifshitz Kosevich formula and of the revised formula calculated for a marginal Fermi liquid, respectively (after Wasserman *et al* [49])

scattering experiments Given this hypothesis, it has been calculated by Wasserman *et al* [49] what the effect will be on the Lifshitz–Kosevich formula They conclude that, although the dHvA frequencies remain unaffected, the amplitude of the oscillations will be reduced because of an enhanced value for the effective mass

$$m^* = m_B \left\{1 + (2/\pi)g^2 N(0)^2[1 + \log(\omega_X/T)]\right\} \qquad (4\,6)$$

where m_B is the effective mass before enhancement, defined in equation (1 5) Note that m^* has become temperature dependent! The degree of suppression is determined by the parameters ω_X and $gN(0)$ In figure 4 7 the influence of this logarithmic temperature dependence is illustrated by plotting the reduction factor as a function of temperature, for the case that $\omega_X = 15\ k_B$, $g^2\Lambda(0)^2 = \pi$ and $m_B = 0\,5\ m_e$

Considering the outcome of our own experiments together with the contemplations in the paragraphs above, we might try to come up with some conclusion with respect to dHvA oscillations in $YBa_2Cu_3O_{7-\delta}$ Until this day the LANL and the YMFD reports have been the only claims on the observation of oscillations Although there have been serious efforts, no other group has published similar results One could argue that, in order to be able to see merely a glimpse of quantum oscillatory behaviour in $YBa_2Cu_3O_{7-\delta}$, it is necessary to apply magnetic fields which are close to B_{c2} (i e , in the order of 100 tesla) In that case the LANL group is the sole claimant of dHvA oscillations, which is scientifically spoken an unsatisfying situation, since – for the near future confirmation by other, independent groups

is not possible. At the same time it would make the YMFD interpretation of their results questionable, to say the least, especially since the Nijmegen experiments have been performed under almost the same conditions.

References

[1] J.G. Bednorz and K.A. Müller, Z. Phys. B **64**, 189 (1986).

[2] M.K. Wu, J.R. Ashburn, C.J. Torng, P.H. Hor, R.L. Meng, L. Gao, Z.J. Huang, Y.Q. Wang, and C.W. Chu, Phys. Rev. Lett. **58**, 908 (1987).

[3] T.M. Rice, Z. Phys. B **67**, 141 (1987).

[4] P. Fulde, Physica C **153-155**, 1769 (1988).

[5] A.J. Arko, R.S. List, R.J. Bartlett, S.-W. Cheong, Z. Fisk, J.D. Thompson, C.G. Olsen, A.-B. Yang, R. Liu, C. Gu, B.W. Veal, J.Z. Liu, A.P. Paulikas, K. Vandervoort, H. Claus, J.C. Campuzano, J.E. Schirber, and N.D. Shinn, Phys. Rev. B **40**, 2268 (1989).

[6] A.L. Wachs, P.E.A. Turchi, Y.C. Jean, K.H. Wetzler, R.H. Howell, M.J. Fluss, D.R. Harshman, J.P. Remieka, A.S. Cooper, and R.M. Fleming, Phys. Rev. B **38**, 913 (1988).

[7] P.E.A. Turchi, A.L. Wachs, Y.C. Jean, R.H. Howell, K.H. Wetzler, and M.J. Fluss, Physica C **153-155**, 157 (1988).

[8] T. Chiba, J. Chem. Phys. **64**, 1182 (1976).

[9] S. Tanigawa, Y. Mizuhara, Y. Hidaka, M. Oda, M. Suzuki, and T. Murakami, Mater. Res. Soc. **5**, 57 (1988).

[10] L.C. Smedskjaer, J.Z. Liu, R. Benedek, D.G. Legnini, D.J. Lam, M.D. Stahulak, and H. Claus, Physica C **156**, 269 (1988).

[11] A. Bansil, R. Pankaluoto, R.S. Rao, P.E. Mijnarends, W. Dlugosz, R. Prasad, and L.C. Smedskjaer, Phys. Rev. Lett. **61**, 2480 (1988).

[12] M.A. Beno, L. Soderholm, D.W. Capone II, D.G. Hinks, J.D. Jorgensen, J.D. Grace, I.K. Schuller, C.U. Segre, and K. Zhang, Appl. Phys. Lett. **51**, 57 (1987).

[13] S. Massida, J. Yu, A.J. Freeman, and D.D. Koelling, Physica C **122**, 198 (1987).

[14] H. Krakauer, W.E. Pickett, and R.E. Cohen, J. Supercond. **1**, 111 (1988).

[15] K.T. Park, K. Terakura, T. Oguchi, A. Yanase, and M. Ikeda, J. Phys. Soc. Jpn. **57**, 3445 (1988).

[16] W.E. Pickett, R.E. Cohen, and H. Krakauer, Phys. Rev. B **42**, 8764 (1990).

[17] J. Yu, S. Massida, A.J. Freeman, and D.D. Koelling, Phys. Lett. A **122**, 203 (1987).

[18] F.M. Mueller, C.M. Fowler, B.L. Freeman, W.L. Hults, J.C. King, and J.L. Smith, Physica B **172**, 253 (1991).

[19] C.M. Fowler, B.L. Freeman, W.L. Hults, J.C. King, F.M. Mueller, and J.L. Smith, Phys. Rev. Lett. **68**, 534 (1992).

[20] F.M. Mueller, Physica B **177**, 41 (1992).

[21] G. Kido, K. Komorita, H. Katayama-Yoshida, T. Takahashi, Y. Kitaoka, K. Ishida, and T. Yoshitomi, in *Advances in Superconductivity III*, edited by K. Kjimura and

H Hayakam (Springer Verlag, Tokyo, 1991), p 237

[22] G Kido, K Komorita, and Y Nakagawa, Physica B **177**, 46 (1992)

[23] F M Mueller (private communications)

[24] V I Nizhankovskii, R N Sheftal, and S G Zybcev (pre-print)

[25] M I Kaganov, I M Lifshitz, and K D Sinel'nikov, Zh eksp teor fiz **32**, 605 (1955) (Sov Phys JETP **5**, 500 (1957))

[26] D E Farrel, B S Chandrasekar, M R DeGuire, M M Fang, V G Kogan, J R Clem, and D K Finnemore, Phys Rev B **36**, 4025 (1987)

[27] PHILIPS PW 1710 spectrometer

[28] Field aligned $YBa_2Cu_3O_{7-\delta}$ powder embedded in epoxy, produced by W L Hults and J L Smith, Los Alamos National Laboratory

[29] DSP-56 Coprocessor board, Ariel Corporation, Highland Park, U S A

[30] D H Lowndes, K M Miller, R G Poulsen, and M Springford, Proc Roy Soc London A **331**, 497 (1973)

[31] P J M van Bentum, H van Kempen, L E C van de Leemput, J A A J Perenboom, L W M Schreurs, and P A A Teunissen, Phys Rev B **36**, 5279 (1987)

[32] J E Graebner and J E Kunzler, J Low Temp Phys **1**, 443 (1969)

[33] A J Arko, Z Fisk, and F M Mueller, Phys Rev B **16**, 1387 (1977)

[34] A J Arko, D H Lowndes, F A Muller, L W Roeland, J Wolfrat, A T van Kessel, H W Myron, F M Mueller and G W Webb, Phys Rev Lett **40**, 1590 (1978)

[35] J E Graebner and M Robbins, Phys Rev Lett **36**, 422 (1976)

[36] L W Gruenberg and L Gunther, Phys Rev **176**, 606 (1968)

[37] Z Tešanović, M Rasolt, and L Xing, Phys Rev B **43**, 288 (1991)

[38] R S Markiewicz, I D Vagner, P Wyder, and T Maniv, Solid State Comm **67**, 43 (1988)

[39] J M Valles Jr , R C Dynes, A M Cucolo, M Gurvitch, L F Schneemeyer, J P Garno, and J V Waszczak, Phys Rev B **44**, 11986 (1991)

[40] M Gurvitch, J M Valles Jr , A M Cucolo, R C Dynes, J P Garno, L F Schneemeyer, and J V Waszczak, Phys Rev Lett **63**, 1008 (1989)

[41] B Batlogg, T T M Palstra, L F Schneemeyer, R B van Dover, and R J Cava, Physica C **153-155**, 1062 (1988),
Y Matsuda, T Hirai, and S Komiyama, Sol St Comm **68** 103 (1988)

[42] D R Harshman, L F Schneemever, J V Waszczak, G Aeppli R J Cava, B Battlog, L W Rupp, E J Ansaldo, and D Ll Williams, Phys Rev B **39**, 851 (1989)

[43] M J Stephen, Phys Rev B **43**, 1212 (1991),
M J Stephen, Phys Rev B **45**, 5481 (1992)

[44] K Maki, Phys Rev B **44**, 2861 (1991)

[45] D Pines and P Nozieres, *The Theory of Quantum Liquids*, Addison-Wesley (1989)

[46] C M Varma, P B Littlewood S Schmitt-Rink, E Abrahams, and A E Ruckenstein, Phys Rev Lett **63**, 1996 (1989)

[47] S M Hayden G Aeppli, H Mook D Rytz, M F Hundley and Z Fisk Phys Rev

Lett. **66**, 821 (1991).

[48] F. Slakey, M.V. Kelin, J.P. Rice, D.M. Ginsberg, Phys. Rev. B **41**, 2109 (1990).

[49] A. Wasserman, M. Springford, and F. Han, J. Phys.: Condens. Matter **3**, 5335 (1991).

Chapter 5

Quantum oscillations in UPt_3 in high magnetic fields

5.1 Introduction

Over the past few years a new branch of metal physics has emerged which is rapidly developing Central are intermetallic compounds containing rare earth (predominantly Ce) or actinide (predominantly U) ions, displaying a very unusual low temperature behaviour Below a characteristic temperature T_{FL} they behave like Fermi liquids, where T_{FL} is in the order of tens of kelvin Here the part of the specific heat that is linear in T, γ, as well as the almost temperature independent magnetic susceptibility $\chi = \partial M/\partial B$ have exceptionally high values when compared to conventional metals This indicates a high density of states at the Fermi surface or, in other words, very high effective quasiparticle masses that can become as large as a few hundred times the free electron mass m_e Because of the presence of quasiparticles with large effective mass these systems are named heavy fermion systems or strongly interacting/correlated fermion systems Members of this family are for example $CeAl_3$, CeB_6, $CeCu_6$, $CeCu_2Si_2$, $CePb_3$, $CeRu_2Si_2$, $CeSn_3$, UBe_{13}, UPt_3, and URu_2Si_2

For temperatures much higher than T_{FL} the systems can be described best in terms of conduction electrons with conventional masses in addition to well localised f electrons ($4f$ for Ce, $5f$ for U) In this temperature range the magnetic behaviour associated with these localised moments is of the Curie- Weiss type It is the existence of interactions between the localised f electrons and the conduction electrons that causes the cross-over to the heavy fermion state at sufficiently low temperatures Thereby the system lowers its energy by losing the magnetic moments associated with the f electrons At the same time the f electrons become part of the Fermi surface, implying that they can no longer be perfectly localised

A closely connected phenomenon, where the localised magnetic moments in a metal are lost, is known as the Kondo effect [1] It deals with the ideal situation of a single magnetic impurity, embedded in a sea of conduction electrons Because of strong many-body effects such an impurity can form a singlet ground state with the surrounding conduction electrons and its moment effectively becomes screened The associated energy gain is $k_B T_K$, where the Kondo temperature T_K can vary between a fraction of a kelvin to hundreds of kelvin It has been known since 1930 [2] that in dilute magnetic alloys at low temperatures the resistivity, instead of dropping monotonically for decreasing temperature, displays a shallow minimum after which it starts to rise again Also in connection with this singlet formation there is an excess specific heat and spin susceptibility, i e , a contribution to the local density of conduction electron states In this single ion case all physical properties scale with respect to T_K, provided that T_K is not too large

Because heavy fermion systems have at least one magnetic ion per unit cell they have sometimes been referred to as 'Kondo lattice " systems Yet it does not mean that the heavy fermion state is a concentrated Kondo state, since interactions *between the magnetic impurities* should be considered As a consequence, the condensation energy as well as other physical properties (for instance the susceptibility per ion) are different from the single-impurity case

There is strong experimental evidence that in the low temperature limit heavy fermion systems can be described as normal Fermi liquids [6], so there is a one-to-one correspondence between the low energy excitations of the strongly correlated f electron system and those of a nearly free electron gas Since this chapter is dedicated to measurements on the compound UPt_3 some of its low temperature properties, which are thought to be characteristic of a Fermi liquid state, will be discussed Although these properties are not systematically observed in all heavy fermion compounds they nevertheless can be regarded as typical

First, the resistivity shows a cross-over to a new regime below 20 K At temperatures lower than approximately 1 5 K the temperature dependence has become quadratic ($\rho = \rho_o + AT^2$) This is indeed characteristic of a Fermi liquid, since $1/\tau \propto (k_B T)^2$ The quantity A is several orders of magnitudes larger than in conventional metals Second, also at very low temperatures, the specific heat C_v is closely linear in T ($C_v = \gamma T$), where $\gamma \approx 420$ mJ/moleK^2 for UPt_3 [7, 8, 9, 10], which is very large compared to 0 7 mJ/moleK^2 for copper In the Fermi liquid model the value of 420 mJ/moleK^2 leads to an average effective quasiparticle mass of $\approx$ 180 m_e [11] Third the low temperature magnetic susceptibility is virtually constant and (again) very large Furthermore the nuclear spin lattice relaxation rate $1/T_1$ shows a linear temperature dependence below 7 K, another indication of Fermi liquid behaviour [12]

However, the strongest justification for the Fermi liquid picture is the direct observation of long-lived fermion quasiparticles *by means of the dHvA effect* [13, 14, 15] A detailed study of the temperature dependence of the dHvA amplitudes yielded effective masses ranging from 15 m_e to 90 m_e, where the value depends on which Fermi surface sheet is considered and depending on the orientation in the magnetic field In section 5 4 the Fermi surface of UPt_3 will be discussed UPt_3 is not the only heavy fermion material for which dHvA measurements have established the existence of heavy quasiparticles on the Fermi surface Other examples are $CeCu_6$ [16, 17, 18, 19], CeB_6 [20, 21, 22], $CeRu_2Si_2$ [15], $CeAl_2$ [15, 18, 23], $CeNi$ [22], and $CeCu_2Si_2$ [24]

Until this point I have not mentioned the intriguing property that several heavy fermion compounds show superconducting and/or magnetic phase transitions at low temperatures UPt_3 is one of them it becomes superconducting below $T_c = 0\ 5$ K, i e , it develops from within the heavy fermion state What is more, the occurrence of antiferromagnetic ordering below 5 K suggests an unusual form of the superconductive ground state, since magnetic moments are usually believed to destroy the superconductive ground state The next section will be devoted to this topic

5.2 Magnetic order and superconductivity

Numerous heavy fermion compounds share the common low temperature feature of developing small ordered moments out of antiferromagnetic spin fluctuations involving different f sites This is also the case for UPt_3 The observation of a $T^3 \ln T$

contribution to the low temperature specific heat was the first indication of spin fluctuations [7] in this material The presence of such a term is not unusual in Fermi liquid theory [25] Spin fluctuations are best discussed in terms of a generalised susceptibility $\chi(\mathbf{q},\omega)$, which measures the response of a system to an applied magnetic field varying in time and space characterised by a wave vector $\mathbf{q}$ and a frequency ω Singularities or resonances in the imaginary part of the susceptibility, $\chi''(\mathbf{q},\omega)$, reveal the spectrum of the magnetic excitations A powerful technique to measure these excitations is thermal neutron scattering The neutrons will interact via the magnetic dipole-dipole interaction with the spins and in this the way probe both the spatial and temporal correlations in the spin density On one hand this can be a static spin density distribution, measured with elastic ($\hbar\omega = 0$) neutron scattering On the other hand it is possible to probe the dynamic excitation spectrum with inelastic ($\hbar\omega > 0$) scattering

Neutron scattering studies of Aeppli *et al* [26] have considerably clarified the fluctuation spectrum of UPt_3 They confirm the existence of inter-site spin fluctuations as well as a large background amplitude corresponding to local spin fluctuations, independent of $\mathbf{q}$ The local magnetisation fluctuates at a typical rate, or energy, of approximately 10 meV On a smaller energy scale of 5 meV, there exists a tendency for neighbouring moments to be weakly antiferromagnetically correlated in the $\mathbf{q} = (0,0,1)$ direction As a function of temperature, these correlations seem to be developing when the temperature is decreased below 17 K, at which temperature a weak maximum is observed in the bulk susceptibility

At a still lower energy of the order of a few tenths of a meV (i e , on a relatively long time scale), the moments are antiferromagnetically correlated in the $\mathbf{q} = (\pm\frac{1}{2},0,1)$ direction (see figure 5 1) It was even more surprising that in this direction and below 5 K also small elastic ($\hbar\omega = 0$) peaks were observed, suggesting static ordering The corresponding ordered moment was determined to be only $(0\ 02 \pm 0\ 01)\mu_B$, or about one percent of the intrinsic $5f$ moments seen in the Curie–Weiss susceptibility Although this ordering was observed in all samples studied by Aeppli and coworkers, as well as in samples of different origin by Taillefer and coworkers [27], it is still not firmly settled whether this magnetic ordering is really intrinsic The reason for this is that the width of the $(\pm\frac{1}{2},0,1)$ peak is not limited by the resolution of the apparatus so there must be some remnant disorder in the samples Furthermore there is no observation yet of a corresponding anomaly in bulk properties such as specific heat or magnetisation

The discovery of a superconducting ground state in several heavy fermion compounds was rather unexpected, since magnetic ions were mainly known to act as pair breakers for the superconducting pairs For superconductivity to occur, there must be an attractive interaction between the quasiparticles In the case of "conventional" superconductors this is possible because of electron-phonon-electron interactions However, the formation of superconducting pairs can also be obtained via other fermion-fermion interactions, i e , without invoking phonons A well-known example is the superfluidity of ^3He In this system a fermion-fermion interaction between the ^3He atoms is generated by the exchange of spin fluctuations (see for ex-

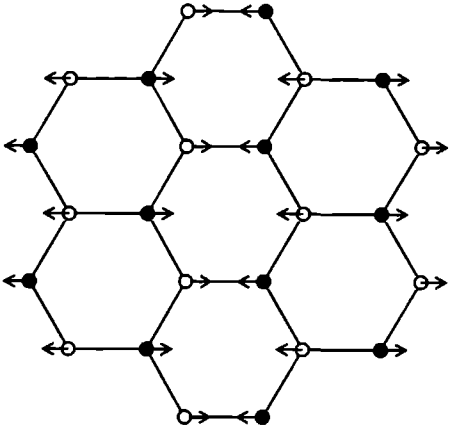

Figure 5.1 Weak static magnetic antiferromagnetic order in the direction $\mathbf{q} = (\frac{1}{2}, 0, 1)$ which is slowly developing below 5 K The open and closed circles refer to uranium ions in adjacent planes of the hexagonal ($SnNi_3$) structure The distance between the planes is $c/2$ (after Aeppli *et al* [26])

ample Leggett [28]) The interaction is attractive for pairs with parallel spin The strongly repulsive short-range part of the interaction is avoided by forming pairs with finite angular momentum and spin-triplet pairing in a $l = 1$ (p-wave) state is found to be the most favourable It has been suggested that a similar situation is the case in heavy fermion systems, where spin fluctuations have been observed and strong local quasiparticle repulsion is caused by the fact that it is energetically unfavourable for two f electrons to occupy the same site Yet there are also numerous differences between ^{3}He and heavy fermion systems, as pointed out in reference [29] For instance the electrons which form the superconducting pairs in the heavy fermion systems are charged, while the ^{3}He atoms are neutral Furthermore, in contrast to ^{3}He atoms, the electrons in a heavy fermion system move about in a periodic lattice

Several low-temperature properties of UPt_3 point at the possibility that the superconductive ground state is unconventional The observation of a power law temperature dependence of ultrasonic attenuation [30] and heat capacity [10, 31] below T_c seem to exclude the presence of an energy gap, which is non-zero over the whole of the Fermi surface, since otherwise the low energy excitations would die out exponentially with temperature Interpretations have been made in terms of a gap parameter with line or point nodes on the Fermi surface, as opposed to a simple scalar parameter

Another peculiarity of the superconducting state is evident when the field-temperature phase diagram is considered In the last three years a number of experiments have revealed the presence of three superconducting phases (see figure 5 2) The most direct evidence for this comes from specific heat measurements [10]

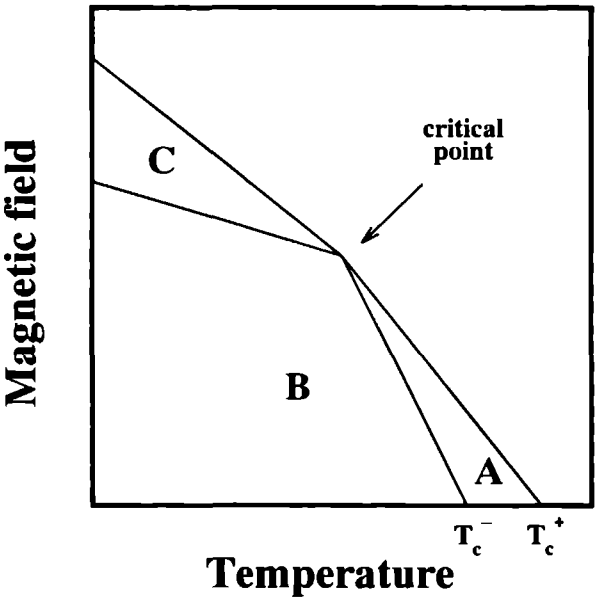

Figure 5.2 Schematic representation of the superconducting phase diagram of UPt_3 in the $B - T$ plane The lines denote the collection of points where anomalies have been observed in the specific heat, ultrasound velocity, and thermal expansion measurements Three phases have been distinguished – labeled A, B, and C – for both $\mathbf{B} \parallel c$ and $\mathbf{B} \perp c$

Instead of one, two sharp discontinuities have been observed in C_v at $T_c^+ = 490$ mK and $T_c^- = 435$ mK Application of a magnetic field [31] causes a lowering of both T_c^+ and T_c^-, as well as a decrease in $(T_c^+ - T_c^-)$ The two transitions merge into each other at a critical point ($B \simeq 0\,5$ T, $T \simeq 400$ mK) for $\mathbf{B} \perp c$ and ($B \simeq 1$ T, $T \simeq 350$ mK) for $\mathbf{B} \parallel c$ Also anomalies in ultrasound attenuation [32], ultrasound velocity [33] and the linear thermal expansion [34] have added proof to the existence of multiple superconducting phases Another indication is the observation of a sharp kink in B_{c1} [35] and B_{c2} [36] as a function of temperature The boundary that separates phases B and C has been seen in ultrasound attenuation [32] and ultrasound velocity [33] measurements

In a recent review by Taillefer *et al* [37] the various superconducting properties are described in more detail and includes a discussion on several proposed models to explain the phase diagram For instance, the smallness of the splitting of the superconductive transition is interpreted in terms of a symmetry breaking field [38, 39] provided by the weak magnetic order below 5 K It distorts the hexagonal symmetry and lifts a degeneracy in T_c Another perspective is of group theoretical origin [40], where it has been inferred that the multiple phases in the $B - T$ di-

agram can be the result of a coupling of the superconducting and magnetic order parameters

5.3 The metamagnetic transition of UPt_3

In order to shed more light on the nature of magnetic interactions in heavy fermion compounds, external magnetic fields can be applied Anomalies in zero field properties, observed at an energy $k_B T^*$, have a corresponding anomaly at the Zeeman energy $\mu_B B^*$ For example UPt_3 shows a maximum in χ at 17 K in zero field, which relates to a strong peak in the low temperature magnetic susceptibility around $B^* = 20$ T [41] To be more specific, the bulk average magnetisation increases linearly below 17 T and shows a step-like increase, centered around 20 T The step size corresponds to a magnetisation jump of $\approx 0\,3\ \mu_B$ per U ion The magnetic field clearly drives the system out of its zero-field ground state and this field-induced transition is called a metamagnetic transition A similar observation is made for $CeRu_2Si_2$, where a maximum in χ at 10 K in zero field corresponds to a maximum in χ at $B^* = 8$ T [42] For both systems the transition becomes more abrupt when the temperature is lowered

However, there are some qualitative differences between the two compounds The transition in $CeRu_2Si_2$ only occurs for a field along the tetragonal c axis and therefore has a one dimensional character, whereas for UPt_3 the transition is seen for all field directions in the $a-b$ hexagonal basal plane, thus showing a two dimensional character Other differences are that $CeRu_2Si_2$ is not a superconductor nor does it show static magnetic ordering

Inelastic neutron scattering experiments on $CeRu_2Si_2$ [43] in magnetic fields yield a strong reduction of slow antiferromagnetic fluctuations when $B \approx 8$ T, while the background of local spin fluctuations survives the transition Such experiments have not been done yet for UPt_3 because of its high value of B^*, so this microscopic signature of the metamagnetic transition in UPt_3 still remains to be confirmed Nevertheless, since there are strong similarities between the magnetic properties of UPt_3 and $CeRu_2Si_2$, there is reason to believe that the metamagnetic transition has a common origin in both compounds

Anomalies in other physical properties have been observed around B^* The coefficient γ of the linear-in-T term in the specific heat exhibits a maximum (about 50% larger than the zero field value) at the metamagnetic transition [44, 45] Also the coefficient A of the quadratic-in-T term in the electrical resistivity shows a maximum at B^*, where it attains almost three times the zero field value [46] Interpreting the field dependence of χ, γ and A, the average effective mass of the quasiparticles appears to increase when the metamagnetic transition is approached and even for fields larger than B^* it remains considerably enhanced

As described in section 5 2 the superconducting state at $B = 0$ develops within the heavy fermion state By applying a magnetic field that is larger than $B_{c2} \approx 2\,5$ T the system is driven normal again, i e , a heavy fermion liquid A pressing question

is of course how this Fermi liquid is affected by the magnetic field and, specifically, what happens at the metamagnetic transition to what extent will the Fermi surface become modified and what will happen to the effective masses of the quasiparticles? These questions are addressed and partially answered in sections 5.5 to 5.7. First the calculated *and measured* Fermi surface of UPt_3 are briefly discussed.

5.4 The Fermi surface of UPt_3

The existence of long-lived quasiparticles with enormously high effective masses was confirmed directly by de Haas – van Alphen measurements. In the case of UPt_3 a detailed study of the temperature and angle dependence of the dHvA oscillations was performed by Taillefer *et al* [13, 14]. This has led to a clear picture of the dimensions and topology of the Fermi surface as well as the mass enhancements for the various Fermi surface sheets. Band structure calculations are a standard tool for understanding the electronic structure in metals. Also in the case of UPt_3 they have been performed, based on density functional theory within the local density approximation (LDA) [47].

It was found that good agreement with the experimentally determined Fermi surface shape is only obtained if the $5f$ electrons on the U ions are treated as itinerant, hybridising with the other conduction electrons. If the $5f$ electrons are forced to occupy core states of the U ions the outcome of the calculations is in clear disagreement with the experiments. It is therefore concluded that the $5f$ electrons are part of the Fermi surface volume.

The Fermi surface of UPt_3 consists of five sheets as illustrated in figure 5.3. It shows the results of calculations by McMullan [48], based on the linear muffin tin orbital (LMTO) method and is in very good agreement with those of Norman *et al* [47]. Sheets (1) and (2) form closed electron-surfaces centered on Γ in the Brillouin zone. Sheet (3) makes up a large electron-surface centered on Γ, as well as closed surfaces around the K point. Furthermore there is a closed hole-surface (5) centered on A, which is disk shaped. Finally, sheet (4) is a hole-surface with interconnecting arms in the MKLH planes. It nearly touches the disk-like sheet (5) in the $A-\Gamma$ direction. In UPt_3, in contrast to many other heavy fermion compounds, *all* observed dHvA frequencies are being accounted for.

Although band calculations fairly well predict the measured Fermi surface topology, they fail to reproduce the large effective masses as measured via the temperature dependence of the dHvA oscillation amplitudes. The masses range from 25 to 90 m_e for the magnetic field along the a axis and from 15 to 50 m_e along the b axis [13, 14]. The higher the dHvA frequency, the larger m^* and the quasiparticles corresponding to the largest Fermi surface part are the heaviest ever observed in any metal. The ratio m^*/m_{CALC} of the measured effective mass m^* and the calculated mass m_{CALC} is very high for all sheets of the Fermi surface, between 12 and 26 depending on the sheet.

All dHvA measurements on heavy fermion systems have been interpreted in

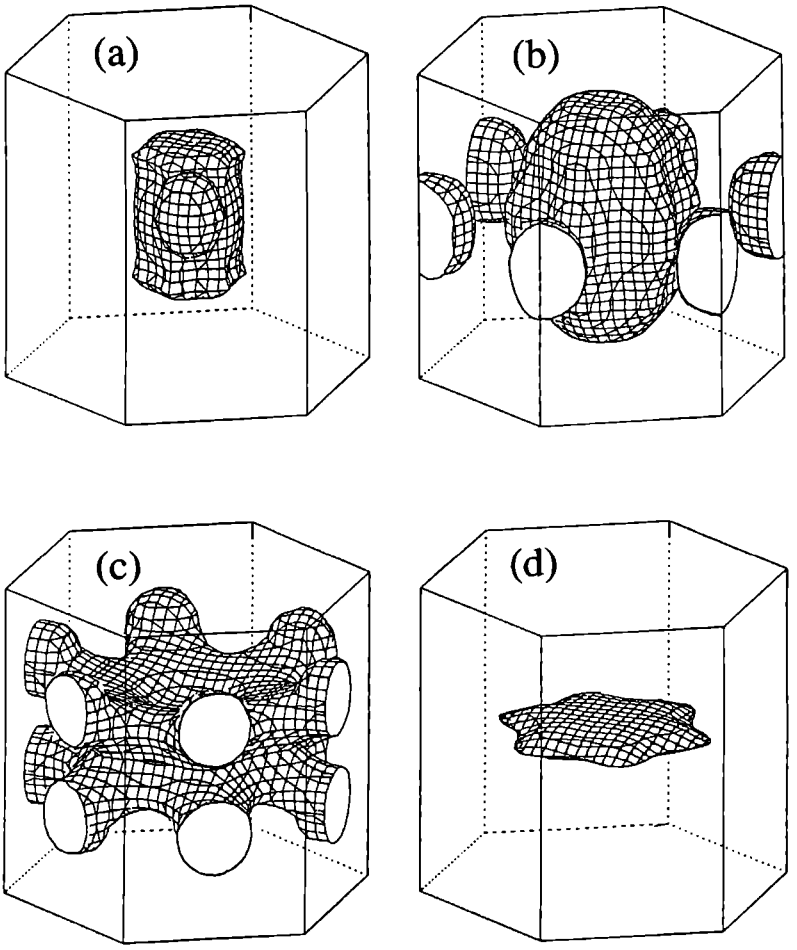

Figure 5.3 Calculated Fermi surface sheets of UPt_3 [48]: (**a**) sheets (1) and (2) are centered on Γ; (**b**) sheet (3) also centered on Γ; (**c**) sheet (4) is centered on A; (**d**) sheet (5) centered on A.

terms of the standard Lifshitz–Kosevich formula, i e , it is assumed that the system is a Fermi liquid Note that the LK expression is derived for independent Bloch electrons without implementing many-body interactions, but in the case of heavy fermion systems these very interactions play a dominating role!

Most theoretical studies of the influence of many-body interactions on the dHvA effect have been confined to systems where the mass enhancement is moderate, leading to the result that the oscillating part of the free energy is hardly influenced except for a renormalisation of the quasiparticle effective mass For heavy fermion compounds the many-body interactions are very strong In order to calculate the dHvA amplitude for heavy fermion compounds, there have been theoretical attempts [49, 50] based on the Anderson model [51] It is concluded that the Lifshitz–Kosevich expression is – apart from a substantial mass enhancement the dHvA - still a good approximation when describing quantum oscillations of the free energy, the dHvA frequency, which provides information on the Fermi surface topology, is essentially unchanged

5.5 Magnetoresistance oscillations in high magnetic fields

In the light of the presence of the metamagnetic transition, it is interesting to study the evolution of the quasiparticle bands as the metamagnetic transition is crossed For the first time this has been studied [52] in the compound $CeRu_2Si_2$, for which band structure calculations [53] also reasonably well account for the measured Fermi surface However, the mass enhancement m^*/m_{CALC} below the transition, which occurs at $B^* = 8$ T, varies considerably (1 to 20) from sheet to sheet and light and heavy quasiparticles seem to *coexist* in this material This is not the case for UPt_3, where all quasiparticle bands are uniformly strongly renormalised Also, in $CeRu_2Si_2$ *only the lightest quasiparticles* can be observed both below and above B^* Their corresponding Fermi surface sheets appear to be only slightly affected by the occurrence of the metamagnetic transition Two surfaces with large masses were observed above the transition but could not be followed into the low field state because the oscillation amplitude decreases rapidly with decreasing field (see equation (1 34)) Finally, since the transition only occurs for $\mathbf{B} \parallel c$, a straightforward study of the field dependence of the Fermi surface topology was not possible in the high field state This uncomplete picture seriously hampers a full understanding of the field dependence of the Fermi surface

Because for $CeRu_2Si_2$ the value $B^* \approx 8$ T, it is relatively easy to study changes in its physical properties Much less accessible is the 20 T metamagnetic transition of UPt_3 With hybrid magnets we are able to explore the high field state of this compound and we have performed a series of experiments in high magnetic fields up to 30 T, observing the quantum oscillatory behaviour of an ultrapure UPt_3 single-crystal, which has been grown in the UHV materials preparation laboratory of the Cavendish Laboratory

Rather than using the dHvA effect we have exploited the related method of measuring the oscillatory behaviour of the resistance, the Shubnikov – de Haas (SdH) effect The effect can be qualitatively understood in terms of the probability of quasiparticle scattering Oscillations of the density of states at the Fermi energy means that the number of states, into which the quasiparticles can scatter, oscillates The relaxation time of excitations is proportional to the number of available states, therefore the resistance will oscillate in pace with the oscillations in the density of states at the Fermi energy The theory of the effect is in fact quite complicated [54], since it involves the problem of electron scattering in a magnetic field Compared to the dHvA method, measuring the resistance is a non-inductive way to extract Fermi surface information Because of the higher noise level of hybrid magnets (section 2 2 2), compared with superconductive magnets, this has been a real advantage

Because of the very high quasiparticle masses in UPt_3 the factor

$$\frac{X_T}{\sinh X_T} \quad \text{with} \quad X_T = 14\,69 \left(\frac{m^*}{m_e}\right) \frac{T}{B} \tag{5 1}$$

which expresses the temperature dependence of the quantum oscillation amplitude, is extremely small, calculated for the typical circumstances $T = 1$ K and $B = 10$ T For $(m^*/m_e) = 1$ this factor is about 0 85, but when $(m^*/m_e) = 100$ it is only $\sim 10^{-41}$! It shows that temperature plays a very dominating role in the observation of quantum oscillations in heavy fermion compounds and that the millikelvin temperatures produced by the plastic-tail dilution refrigerator are an absolute prerequisite in order to compensate for the high masses

Finally, the role of sample purity is very important and often underestimated The damping of the oscillation amplitude is reflected in the Dingle factor – see equation (1 30) dHvA measurements on UPt_3 by Taillefer *et al* [13] have revealed an effective mean free path $l_e \approx 2000$ Å (as defined in section 1 4 2) for the largest Fermi surface sheet, derived from the field dependence of the dHvA oscillation amplitude These samples were prepared in ultrahigh vacuum using zone-refining In order to demonstrate the influence of the negative-exponential Dingle factor one can calculate the relative decrease of the signal (for example at $B = 10$ T) in case the effective mean free path is 1000 Å, 500 Å, or 300 Å instead of 2000 Å the signal strength will decrease by a factor of $1\,2 \times 10^{-2}$, $1\,8 \times 10^{-6}$ and $1\,9 \times 10^{-13}$, respectively It shows the importance of sample preparation in relation to quantum oscillation experiments! In this respect, application of high magnetic fields can partially neutralise the influence of impurities

The next two sections describe the results of a series of quantum oscillation measurements on UPt_3, applying magnetic fields up to 30 T

5.6

Observation of heavy fermion quasiparticles in UPt_3 above the metamagnetic transition*

S. R. Julian[a], P. A. A. Teunissen[b], and S. A. J. Wiegers[b]

(a): Cavendish Laboratory, Madingley Road, Cambridge, CB3 OHE, UK
(b): High Field Magnet Laboratory and Research Institute for Materials, University of Nijmegen, Toernooiveld, NL-6525 ED Nijmegen, The Netherlands

Abstract. Quantum oscillations of the transverse magnetoresistance have been observed in the heavy fermion metal UPt_3, in fields up to 24.5 T applied in the basal plane, providing the first observation of the quasiparticle Fermi surface above the metamagnetic transition. The observed quasiparticle masses remain strongly renormalised in the high field state, ranging from 30 to approximately 100 times the bare electron mass.

Introduction. The intermetallic compound UPt_3 offers an outstanding example of the fascinating complexity of the behaviour that can result from the involvement of f electrons in the Fermi surface. At low temperature UPt_3 has a large linear specific heat coefficient, $\gamma \approx 420$ mJ/molK^2 [41, 55] which de Haas – van Alphen (dHvA) experiments have shown to be explainable in terms of fermion quasiparticles with very large effective masses, ranging from 25 to approximately 90 times the bare electron mass [14]. UPt_3 also has a novel, multi-component superconducting phase diagram, and is very weakly antiferromagnetic below 5 K (for a recent review see reference [37]). Finally, the subject of this paper is a metamagnetic-like transition at $H_c \approx 20$ T with H in the basal plane, where the internal magnetisation jumps by about 0.3 μ_B per uranium atom [41]. The signature of this transition is a peak in the differential magnetic susceptibility, $\chi_M = dM/dH$, which becomes narrower as the temperature is lowered. This peak is accompanied by a weaker peak in γ, which attains a value of about 625 mJ/molK^2 at H_c [44, 45].

Well characterised metamagnetic transitions occur in two heavy fermion metals, UPt_3 and $CeRu_2Si_2$ (reviewed in reference [37]). The detailed mechanism of the transition is not established, and it is hoped that Fermi surface measurements will clarify the situation. The main questions to be addressed are whether the Fermi surface is rearranged at the transition by, for example, exchange splitting of the quasiparticle bands, or, more radically, localisation of the f electrons, and whether the quasiparticles continue to be as strongly renormalised in the high field state. If the Fermi surface topology changes at the metamagnetic transition, then it will be

* This section has been published in Physica B **177**, 135 (1992).

interesting to see if the success of the LDA Fermi surface calculations [47] extends to the high field state Howard and coworkers [15, 52] have in fact observed dHvA oscillations in the high field state of $CeRu_2Si_2$ The transition in this material is however only accessible with the field near the c axis, so determination of the high field Fermi surface topology was not possible Furthermore the low value of the transition field (8 T for $\mathbf{H} \parallel c$) made it impossible to follow surfaces with large masses – two were seen above the transition – into the low field state

The purpose of the present work is thus to determine quasiparticle masses and the Fermi surface topology in UPt_3 above the metamagnetic transition The quantum oscillatory magnetoresistance rather than the dHvA effect is being used following the recent observation of remarkably strong oscillations of the Shubnikov – de Haas (SdH) type in ultrapure single-crystal whiskers of UPt_3 [56], which followed the observation of weak magnetoresistance oscillations in a previous generation of samples [57] These measurements [56], at temperatures as low as 17 mK in fields up to 14 5 T, have found quasiparticle bands ranging in size from 1 5 MG to approximately 60% of the Brillouin zone area, some of which were observed in earlier dHvA work [14], while others represent previously unobserved quasiparticle bands with masses ranging up to 200 m_e, the heaviest quasiparticles yet seen in a heavy fermion system

Experiment. Fermi surface studies using quantum oscillations present considerable technical challenges, especially in the realm of sample preparation, because normally the signal level drops rapidly with increasing quasiparticle mean free path The sample used in this study is a $50\,\mu\text{m} \times 160\,\mu\text{m} \times 4\,\text{mm}$ single-crystal whisker grown in ultra-high vacuum The magnetoresistance oscillations in the sample are at least a factor of ten larger than those observed in the previous generation of samples [36, 46] This demonstrates an improvement in quality that is partially reflected in the value of ≈ 3000 for the ratio of the room temperature resistance to the extrapolated 0 K resistance (averaged over length), an improvement by a factor of two over what was previously attained

The experiments were done in the 25 T hybrid magnet at the Nijmegen High Field Magnet Laboratory [58] To reach the low temperatures required for observation of quantum oscillations in large-γ systems a dilution refrigerator [59] with a room temperature diameter of 32 mm, designed and built at the High Field Magnet Laboratory, was used This refrigerator has one continuous heat exchanger in which the dilute phase occupies a long spiral channel machined in a 16 mm diameter epoxy rod, 40 cm in length while the concentrated phase flows inside a 0 3 mm inner diameter copper-nickel capillary doubly spiraled inside the channel The channel is sealed by a close fitting epoxy sleeve, with a plastic to metal seal at the 1 K plate Temperatures as low as 30 mK have been obtained with the first version of this refrigerator The sample mounted below the mixing chamber on a platform that can be rotated in situ to change the angle of the field in the basal plane has reached temperatures as low as 50 mK The field angle relative to the crystal axes is de-

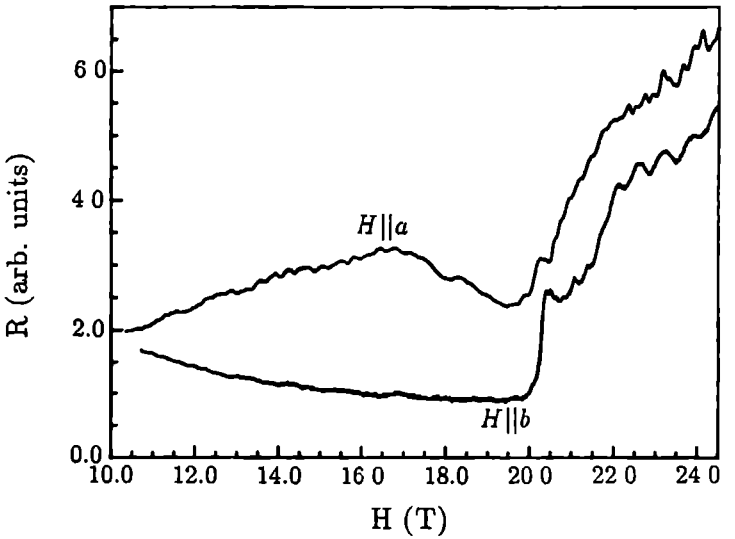

Figure 5.4 Resistance, in arbitrary units, as a function of field with the field roughly parallel to the a axis (top curve) and the b axis (bottom curve) The lower curve has been shifted downwards so that the curves do not overlap The metamagnetic transition is marked by a sharp increase in the resistance between 20 and 20 5 T Quantum oscillations in the magnetoresistance are clearly visible above the metamagnetic transition, particularly above about 22 T, where the slope of the non-oscillatory magnetoresistance decreases

termined using the angle dependence of the non-oscillatory magnetoresistance [46], and by comparing frequencies seen below 14 5 T with previous dHvA [14] and SdH [56] results Heat sinking is via high purity silver wires fed through a conical plug into the mixing chamber to some sintered silver powder Current and voltage leads to the sample are arranged in such a way that pick-up from the field is minimised, to the extent that at the frequencies used ($\approx$ 1000 Hz), noise arising from vibrations and flux noise in the magnet is reduced close to the level of the Johnson noise of the lead resistance, eliminating the need of a modulation field

Results. In figure 5 4 the magnetoresistance, $R(H)$, along the two symmetry directions in the basal plane is plotted as a function of field at 55 mK In both scans quantum oscillations are clearly observable both above and below H_c, which is marked by a sudden increase of $R(H)$ just above 20 T, as found in reference [46] The high frequency "fuzz" below 20 T in the lower scan is noise

For approximately 2 T on either side of the transition the oscillations are weak and their frequencies appear to be somewhat unstable The weakening of the oscillations is consistent with the peak in γ at H_c, but inhomogeneities in the non-linear magnetisation and magnetostriction near the transition may equally well be respon-

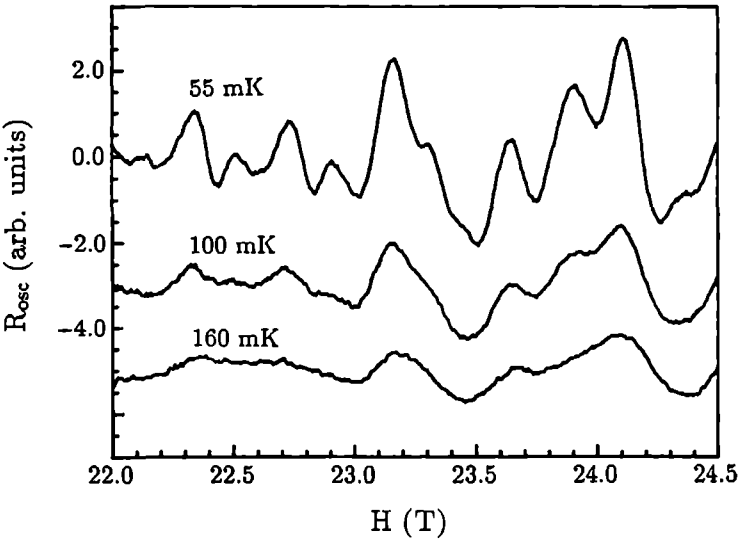

Figure 5.5 Temperature dependence of magnetoresistance oscillations between 22 and 24 5 T The field is oriented within a few degrees of the *a* axis, and the non-oscillatory background has been subtracted from the data The fact that increasing the temperature from 55 to 160 mK damps the oscillations so strongly implies that there are no light quasiparticles in this field range

sible for both the weakness and the instability of the signals The signals close to the transition are still further being analysed, and will not be discussed further here Above the transition the oscillations stabilise at about 22 2 T, the field at which the magnetoresistance flattens out, an effect seen clearly only near the symmetry axes

Mass studies were done with the field close to the *a* axis, where the strongest oscillations are found In figure 5 5, typical scans above 22 T are plotted, showing the strong damping of the oscillations by increasing temperatures These data have been analysed assuming that the expression of Lifshitz and Kosevitch [60] can be applied In figure 5 6 the resulting frequency spectrum of the magnetoresistance oscillations observed with the field between 22 2 and 24 5 T near the *a* axis, is plotted, and the effective mass associated with each frequency shown No light masses are observed Indeed, comparing orbits of similar size, these masses are as large or larger than those seen in UPt_3 below 14 5 T [14] The specific heat coefficient γ in this field range in 20 to 30% larger than between 10 and 14 T [44, 45] so the observed masses are consistent with an interpretation in which γ is due to fermion quasiparticles above as well as below, the metamagnetic transition

A definitive statement about the topology of the Fermi surface above H_c must wait until the dependence of the frequencies on angle has been analysed Some cautionary comments are in order however Comparing figure 5 6 with frequencies observed on the *a* axis below the transition shows two points of disagreement a

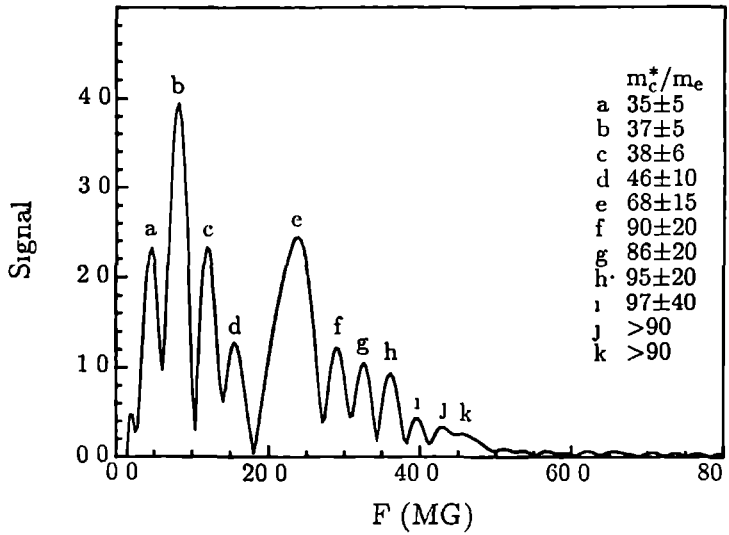

Figure 5.6 Frequency spectrum of magnetoresistance oscillations observed with the field between 22 2 and 24 5 T oriented near the a axis at 55 mK The ratio of the effective mass m^* to the bare electron mass m_e is given for each peak

90 m_e surface at 60 MG seen below the transition [14, 56] is not seen above, and a series of peaks with equally large masses found above the transition were not seen on dHvA experiments below the 14 5 T These discrepancies might be trivially explained, however, so they do not constitute proof that a Fermi surface rearrangement has taken place For example, the 60 MG quasiparticles may be heavier above the transition than below, and so be too weak to be seen at 55 mK at 24 T, while the lower frequencies, or at least one very much like it, has in fact been observed within 10° of the a axis in magnetoresistance measurements below 14 T, so it may not be a new feature of the high field state Only clear topological differences qualify as a demonstration of a substantial Fermi surface rearrangement It is worth noting that because the peaks between 28 and 42 MG are evenly spaced and have similar masses, an obvious and attractive interpretation is that they are due to a spin split surface on which the splitting has zeroes at four symmetric points Evidence for the existence of such zeroes comes from preliminary calculations by McMullan [56]

The frequency spectrum of $R(H)$ with H between 22 2 and 24 5 T oriented near the b axis (the lower scan in figure 5 4) shows only a single, strong, well defined frequency near 8 5 MG, in marked contrast to the large number of frequencies

observed near the a axis.

Conclusion. Preliminary results of a Fermi surface study above the metamagnetic transition in UPt_3 have been presented. For fields above 22 T there are well defined quantum oscillations in the transverse magnetoresistance. When these are analysed to derive Fermi surface areas and quasiparticle masses, the masses are found to be of a similar size to those observed in the low field state, so that the metamagnetic transition does not cause a dramatic change in the quasiparticle mass. The masses found are of such a size that, barring pathologically shaped Fermi surfaces, they should be sufficient to explain most or all of the linear specific heat observed above the metamagnetic transition.

Future work will concentrate on the angle dependence of the frequencies, the field dependence of the quasiparticle masses, construction of a Fermi surface model for the high field state, and on understanding the behaviour of the frequencies as the metamagnetic transition is approached.

Acknowledgements. The authors are indebted to G.G. Lonzarich for help and advice given at several stages of this investigation, and wish also to thank J.A.A.J. Perenboom and A. de Visser for helpful discussions. Access to the Nijmegen High Field Magnet Laboratory was made possible by the Large Installations Plan of the European Community.

5.7

Fermi surface of UPt_3 from 3 to 30 T: Field-induced quasiparticle band polarisation and the metamagnetic transition*

S. R. Julian[a], P. A. A. Teunissen[b], and S. A. J. Wiegers[b]

(a): Cavendish Laboratory, Madingley Road, Cambridge, CB3 OHE, United Kingdom
(b): High Field Magnet Laboratory and Research Institute for Materials, University of Nijmegen, Toernooiveld, NL-6525 ED Nijmegen, The Netherlands

Abstract. The magnetic-field dependence of the Fermi surface of UPt_3 has been studied up to 30 tesla from 17 to 150 mK using the quantum oscillatory magnetoresistance. Near the 20 T metamagnetic transition rapid changes in the frequency spectrum indicate strong nonlinear magnetic splitting of the quasiparticle bands; weaker nonlinear splitting is seen at all fields. Above the transition the mass enhancement remains very large, and masses exceeding $100\,m_e$ have been observed. Below the transition a surface with mass $170\,m_e$ has been found.

The enormous magnetic susceptibility of the heavy fermion metals means that large magnetic polarisations can be induced by laboratory scale magnetic fields. For example, UPt_3 below 1 K [61] is a Pauli paramagnet up to $H = 17$ T, and over this range the magnetic moment per uranium atom increases linearly from 0 to $\sim 0.3\,\mu_B$. Above 17 T the moment grows even faster, as the differential magnetic susceptibility, $\chi(H) = dM(H)/dH$, shows an upturn which culminates in a sharp peak at 20 T: the so called metamagnetic transition [37]. The induced moment thus reaches $\sim 0.6\,\mu_B$ per uranium atom at 22 T [41], a polarisation comparable to that of ferromagnetic nickel.

A central question is whether the induced magnetisation can be described in terms of a difference between the up- and down-spin Fermi surface volumes. This is the case for example with the spontaneous magnetisation of iron at $T = 0$ [62], but not with gadolinium, where most of the moment arises from localised f electrons, which polarise the conduction bands by exchange [63]. At low fields the f electrons in UPt_3 are delocalised [14, 47], in which case large field-induced spin splitting of the bands should occur. Once the system is polarised Luttinger's theorem can break down however, and non-Fermi liquid magnetic degrees of freedom may appear accompanied by a change in the total Fermi surface volume.

* This section has been published in Physical Review B **46**, 9821 (1992).

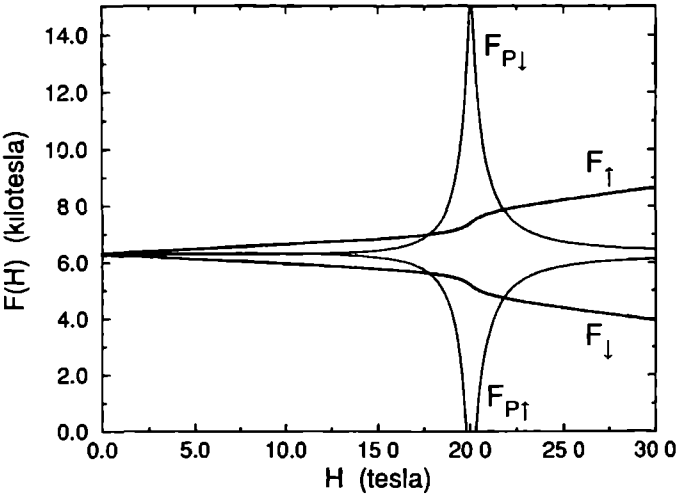

Figure 5.7 Variation with field of the "instantaneous" frequency $F_\sigma(H)$, compared to that of the measured frequency $F_{p\sigma}(H)$, for a simplistic model of band magnetism in which the difference in up- and down-pseudospin extremal areas is proportional to the magnetisation Note that the larger surface can produce the smaller frequency

We note that neither the underlying mechanism of the metamagnetic transition, nor the nature of the high field state, are understood although several theories exist [64] One of the major stumbling blocks is uncertainty over the role of quasiparticle band polarisation in the transition

In this paper we present measurements of the quantum oscillatory magnetoresistance of UPt_3 *both above and below the metamagnetic transition* We have found compelling evidence that the quasiparticle bands are subject to a strong nonlinear spin splitting at the metamagnetic transition Furthermore we have observed nonlinear spin splitting of the Fermi surface *when* $M(H)$ *is itself linear* (i e , far from the metamagnetic transition), suggesting that the Pauli paramagnetism of heavy fermion metals is not a straightforward phenomenon Finally, our measurements confirm by direct observation that above the metamagnetic transition the polarised quasiparticles remain very massive, the largest mass seen above 20 T being 110 m_e These findings stem from observations of large, heavy, *thermodynamically dominant* Fermi surface sheets in the system, a condition which must be satisfied before rigorous comparisons with either thermodynamic measurements or band structure and many body calculations can be made We note that these conditions have not yet been reached in other heavy fermion systems with field-induced transitions [37, 24]

Magnetoresistance oscillations (sometimes called the Shubnikov - de Haas (SdH) effect) are produced by modulation of the density of states as Landau levels pass through extremal cross sections of the Fermi surface When an extremal cross

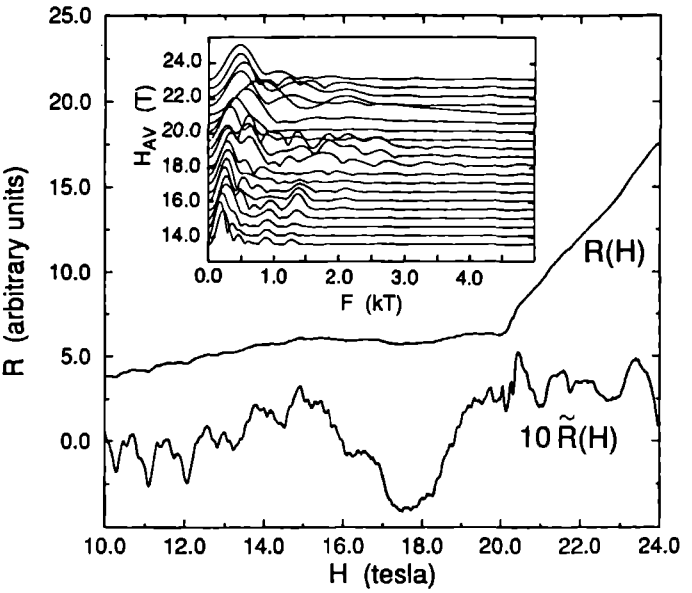

Figure 5.8 Variation from 10 to 24 T of the magnetoresistance before ($R(H)$) and after ($\tilde{R}(H)$) subtraction of the non-oscillatory background. Inset: the corresponding variation with field of the frequency spectrum. The spectra are the Fourier transforms (in $1/H$) of consecutive, overlapping, 2 T wide sections, centered on H_{av}. A striking modification of the spectrum is seen as the transition is approached. The field is 22° from the a axis in the basal plane, at $T \approx 60$ mK.

section A_σ is field *independent* the modulation is periodic in $1/H$ with frequency $F_\sigma = (\hbar/2\pi e)A_\sigma$ [65], but a central feature of our measurements is the observation of field *dependence* of the Fermi surface, in which case the experimentally measured quantity is the "projected" frequency [66] $F_{p\sigma}(H) = F_\sigma(H) - H\mathrm{d}F_\sigma(H)/\mathrm{d}H + \cdots$. In order to illustrate this important technical point, we show in figure 5.7 the field-dependence of the frequencies for a very simplistic model of the magnetisation process in UPt_3 in which the difference between the up- and down-pseudospin Fermi surface extremal areas, $A_\uparrow(H) - A_\downarrow(H)$, is proportional to $M(H)$. Evidently, $F_{p\sigma}$ may be very different from F_σ. When F_σ varies linearly with H, $F_{p\sigma}$ is constant. When F_σ has upward (downward) curvature, $F_{p\sigma}$ *falls (rises)*, the rise or fall being disproportionately large when H is large. The insensitivity to linear changes in the Fermi surface with field means that we are unable to directly compare the induced moment and the band splitting, so that supporting computational Fermi surface modeling will be required in order to test for localised f electron magnetic degrees of freedom.

Our results consist of transverse magnetoresistance measurements on ultrapure

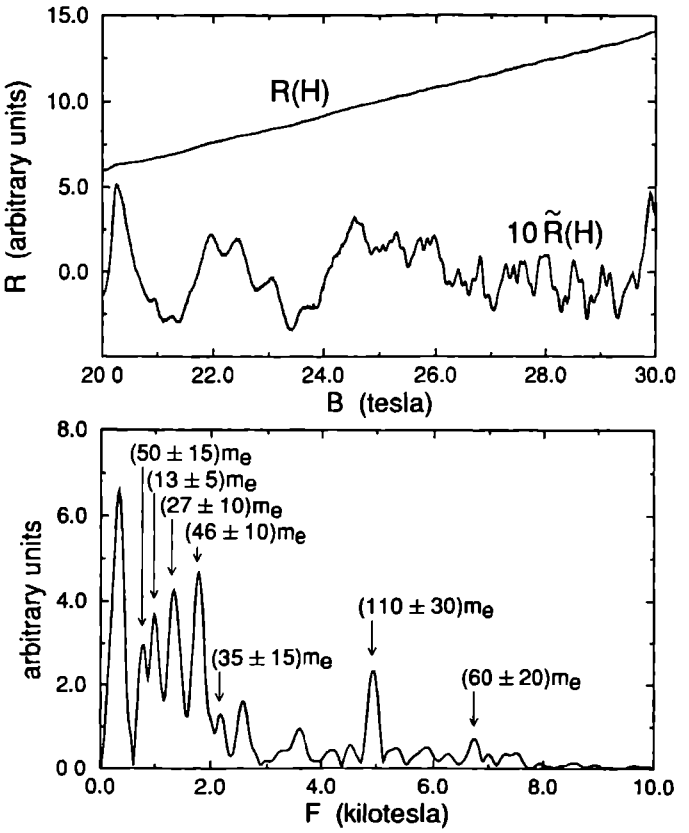

Figure 5.9 Variation from 20 to 30 T of the magnetoresistance before ($R(H)$) and after ($\tilde{R}(H)$) subtraction of the non-oscillatory background, with the field parallel to the b axis. The frequency spectrum for $25\,\mathrm{T} < H < 30\,\mathrm{T}$ is also shown, with the effective mass given for those prominent peaks which are not harmonics. The weak, unlabeled peaks appear only at the high field end of the scan, and we believe them to be harmonics of the larger peaks, or possibly "quantum interference" [68] orbits.

single-crystal whiskers of UPt_3. The magnetic field was applied in the basal plane of the hexagonal structure, and the current was parallel to the c axis. Measurements at temperatures between 17 and 100 mK, and fields from 0 to 14.4 T, were made at the Cavendish Laboratory using a top loading dilution refrigerator and superconducting magnet system specially designed for low noise quantum oscillation experiments. Data at temperatures between 30 and 150 mK, from 10 to 30 T, were taken at the Nijmegen High Field Magnet Laboratory. The sample was cooled by a plastic dilution refrigerator [59], which was placed into a ^{4}He cryostat mounted

in a 30 T hybrid magnet To vary *in situ* the angle of the field with respect to the crystal axes the sample was mounted below the mixing chamber on a rotating platform, controlled by a wire from the top of the system The sample was heat sunk with a silver wire to a piece of sintered silver powder in the mixing chamber

The behaviour of the SdH frequencies near 20 T supports the notion that the bands split nonlinearly at the metamagnetic transition In figure 5 8 a typical magnetoresistance scan from 10 to 24 T is shown, with the corresponding quantum oscillation spectrum as a function of field Below 16 T the oscillation frequencies show only weak field dependence (discussed below) But as the metamagnetic transition is approached a radical modification occurs, as the oscillations first weaken near 17 T, and then reappear with a completely different spectrum which contains higher frequencies and is strongly field dependent This modification is reproducible, and is much too large to be due to the contribution of the nonlinear magnetisation to the internal field, since $\mu_0 M(H)$ changes by only about 0 03 T across the transition While some of this modification may arise from "magnetic breakdown" [65], the natural explanation of the high frequencies seen near the transition is back projection of the nonlinearly changing extremal areas (as per F_{p_1} in figure 5 7), compelling evidence that the bands split nonlinearly near the transition This implies that theoretical models of the heavy fermion metamagnetic transition cannot ignore the magnetism of the quasiparticle bands, whether or not additional magnetic degrees of freedom are assumed to be present Furthermore from these data it is clear that polarisation of the Fermi surface associated with the metamagnetic transition is spread out over a range of several tesla, although a further stepwise change at 20 T cannot at this stage be ruled out

The quasiparticle masses derived from our measurements show that heavy quasiparticles survive into the high field state Figure 5 9 shows typical magnetoresistance data between 20 and 30 T with the field parallel to the b axis, along with the corresponding Fourier spectrum The effective mass associated with each frequency was determined from the temperature dependence of the oscillation amplitudes using the Lifshitz–Kosevich formula [65], thus assuming that the system is a Fermi liquid The peak at 5 0 kT has an effective mass of $(110 \pm 30)\, m_e$, which is one of the largest ever observed All of the masses, both in figure 5 9 and on the a axis [67], show that the quasiparticle mass renormalisation has a similar strength above the transition as it has below (masses below the transition are given in reference [14]), *confirming that the high field state is a heavy electron liquid* in which most or all of the large linear specific heat observed above 20 T [44, 45] can be explained in terms of massive charged fermion quasiparticles

In figure 5 10 the dependence of the frequency spectrum on field orientation in the basal plane is shown, from which topological features of the Fermi surface can be determined Figure 5 10(a) shows the clearest features above the metamagnetic transition, while for comparison figure 5 10(b) shows those below The high field data are more difficult to interpret, perhaps because variations in the projected frequency at these fields may be more the result of variations in $H\,\mathrm{d}F(H)/\mathrm{d}H$ than in $F(H)$, but also simply because more peaks appear above the transition than

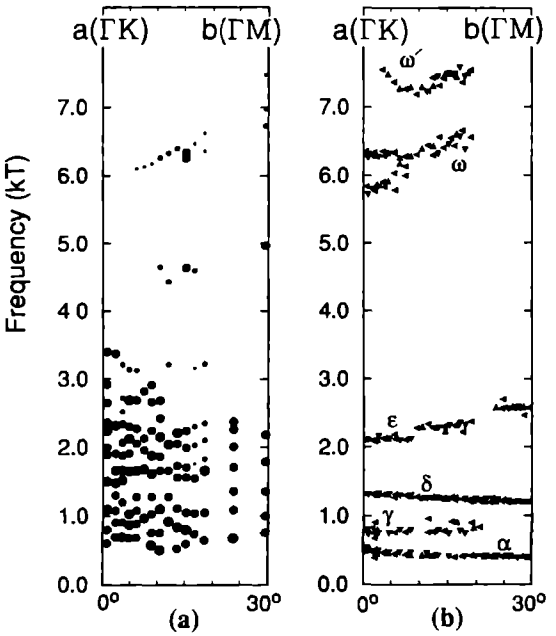

Figure 5.10 Variation of the fundamental SdH frequencies with field orientation in the basal plane (a) for $25\,\mathrm{T} < H < 30\,\mathrm{T}$, at $50 < T < 100\,\mathrm{mK}$, (b) for $H < 14\,\mathrm{T}$ and $T = 17\,\mathrm{mK}$ Some simplification has been achieved by including only those peaks that appear over a range of adjacent angles In figure (a) the size of each point reflects the intensity of the peak, the smallest points arising from weak signals that appear only near 30 T The frequency branch marked ω in figure (b) appears to survive unchanged into the high field state The branch marked ω', not seen in a previous de Haas-van Alphen study [14], has a mass of $170 \pm 35\, m_e$ – the largest value found in any system to date. We believe the ω and ω' branches to be the spin split components of one Fermi surface sheet

below This is likely due to spin splitting of the Fermi surface (as in figure 5 7, where what appears to be one frequency below the transition is resolved into two frequencies above), although some peaks may be due to magnetic breakdown [65] Nevertheless, several features are clear A frequency starting at 1 5 kT on the a axis rises gradually to 1 65 kT on the b axis Several strong frequencies appear between 2 0 and 2 5 kT and persist across most of the diagram Furthermore a strong peak at 5 0 kT is seen on the b axis (also shown in figure 5 9) and a series of weaker peaks, rising from 6 2 to 6 5 kT, is observed as the field is rotated away from the a axis This latter feature matches the band marked ω on figure 5 10(b), implying that this frequency may be unaffected by the metamagnetic transition, a remarkable result Calculation of the field-dependent band structure is required to determine

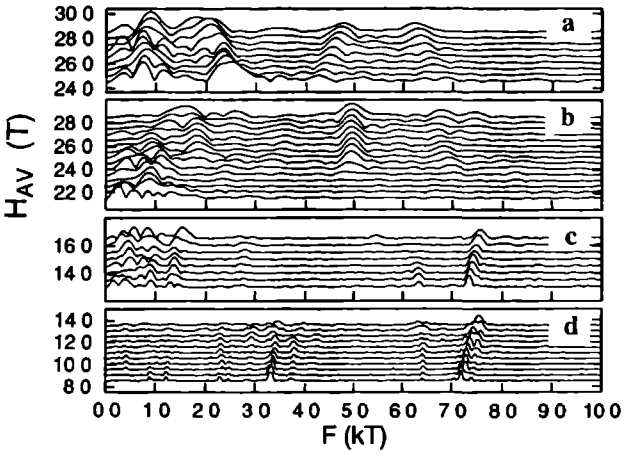

Figure 5.11 Field dependence of the SdH frequencies in UPt_3 in field regions where $M(H)$ varies linearly with H Each spectrum is from a 2 T wide interval centered on H_{av} The shifts are due to nonlinear change of the corresponding extremal area with field The conditions for these scans were (a) 23 T < H < 30 T, T = 70 mK, H 18° from the a axis, (b) 20 T < H < 30 T, T = 70 mK, H parallel to the b axis, (c) 12 T < H < 17 5 T, $T \approx$ 40 mK, H 10° from the a axis, (d) 7 T < H < 14 4 T, T = 17 mK, H 12° from the a axis

if the observed frequencies arise from magnetic splitting of, or magnetic breakdown between, sheets which retain the topology of the low field Fermi surface, or whether a topological rearrangement or, more radically, a change in volume, of the Fermi surface has occurred

Finally, we present evidence of nonlinear magnetic splitting of the quasiparticle bands at fields *where* $M(H)$ *is itself varying linearly with* H This is a new phenomenon, distinct from the nonlinearities seen near 20 T, because there $M(H)$ is itself nonlinear

Figures 5 11(a) and (b) illustrate the field-dependence of the highest frequencies seen above the metamagnetic transition Some frequencies show a clear field dependence (for example the 2 5, 4 5 and 6 5 kT peaks in figure 5 11(a), while others (the 5 0 kT frequency in figure 5 11(b) do not

Figures 5 11(c) and (d) show field-dependent frequencies below 20 T The peak which rises from 7 2 to 7 5 kT in figure 5 11(d) corresponds to the ω' frequency in figure 5 10(b) – a frequency not seen in a previous de Haas–van Alphen study [14] Its appearance was a surprise since LDA band structure calculations predict only one large orbit when the field is in the basal plane, and this had already been identified with the ω frequency of figure 5 10(b) (the field-independent peak at 6 4 kT in figures 5 11(c) and (d)) [14, 47] The clue to the origin of the ω' frequency lies in its quasilinear upward shift with increasing field extrapolating this dependence

to $H = 0$ we find that in zero field the ω and ω' frequencies coincide This is compelling evidence that these are the spin split components of one surface Thus the roughly constant, negative second derivative with field of the ω' extremal area indicated by the behaviour shown in figures 5 11(c) and (d), compared to the (at most) linear field-dependence of the ω surface, demonstrates that subtle, nonlinear quasiparticle band splitting underlies the apparently simple Pauli paramagnetism of the heavy fermion metals, a point is underscored by the differing masses of these surfaces at 12 T, with the field 12° from the a axis, the ω orbit has an effective mass of $(120 \pm 30)\, m_e$, compared to $(170 \pm 35)\, m_e$ for the ω' surface, which is the largest quasiparticle mass observed to date in any system

The authors have benefited from the insight and advice of G G Lonzarich and J A A J Perenboom Access to the Nijmegen High Field Magnet Laboratory was made possible by the Large Installations Plan of the European Community One of us (SRJ) is grateful to NSERC of Canada and to the UK SERC for financial support

References

[1] J Kondo, Prog Theor Phys **32**, 37 (1964)

[2] W Meissner and B Voigt, Ann Phys **7**, 761 and 892 (1930)

[3] M A Ruderman and C Kittel, Phys Rev **96**, 99 (1954)

[4] T Kasuya, Prog Theor Phys **16**, 45 (1956)

[5] K Yosida, Phys Rev **106**, 893 (1957)

[6] D Pines and P Nozieres, *The Theory of Quantum Liquids*, Addison–Wesley (1989)

[7] A de Visser, J J M Franse, A Menovsky, and T T M Palstra, Physica B **127**, 442 (1984)

[8] G R Stewart, Rev Mod Phys **56**, 755 (1984)

[9] G E Brodale, R A Fisher, N E Phillips, G R Stewart, and A L Giorgi, Phys Rev Lett **57**, 234 (1986)

[10] R A Fisher, S Kim, B W Woodfield, N E Phillips, L Taillefer, K Hasselbach, J Flouquet, A L Giorgi, and J L Smith, Phys Rev Lett **62**, 1411 (1989)

[11] A de Visser, L Puech, W Joss, A Menovsky, and J J M Franse, Jpn J Appl Phys **26**, 513 (1987)

[12] Y Kohori, H Shibai, T Kohara, Y Oda, Y Kitaoka, and K Asayama, J Magn & Magn Mater **76&77**, 478 (1988)

[13] L Taillefer, R Newbury, G G Lonzarich, Z Fisk, and J L Smith, J Magn & Magn Mater **63&64**, 372 (1987)

[14] L Taillefer and G G Lonzarich, Phys Rev Lett **60**, 1570 (1988)

[15] G G Lonzarich, J Magn & Magn Mater **76&77**, 1 (1988)

[16] P H P Reinders, M Springford, P T Coleridge, R Boulet, and D Ravot, Phys Rev Lett **57**, 1631 (1986)

[17] P H P Reinders, M Springford, P T Coleridge, R Boulet, and D Ravot, J Magn & Magn Mater **64&64**, 297 (1987)

[18] M Springford and P H P Reinders, J Magn & Magn Mater **76&77**, 11 (1988)

[19] S Chapman, M Hunt, P Meeson, P H P Reinders, M Springford, and M Norman, J Phys Condens Matter **2**, 8123 (1990)

[20] W Joss, J M van Ruitenbeek, G W Crabtree, J L Tholence, A P J van Deursen, and Z Fisk, Phys Rev Lett **59**, 1609 (1987)

[21] W Joss, J M van Ruitenbeek, G W Crabtree, J L Tholence, A P J van Deursen, and Z Fisk, J Appl Phys **63**, 3893 (1989)

[22] Y Onuki, T Komatsubara, P H P Reinders, and M Springford, J Phys Soc Jpn **58**, 3698 (1989)

[23] P H P Reinders and M Springford, J Magn & Magn Mater **79**, 295 (1989)

[24] M Hunt, P Meeson, P-A Probst, P H P Reinders, M Springford, W Assmus, and W Sun, J Phys Condens Matter **2**, 6859 (1990)

[25] A Auerbach and K Levin, J Appl Phys **61**, 3162 (1987)

[26] G Aeppli, E Bucher, C Broholm, J K Kjems, J Baumann, and J Hufnagl, Phys Rev Lett **60**, 615 (1988),

G Aeppli, E Bucher, A I Goldman, G Shirane, C Broholm, and J K Kjems, J Magn & Magn Mater **76&77**, 385 (1988)

[27] L Taillefer, K Behnia, K Hasselbach, J Flouquet, S M Hayden, and C Vettier, J Magn & Magn Mater **90&91**, 623 (1990)

[28] A J Leggett, Rev Mod Phys **47**, 331 (1975)

[29] A J Leggett, J Magn & Magn Mater **64&64**, 406 (1987)

[30] Y J Qian, M -F Xu, A Schenstrom, H -P Baum, J B Ketterson, D G Hinks, M Levy, and B K Sarma, Solid State Comm **63**, 599 (1987)

[31] K Hasselbach, L Taillefer, and J Flouquet, Phys Rev Lett **63**, 93 (1989)

[32] A Schenstrom, M -F Xu, Y Hong, D Bein, M Levy, B K Sarma, S Adenwalla, Z Zhao, T Tokuyasu, D W Hess, J B Ketterson, J A Sauls, and D G Hinks, Phys Rev Lett **62**, 332 (1989)

[33] S Adenwalla, S W Lin, Q Z Ran, Z Zhao, J B Ketterson, J A Sauls, L Taillefer, D G Hinks, M Levy, and B K Sarma, Phys Rev Lett **65**, 2298 (1990)

[34] K Hasselbach, A Lacerda, A de Visser, K Behnia, L Taillefer, and J Flouquet, J Low Temp Phys **81**, 299 (1990)

[35] E Vincent, J Hammann, L Taillefer, K Behnia, N Keller, and J Flouquet, J Phys Condens Matter **3**, 3517 (1991)

[36] L Taillefer, F Piquemal, and J Flouquet, Physica C **153-155**, 1631 (1988)

[37] For a recent review see L Taillefer, J Flouquet, and G G Lonzarich, Physica B **169**, 257 (1991)

[38] R Joynt, Supercond Sci Technol **1**, 210 (1988)

[39] M Sigrist, R Joynt, and T M Rice, Europhys Lett **3**, 629 (1987)

[40] R Joynt, V P Mineev, G E Volovik, and M E Zhitomirsky, Phys Rev B **42**, 2014 (1990)

[41] P H Frings, J J M Franse, F R de Boer, and A Menovsky J Magn & Magn Mater **31-34**, 240 (1983)

[42] P Haen, J Flouquet, F Lapierre, P Lejay, and G Remenyi, J Low Temp Phys **67**, 391 (1987)

[43] J Rossat-Mignod, L P Regnault, J L Jaccoud, C Vettier, P Lejay, J Flouquet, E Walker, D Jaccard, and A Amato, J Magn & Magn Mater **76&77**, 376 (1988)

[44] T Muller, W Joss, and L Taillefer, Phys Rev B **40** 2614 (1989)

[45] H P van der Meulen, Z Tarnawski, A de Visser J J M Franse, J A A J Perenboom, D Althof, and H van Kempen, Phys Rev B **41**, 9352 (1990)

[46] L Taillefer, J Flouquet, and W Joss, J Magn & Magn Mater **76&77**, 218 (1988)

[47] M R Norman, R C Albers, A M Boring, and N E Christensen, Solid State Comm **68**, 245 (1989)

[48] G J McMullan, (unpublished data)

[49] J W Rasul, Phys Rev B **39**, 663 (1989)

[50] A Wasserman, M Springford, and A C Hewson, J Phys Condens Matter **1**, 2669 (1989)

[51] P Fulde, J Phys F Met Phys **18**, 601 (1988)

[52] B.K. Howard, Ph.D. Thesis, University of Cambridge (July 1989).

[53] G. Zwicknagl, E. Runge, and N.E. Christensen, Physica B **163**, 97 (1990).

[54] E.N. Adams and T.D. Holstein, J. Phys. Chem. Sol. **10**, 254 (1959).

[55] G.R. Stewart, Z. Fisk, J.O. Williams, and J.L. Smith, Phys. Rev. Lett. **52**, 679 (1984).

[56] S.R. Julian *et al.*, to be published.

[57] L. Taillefer and G.G. Lonzarich, unpublished data.

[58] J.A.A.J. Perenboom and K. van Hulst, Physica B **155**, 74 (1989).

[59] Described in chapter 3.

[60] I.M. Lifshitz and A.M. Kosevich, Sov. Phys. JETP **2**, 636 (1956).

[61] Throughout this discussion we assume that the applied field is in the basal plane, and we ignore the superconducting portion of the field-temperature phase diagram. At $T = 0\,\mathrm{K}$ this requires fields larger than $H_{c2} \sim 3\,\mathrm{T}$.

[62] G.G. Lonzarich in *Electrons at the Fermi surface*, edited by M. Springford (Cambridge University Press, Cambridge, 1980).

[63] P.G. Mattocks and R.C. Young, J. Phys. F: Met. Phys. **7**, 1219 (1977).

[64] D.M. Edwards, Physica B **169**, 271 (1991);
S.M.M. Evans, Europhysics Letters **17**, 469 (1992);
R. Konno, J. Phys. Condens. Matter **3**, 9915 (1991);
Y. Kuramoto and K. Miyake, J. Phys. Soc. Jpn. **59**, 2831 (1990);
F.J. Ohkawa, Solid State Comm. **71**, 907 (1989);
M. Acquarone, J. Magn. & Magn. Mater. **108**, 181 (1992).

[65] See, for example, D. Shoenberg, *Magnetic Oscillations in Metals* (Cambridge University Press, Cambridge, 1984). Strictly speaking the quantum oscillation frequency is a function of the internal field B, instead of the applied field H. But despite the large induced moment per uranium atom in UPt_3, the contribution of the magnetisation to the internal field is negligible compared to H.

[66] J.M. van Ruitenbeek, W.A. Verhoef, P.G. Mattocks, A.E. Dixon, A.P.J. van Deursen, and A.R. de Vroomen, J. Phys. F: Met. Phys. **12**, 2919 (1982);
T.I. Sigfusson, G.G. Lonzarich, and N.R. Bernhoeft, J. Phys. F: Met. Phys. **14**, 2141 (1984).

[67] S.R. Julian, P.A.A. Teunissen, and S.A.J. Wiegers, Physica B **177**, 135 (1992).

[68] See, for example, A.B. Pippard, *Magnetoresistance in Metals* (Cambridge University Press, Cambridge, 1989).

Summary

This thesis deals with quantum oscillations in metallic systems in very high static magnetic fields, at very low temperatures The periodicity of the oscillations provides valuable information on the Fermi surface dimensions, while analysis of the oscillation amplitude as a function of applied temperature and magnetic field yields information on the cyclotron effective masses and the scattering rate of the electron-quasiparticles The oscillations are periodic with the inverse of the magnetic field They are the result of Landau states moving through the Fermi surface as the magnetic field is varied, causing abrupt periodic variations in the free energy Oscillations can be observed in several thermodynamic and transport properties In this thesis we make use of the de Haas – van Alphen (dHvA) effect and the Shubnikov – de Haas (SdH) effect, which stand for oscillatory behaviour of the magnetisation and resistivity, respectively In chapter 1 the principal aspects of the theory of these oscillations are briefly summarised

The following two chapters discuss the techniques that are used to create the necessary conditions for the observation of these quantum oscillations Chapter 2 describes the experimental dHvA set-up used for measurements in high magnetic fields, generated by a Bitter coil magnet The relatively small oscillations in the magnetisation are detected by means of a field modulation technique The time-varying magnetisation of the sample will induce a voltage in a balanced pair of pick-up coils, surrounding the sample Noise in this pick-up voltage, caused by the high-field magnets, can seriously hamper the observation of quantum oscillations, and special precautions are needed to reduce the noise level To this end an electronic feedback mechanism has been developed, which suppresses the magnetic field noise in a small volume around the sample

In chapter 3 a dilution refrigerator is described, which is specially designed to provide millikelvin temperatures in hybrid magnets It has been used in the experiments described in the last two chapters The trouble with conventional dilution refrigerators is that they are made of metal Therefore eddy currents, induced in the mixing chamber and heat exchangers by a time-varying field, will cause significant heating The new refrigerator has been constructed using plastic materials It has one continuous heat exchanger and achieves a base temperature of 25 mK

Chapter 4 deals with the dHvA effect in high-T_c superconductors Since the discovery of these materials, considerable scientific effort has been invested in the clarification of their electronic ground state, and many theoretical models on high-temperature superconductivity have been proposed The experimental observation of the existence of a Fermi surface in these materials would place a severe constraint on the choice of models Although photoemission studies and positron annihilation experiments have provided some proof for the existence of a Fermi surface in high-T_c

compounds, a direct ground state measurement of the Fermi surface by means of a quantum oscillation experiment should give the definite answer After recently reported claims of observations of dHvA oscillations in the compound $YBa_2Cu_3O_{7-\delta}$, we have set out to independently reproduce these results, using the experimental set-up described in chapter 2 Apart from the field modulation technique we have used 'pulsed" fields, obtained by very quickly ramping the field of a Bitter magnet In spite of extensive investigations, no sign of oscillations has been found We have tried to explain these negative results and arrive at the conclusion that, even at a maximum field of 20 T, the oscillations in $YBa_2Cu_3O_{7-\delta}$ - if present - are too feeble to be detected

Chapter 5 is dedicated to the heavy fermion compound UPt_3 It belongs to a class of intermetallic compounds containing rare earth (mostly Ce) or actinide (mostly U) ions "Heavy" refers to the presence at low temperatures – of conduction electrons with strongly enhanced mass, when compared with those in conventional metals The enhancement is associated with the strongly interacting *f*-electrons of the U or Ce atoms The existence of these quasiparticles has already been confirmed by dHvA measurements Interactions between the quasiparticles can lead to instabilities of the ground state, so that for example superconductivity, antiferromagnetism and metamagnetism may occur In chapter 5 we concentrate on the field-induced metamagnetic transition of UPt_3, which occurs at 20 T Although there is evidence that the transition is related to the breaking of short-range antiferromagnetic correlations when a magnetic field is applied, neither the underlying mechanism of the transition nor the high-field state is well understood In order to clarify the situation we have performed SdH measurements on an ultrapure single-crystal of UPt_3 up to a magnetic field of 30 T Rapid changes in the oscillation frequency spectrum near 20 T indicate strong nonlinear magnetic splitting of the quasiparticle bands Nonlinear splitting is also seen at fields considerably lower and higher than 20 T, although the effect is weaker Below the metamagnetic transition a surface with an effective mass of 170 times the free electron mass has been observed which is the largest seen to date Finally it is established that the mass enhancement above the transition is still very large and that like below 20 T no light quasiparticles are present

Samenvatting

Dit proefschrift handelt over quantum oscillaties in metallische systemen in zeer hoge statische magneetvelden bij zeer lage temperaturen De periode van de oscillaties levert waardevolle informatie omtrent de afmetingen van het Fermi oppervlak, terwijl analyse van de oscillatie-amplitude, als functie van temperatuur en magnetische veldsterkte, kennis oplevert over de cyclotron effectieve massa en de verstrooiing van de elektron-quasideeltjes De oscillaties zijn periodiek in de reciproke veldsterkte Ze zijn het gevolg van het schuiven van Landau niveau's door het Fermi oppervlak wanneer het magneetveld wordt gevarieerd, hetgeen abrupte periodieke variaties in de vrij energie veroorzaakt Oscillaties kunnen worden waargenomen in verschillende thermodynamische en transport eigenschappen In dit proefschrift wordt gebruik gemaakt van zowel het de Haas – van Alphen (dHvA) effect als het Shubnikov – de Haas (SdH) effect, welke respectievelijk oscillerend gedrag van magnetisatie en elektrische weerstand betreffen In hoofdstuk 1 worden de voornaamste aspecten van de theorie achter deze oscillaties kort samengevat

In de volgende twee hoofdstukken worden de technieken besproken die gebruikt worden om de condities te scheppen waaronder quantum oscillaties kunnen worden waargenomen Hoofdstuk 2 beschrijft de experimentele dHvA-opstelling, die gebruikt wordt voor metingen in sterke magneetvelden, opgewekt door een Bitter magneet De relatief zwakke oscillaties in de magnetisatie worden gedetecteerd met behulp van een veldmodulatie techniek De variërende magnetisatie van een preparaat induceert een spanning in een gebalanceerd paar oppikspoeltjes, welke het preparaat omhullen Ruis in deze oppikspanning, veroorzaakt door de hoge-veld magneten, kan het waarnemen van quantum oscillaties ernstig bemoeilijken en speciale maatregelen zijn daarom nodig om het ruisniveau te reduceren Hiertoe is een elektronisch terugkoppelmechanisme ontwikkeld, die de ruis in het magneetveld in een klein volume rond het preparaat onderdrukt

In hoofdstuk 3 wordt een mengkoelmachine beschreven, die er speciaal voor is ontworpen om millikelvin temperaturen beschikbaar te hebben in hybride magneten Deze is gebruikt voor de metingen beschreven in de laatste twee hoofdstukken Het nadeel van conventionele mengkoelers is dat ze van metaal gemaakt elektrische stromen, opgewekt door een veranderend magneetveld, kunnen dan in de mengkamer en warmtewisselaars opwarming veroorzaken De nieuwe koelmachine is geconstrueerd met gebruikmaking van plastic materialen, heeft een continue warmtewisselaar en haalt een bodemtemperatuur van 25 mK

Hoofdstuk 4 behandelt het dHvA effect in hoge-T_c supergeleiders Sinds de ontdekking van deze materialen is aanzienlijke wetenschappelijke inspanning geleverd om duidelijkheid te brengen in hun elektronische grondtoestand en een aantal theoretische modellen voor hoge-temperatuur supergeleiding zijn voorgesteld

Experimentele waarneming van een Fermi oppervlak in deze materialen zou een aanzienlijke beperking betekenen van het aantal mogelijke modellen Hoewel fotoemissie studies en positron-annihilatie experimenten in enige mate bewijs leveren voor het bestaan van een Fermi oppervlak in hoge-T_c materialen, zal een directe grondtoestand-meting van het Fermi oppervlak door middel van een quantum oscillatie experiment het beslissende antwoord moeten geven Na recente rapportages over het waarnemen van dHvA oscillaties in de supergeleider $YBa_2Cu_3O_{7-\delta}$ hebben we gepoogd om deze resultaten onafhankelijk te reproduceren, met gebruikmaking van de experimentele opstelling zoals beschreven in hoofdstuk 2 Naast de veldmodulatie techniek hebben we met "gepulste" magneetvelden gewerkt, door het veld van een Bitter magneet snel te varieren Ondanks uitgebreid onderzoek is geen enkele oscillatie waargenomen We hebben getracht oorzaken te vinden voor deze negatieve resulaten en komen tot de conclusie dat, zelfs bij een veldsterkte van 20 T, de oscillaties in $YBa_2Cu_3O_{7-\delta}$ – indien aanwezig – te zwak zijn om waargenomen te kunnen worden

Hoofdstuk 5 is gewijd aan de zware-fermion verbinding UPt_3 Het behoort tot de klasse van intermetallische verbindingen, welke zeldzame-aarde- (voornamelijk Ce) of actinide- (voornamelijk U) ionen bevatten "Zwaar" verwijst naar de aanwezigheid – bij lage temperatuur – van ladingsdragers met een in vergelijking met conventionele metalen sterk verhoogde effectieve massa Deze verhoging is verbonden met sterke interacties tussen de f-elektronen van de U of Ce atomen De directe bevestiging van het bestaan van deze quasideeltjes is reeds geleverd door dHvA metingen Interacties tussen de quasideeltjes kunnen leiden tot instabiliteiten van de grondtoestand, bijvoorbeeld supergeleiding, antiferromagnetisme en metamagnetisme In hoofdstuk 5 wordt de aandacht gericht op de magneetveldgeinduceerde metamagnetische overgang van UPt_3, die optreedt bij 20 T Ofschoon er aanwijzingen zijn dat de overgang gerelateerd is aan het verbreken van antiferromagnetische correlaties wanneer een magneetveld wordt aangelegd, is noch het onderliggende mechanisme van de overgang, noch de hoge-veld toestand begrepen In een poging hierin opheldering te brengen hebben we SdH metingen uitgevoerd aan een ultra-puur éénkristal van UPt_3 in magneetvelden tot 30 T Snelle veranderingen in het frequentiespectrum van de oscillaties in de buurt van 20 T duiden op sterke, niet-lineaire magnetische opsplitsing van de energiebanden Niet-lineaire opsplitsing is ook gezien voor velden die aanzienlijk hoger en lager zijn dan 20 T, echter het effect is zwakker Onder de metamagnetische overgang is een Fermi oppervlak gedeelte waargenomen met een effectieve massa van 170 maal de vrije elektron massa, de grootste massa die ooit gemeten is Tenslotte is vastgesteld dat boven de overgang de massa's nog steeds erg groot zijn en dat lichte quasideeltjes, net als onder de overgang, volledig afwezig zijn

List of Publications

Tunneling Measurements on the High-T_c Superconductors $La_{1.85}Sr_{0.15}CuO_{4-\delta}$ and $YBa_2Cu_3O_{7-\delta}$
P J M van Bentum, L E C van de Leemput, L W M Schreurs, P A A Teunissen, and H van Kempen,
Physical Review B **36**, 843 (1987)

High-field Measurements on the High-T_c Superconductors $La_{1.85}Sr_{0.15}CuO_{4-\delta}$ and $YBa_2Cu_3O_{7-\delta}$
P J M van Bentum, H van Kempen, L E C van de Leemput, J A A J Perenboom, L W M Schreurs, and P A A Teunissen,
Physical Review B **36**, 5279 (1987)

Single-electron Tunneling Observed with Point-contact Tunnel Junctions
P J M van Bentum, H van Kempen, L E C van de Leemput, and P A A Teunissen,
Physical Review Letters **60** (1988)

Comparative Study of the Energy Gap in $YBa_2Cu_3O_{7-\delta}$
P J M van Bentum, H F C Hoevers, L E C van de Leemput, L W M Schreurs, P A A Teunissen, and H van Kempen,
Physica C **153–155**, 1379 (1988)

High-field Measurements on $La_{1.85}Sr_{0.15}CuO_{4-\delta}$ and $YBa_2Cu_3O_{7-\delta}$
P J M van Bentum, H van Kempen, L E C van de Leemput, J A A J Perenboom, L W M Schreurs, E van der Steen, and P A A Teunissen,
Physica C **153–155**, 1485 (1988)

Determination of the Energy Gap in $YBa_2Cu_3O_{7-\delta}$ by Tunneling, Far-Infrared Reflection and Andreev Reflection
P J M van Bentum, H F C Hoevers, H van Kempen, L E C van de Leemput, M J F M de Nivelle, L W M Schreurs, R T M Smokers, and P A A Teunissen,
Physica C **153–155**, 1718 (1988)

High Magnetic Field and Tunneling Measurements on the High T_c Superconductors $La_{1.85}Sr_{0.15}CuO_4$ and $YBa_2Cu_3O_{7-\delta}$
P J M van Bentum, J C Fuggle, R A de Groot, H van Kempen, L E C van de Leemput, J A A J Perenboom, L W M Schreurs, and P A A Teunissen,
Proceedings of the First European Workshop on High-T_c Superconductors and Potential Applications, Genua, Italy 1-3 July 1987

The Energy Gap of $YBa_2Cu_3O_{7-\delta}$ Tunneling, Far-Infrared Reflection and Andreev Reflection
H van Kempen, P J M van Bentum, H F C Hoevers, L E C van de Leemput, L W M Schreurs, R T M Smokers, and P A A Teunissen,
Proceedings Latin American Conference on High-T_c Superconductors, Progress in High Temperature Superconductivity **9**, 175 (World Scientific, Singapore, 1988)

Comparison of Three Methods to Determine the Energy Gap of $YBa_2Cu_3O_{7-\delta}$
P J M van Bentum, H F C Hoevers, L E C van de Leemput, M J F M de Nivelle, L W M Schreurs, R T M Smokers, P A A Teunissen, and H van Kempen,
Physica Scripta **T25**, 91 (1989)

Anisotropy of the Critical Fields of High-T_c Superconductors
P J M van Bentum, H van Kempen, J A A J Perenboom, L W M Schreurs, P A A Teunissen, and H J L van der Steen,
Physica B **155**, 160 (1989)

Observation of Heavy Fermion Quasiparticles in UPt_3 Above the Metamagnetic Transition
S R Julian, P A A Teunissen, and S A J Wiegers,
Physica B **177**, 135 (1992)

The Fermi Surface of UPt_3 from 3 to 30 T Field-Induced Quasiparticle Band Polarisation and the Metamagnetic Transition
S R Julian, P A A Teunissen, and S A J Wiegers,
Physical Review B **46**, 9821 (1992)

Observation of the Fractional Quantum Hall Effect in GaAs-(Ga,Al)As Quantum Well Structures
C V Brown, C J G M Langerak, P C Main, L Eaves, T J Foster, M Henini, P A A Teunissen, and J A A J Perenboom,
To be published in Physica B

Precision of the Hall Quantisation in Naturally Occuring Two-Dimensional-System HgCdMnTe Bicrystals
G Grabecki, A Wittlin, T Dietl, P A A Teunissen, S A J Wiegers, and J A A J Perenboom,
To be published in Semiconductor Science and Technology

Curriculum Vitae van P.A.A. Teunissen

geboren op 20 juni 1965 te Eindhoven

1977-1983	Opleiding Gymnasium B aan het St. Janslyceum te 's-Hertogenbosch.
1983-1988	Studie Natuurkunde aan de Katholieke Universiteit te Nijmegen, afstudeerwerk: tunnelmetingen en kritisch veld metingen aan de hoge T_c supergeleiders $La_{1.85}Sr_{0.15}CuO_{4-\delta}$ en $YBa_2Cu_3O_{7-\delta}$.
1988-1992	Promotiewerkzaamheden op de afdeling Experimentele Vaste Stof Fysica I van de Katholieke Universiteit Nijmegen onder leiding van Prof. Dr. A.R. de Vroomen en Prof. Dr. H. van Kempen en dagelijkse begeleiding van Dr. J.A.A.J. Perenboom.